APPENDIX 3.9.5
NUHOMS® EOS-TC BODY STRUCTURAL ANALYSIS

Table of Contents

3.9.5 NUHOMS® EOS-TC BODY STRUCTURAL ANALYSIS 3.9.5-1

3.9.5.1 General Information 3.9.5-1

3.9.5.2 EOS Transfer Cask Accident (Side and End) Drop Evaluation for 65g Static Load 3.9.5-1

3.9.5.3 Lead Gamma Shielding Slump Evaluation 3.9.5-2

3.9.5.4 EOS Transfer Cask Trunnions and Local Shell Stress Evaluation 3.9.5-3

3.9.5.5 EOS Transfer Cask Neutron Shield Shell Structural Evaluation *3.9.5-9*

3.9.5.6 EOS Transfer Cask, Trunnion, and Neutron Shield Shell Fatigue Requirements *3.9.5-14*

3.9.5.7 References *3.9.5-15*

List of Tables

Table 3.9.5-1 EOS-TCMAX Stress Result Summary Table – 65g Side Drop *3.9.5-16*
Table 3.9.5-2 EOS-TCMAX Stress Result Summary Table – 65g Top End Drop..... *3.9.5-17*
Table 3.9.5-3 EOS-TCMAX Stress Result Summary Table – 65g Bottom End Drop *3.9.5-18*
Table 3.9.5-4 Stress Result Summary Table for the Trunnions *3.9.5-19*
Table 3.9.5-5 Acceptance Criteria for the Stress Evaluation *3.9.5-21*
Table 3.9.5-6 Stress Result Summary for the Neutron Shield Panel model *3.9.5-22*
Table 3.9.5-7 Weld Stress Result Summary for the Neutron Shield Panel model..... *3.9.5-23*

List of Figures

Figure 3.9.5-1 3D Half Symmetric Finite Element Model for Drop Loads *3.9.5-24*

Figure 3.9.5-2 Pressure Load and Boundary Condition Plots – 65g Side Drop *3.9.5-25*

Figure 3.9.5-3 Pressure Load and Boundary Condition Plots – 65g End Drop..... *3.9.5-26*

Figure 3.9.5-4 Stress Intensity (psi) plot for EOS-TCMAX – 65g Side Drop *3.9.5-27*

Figure 3.9.5-5 Deformation plot (in.) for EOS-TCMAX (scaled up) – 65g Side Drop *3.9.5-27*

Figure 3.9.5-6 Stress Intensity (psi) plot for EOS-TCMAX – 65g Top End Drop *3.9.5-28*

Figure 3.9.5-7 Stress Intensity (psi) plot for EOS-TCMAX – 65g Top End Drop *3.9.5-28*

Figure 3.9.5-8 Upper Trunnion Sectional View *3.9.5-29*

Figure 3.9.5-9 Cut Section Finite Element Model of EOS-TCMAX (Top and Bottom) *3.9.5-30*

Figure 3.9.5-10 Pressure Load and Boundary Condition Plots *3.9.5-31*

Figure 3.9.5-11 Stress Intensity (psi) Plot for Load Case 3g..... *3.9.5-32*

Figure 3.9.5-12 Stress Intensity (psi) Plot for Load Case Horizontal Transfer on Skid *3.9.5-33*

Figure 3.9.5-13 EOS-TC108 Meshed Model *3.9.5-34*

Figure 3.9.5-14 EOS-TC125 Meshed Model *3.9.5-35*

Figure 3.9.5-15 EOS-TC108 Neutron Shield Panel Stress Intensity (P_m+P_b) Plot Load Case E1 ..... *3.9.5-36*

Figure 3.9.5-16 EOS-TC108 I-Beam Stress Intensity (P_m+P_b) Plot Load Case E1 ..... *3.9.5-37*

Figure 3.9.5-17 EOS-TC135 Neutron Shield Shell Stress Intensity Plot under Pressure Load (40 psig) *3.9.5-38*

Figure 3.9.5-18 EOS-TC135 I-Beam Stress Intensity Plot under Pressure Load (40 psig)..... *3.9.5-39*

Figure 3.9.5-19 EOS-TC125 Temperature Distribution Plot *3.9.5-40*

Figure 3.9.5-20 EOS-TC108 Temperature Distribution Plot *3.9.5-41*

Figure 3.9.5-21 Bottom and Top, respectively, End Drops - Load 65g - Lead Slump Displacements..... *3.9.5-42*

3.9.5 NUHOMS® EOS-TC BODY STRUCTURAL ANALYSIS

3.9.5.1 General Information

This appendix covers the structural evaluation of the transfer cask (TC) when carrying a loaded DSC. The TC structure is designed to American Society of Mechanical Engineers (ASME) NF-3200 [3.9.5-3] stress limits to the greatest degree practical. The trunnions and trunnion welds to the TC top ring are designed to American National Standards Institute (ANSI) N14.6 [3.9.5-2] stress limits for non-redundant lifting. Structural evaluation of the TC for the missile impact load cases is covered in Appendix 3.9.7, and not presented in this Appendix.

A geometric- and load-bounding representation, enveloping the three EOS-TCs (EOS-TC108, EOS-TC125 and EOS-TC135), is referred to as EOS-TCMAX in this evaluation. The geometric dimensions for this bounding model are selected to yield the most bounding stresses and deformations.

3.9.5.2 EOS Transfer Cask Accident (Side and End) Drop Evaluation for 65g Static Load

The purpose of this section is to summarize the structural evaluation of the EOS-TC for the postulated accident side and end drop conditions. The Service Level D drop evaluations are done by means of 3-D elastic-plastic model. Structural integrity of the design is evaluated by means of plastic analysis criteria of Reference [3.9.5-3].

3.9.5.2.1 Material Properties

Mechanical properties of cask components are evaluated at a temperature of 400°F that exceeds the maximum temperature of cask body for all cask designs. A bilinear stress-strain curve with a 5% tangent modulus is used for steel components. The lead material is modeled by bilinear kinematic hardening method. All the EOS-TC material properties are listed in Chapter 8.

3.9.5.2.2 Design Criteria

The EOS-TC is analyzed using ASME code, Section III, Appendix F requirements service level D allowable stresses for plastic analysis.

3.9.5.2.3 Methodology

ANSYS [3.9.5-4] is used for the evaluation of side and end drop loads. A static load of 65g is applied and a plastic evaluation is performed for the postulated accident drop loads and compared against the Level D stress allowables.

A 65g drop load is considered bounding for the cask design in the accident conditions. Combination of side and end drop are considered bounding for the corner drop, since the corner accidents decelerations are significantly below 65g magnitude.

3.9.5.2.3.1 Finite Element Model

A 3D half symmetric model is used to perform accident drop evaluations. ANSYS SOLID185 elements were used to model the EOS-TC components. ANSYS Surface to Surface contact CONTA173 were used to model the contacting surface. Top cover bolts were modeled using COMBIN39 spring elements. Welds are modeled by means of nodal couples in all three directions. The finite element model is shown in Figure 3.9.5-1.

3.9.5.2.3.2 Loads and Boundary Conditions

For the side drop evaluation the DSC weight is specified using a cosine distributed pressure load for an angle span of 90°. Symmetry boundary conditions are applied on the cut plane. On the impact side the EOS-TC structural shell is fixed for a small 15° arc in radial direction and over total length. The applied pressure load and the boundary conditions are shown in Figure 3.9.5-2.

For the end drop evaluation the DSC weight is uniformly distributed on the lid/inner bottom end plate. Symmetry boundary conditions are applied on the cut plane. The cask is supported at the impacting surface for the top and bottom end drop. The applied pressure load and the boundary conditions are shown in Figure 3.9.5-3.

3.9.5.2.3.3 Results

The maximum stress intensity and the deformation plots for the 65g side drop are shown in Figure 3.9.5-4 and Figure 3.9.5-5. As shown in Table 3.9.5-1, all stresses are within allowable limits for the side drop condition.

The maximum stress intensity for the 65g top and bottom end drop are shown in Figure 3.9.5-6 and Figure 3.9.5-7. As shown in Table 3.9.5-2 and Table 3.9.5-3, all stresses are within allowable limits for the both top and bottom end drop condition.

3.9.5.3 Lead Gamma Shielding Slump Evaluation

The extent of lead slump in the TC during a vertical/end drop scenario is presented exclusive of side drop results, as a side drop would induce only negligible amounts of slump in the lead shielding.

The lead material conforms to the ASTM B29 specification for standard commercial lead, except that the density is increased from the reference 0.41 lb/in^3 to 0.615 lb/in^3 in order to conservatively bound the largest weight of shielding available.

The lead is assumed to fill the available cavity in the TC, such that any deformation of the inner shell will be carried into the lead shielding. The material is modeled with a multi-linear, kinematic hardening stress response to applied strains as detailed in Chapter 8.

The lead slump is modeled as subjected to a conservative 65g vertical load. This load induces a maximum slump of 2.2 inches in the vertical direction. The mesh for this vertical load is shown in Figure 3.9.5-3, while the displacements of the lead under top and bottom 65g accelerations are shown in Figure 3.9.5-21.

See Chapter 12 for the shielding evaluation of this slump.

3.9.5.4 EOS Transfer Cask Trunnions and Local Shell Stress Evaluation

The purpose of this section is to summarize the structural evaluation of the EOS-TC upper trunnions, the welds between the top/bottom rings and the upper/lower trunnions, respectively, and the shell stresses during lifting and handling operations for transfer conditions.

The EOS-TC is lifted by the two upper trunnions. Two lower pocket trunnions in the bottom ring of the cask form the rotational axis for the cask on the support skid during up-ending and down-ending of the cask. These lower pocket trunnions also provide support for the bottom end of the cask during transfer operations.

A geometric- and load-bounding representation, enveloping the three EOS-TCs (EOS-TC108, EOS-TC125 and EOS-TC135), is referred to as EOS-TCMAX in this evaluation. The geometric dimensions for this bounding model are selected to yield the most bounding stresses and deformations.

The evaluation is performed in the following steps:

- The upper trunnions, bottom ring and the welds between the trunnions and the shell are evaluated using hand calculations.
- The cask shell stresses are evaluated using ANSYS code [3.9.5-4].

The material properties are as measured at a conservative 400 °F.

3.9.5.4.1 Methodology and Acceptance Criteria

The conservatively bounding weights of the EOS-TC and DSC components employed for the analysis are as follows:

- Unloaded EOS-TC135 136,000 lb
- Loaded EOS-37PTH DSC 134,000 lb
- Total 270,000 lb

The upper trunnions and trunnion welds to the cask top ring are designed in accordance with the allowable stresses defined by ANSI N14.6 [3.9.5-2] for a non-redundant lifting device.

For the vertical configuration, the dead weight load includes the self-weight of the loaded EOS-TC with the bounding EOS-37PTH DSC payload full of water. This load considers the EOS-TC hanging vertically by the two upper trunnions. The weight of the DSC is applied as a uniform pressure on the bottom end plate of the EOS-TCMAX. A dynamic load factor (DLF) of 1.15 is used to include the effects of dynamic interactions.

During transfer of the EOS-TC on the trailer, the EOS-37PTH DSC will rest on the EOS-TC inner shell. The EOS-37PTH DSC weight is therefore applied as a pressure to the inner shell using a cosine shaped load amplitude variation. The EOS-TC will be in contact with the saddle, latch and the lower trunnion pockets; the lower trunnion pocket was modeled in ANSYS as vertically constrained nodes. Similarly, the semicircular half section of the upper trunnion is constrained in radial direction. See Figure 3.9.5-10 for a diagram showing the boundary conditions for various loading conditions.

During down-ending operations on the transfer trailer, the EOS-TC will rotate about the lower trunnion pockets, at which time, the contact between the lifting yoke and the upper trunnion will separate and the total load will be supported by the lower trunnion pockets.

For thermal stress analysis, temperature profiles and maximum component temperatures are based on the thermal analyses described in Chapter 4. Only two load cases are evaluated for thermal stress analysis, depending on the bounding cases, based on the maximum reported temperatures for normal and off-normal conditions. Displacement constraints are applied simply to prevent rigid body motion.

For all analyses except thermal analysis material properties are taken at a conservative temperature of 400 °F. The allowable stresses for the EOS-TC components are obtained from Chapter 3, Table 3-3 and is reproduced for the pertaining load cases in Table 3.9.5-4.

3.9.5.4.2 Trunnion and Weld Evaluation

The EOS-TC has two upper trunnions to lift the cask during the lifting and handling operations. The upper trunnions are welded to the cask through partial penetration groove welds with fillet covers.

The upper trunnions are single shoulder trunnions as shown in Figure 3.9.5-8. The upper trunnions are evaluated for its critical section, Section A-A shown in Figure 3.9.5-8, for the maximum total weight of the TC.

The maximum total weight is calculated as:

$$F_v = W_L \text{ x } DLF / N_{tr} = 155{,}250 \text{ lb}$$

Where,

F_v = Maximum lift weight
W_L = Total weight of the TC and DSC = 270,000 lb
DLF = Dynamic load factor = 1.15
N_{tr} = Number of trunnions = 2

The shear stress in Section A-A for 1g is:

$$\text{Shear Stress (ksi)} = F_v/S_{AA} = 3.29 \text{ ksi}$$

Where S_{AA} is the section area and the bending stress is:

$$\frac{M_{AA}}{I_{AA}} \times \frac{D_1}{2} = 6.59 \text{ ksi}$$

Where,

M_{AA} = Bending moment at Section A-A
I_{AA} = Moment of Inertia at Section A-A, and
D_1 = Trunnion diameter.

At a service load level of 1g the maximum stress intensity within the upper trunnion itself is 9.31ksi, leading to 6g and 10g stress intensities of 55.9 ksi and 93.1 ksi, respectively.

The upper trunnion is welded to the top ring via a 1.25 inch partial penetration groove weld with a 3/8 inch fillet cover. *These welds are also evaluated per the ANSI 14.6 criteria.* The direct shear load on the trunnion is considered to be resisted by contact/bearing due to the very tight tolerances to which the parts are machined.

Per Paragraph 4.2.1.1 of ANSI N14.6 [3.9.5-2], the combined shear stress and the maximum tensile stress are compared to the material yield and ultimate strengths considering safety factors of 6 and 10, respectively. Both the base metal and weld metal stresses are evaluated. Only the ultimate stress of the weld metal is considered. For the base metal, both yield and ultimate stress checks are performed.

The normal stress, f_n, and shear stress, f_v, components on each critical plane of the weld are calculated and then the combined maximum equivalent stress is calculated and compared to the bounding allowable stress for the trunnion base metal, weld metal, and top ring base metal. The maximum equivalent stress is calculated as:

$$f_{eqv} = \sqrt{(f_n)^2 + 3(f_v)^2}$$

The bending moment considered in the weld is calculated as the shear load, F_v times the moment arm of 2.62, which is the distance from the load application to the top ring:

$$M = F_v \times 2.62 = 155{,}250 \text{ lbs} \times 2.62 \text{ in} = 406{,}755 \text{ in} - \text{lbs}$$

Therefore, the bending load on the weld is

$$f_b = \frac{M}{I_{weld}} = \frac{406{,}755}{78.54} = 5{,}179\ lb/in$$

Where,

$$I_{weld} = \frac{\pi}{4}(D_2)^2 = 78.54 in^2$$

The trunnion base metal shear stress, f_{vTBM}, is caused by the bending load of 5,179 lb/in calculated above. The base metal length is the depth of the J-groove, 1.25 inch, plus the 3/8 inch cover, for a total length of 1.625 inches.

$$f_{vTBM} = \frac{5{,}179\ lb/in}{1.625\ in} = 3{,}187\ psi$$

The maximum equivalent stress is, therefore:

$$f_{eqv,TBM} = \sqrt{3} f_{vTBM} = 5{,}520\ psi$$

The minimum throat distance through the weld metal is $\sqrt{1.25^2 + 0.375^2} = 1.305$ *inches. The weld throat is inclined at an angle of* $\tan^{-1}\frac{0.375}{1.25} = 16.7$ *degrees. The stress on the minimum throat is a combination of tension and shear.*

$$f_{v,weld} = \frac{5{,}179\ lb/in}{1.305\ in}\cos(16.7) = 3{,}801\ psi$$

$$f_{n,weld} = \frac{5{,}179\ lb/in}{1.305\ in}\sin(16.7) = 1{,}140\ psi$$

The weld metal maximum equivalent stress is:

$$f_{eqv,weld} = \sqrt{\left(f_{n,weld}\right)^2 + 3\left(f_{v,weld}\right)^2} = \sqrt{(1{,}140)^2 + 3(3{,}801)^2} = 6{,}682\ psi$$

*The cask top ring base metal stress components are conservatively calculated considering a 45-degree weld bevel. The actual length of base metal for the J-groove geometry is larger. The length of the beveled edge is, therefore, taken as 1.414*1.25=1.77 inches. The top ring base metal shear stress is:*

$$f_{vTRBM} = \frac{5{,}179\frac{lb}{in}}{1.77\ in}\cos(45) = 2{,}069\ \text{psi}$$

The top ring base metal normal stress is:

$$f_{nTRBM} = \frac{5{,}179\frac{lb}{in}}{1.77in} \times \sin(45) = 2{,}069\ \text{psi}$$

The base metal maximum equivalent stress is, therefore:

$$f_{eqv,TRBM} = \sqrt{(f_{nTRBM})^2 + 3(f_{vTRBM})^2} = \sqrt{2{,}069^2 + 3 \times 2{,}069^2} = 4{,}138\ psi$$

The allowable stresses for each of these stress components are as follows:

Trunnion base metal allowable stress:

$$F_{TBM} = \min\left(\frac{S_y}{6}, \frac{S_u}{10}\right) = \min\left(\frac{82.8}{6}, \frac{113.7}{10}\right) = \min(13.8, 11.4) = 11.4\ ksi$$

Top ring base metal allowable stress:

$$F_{TRBM} = \min\left(\frac{S_y}{6}, \frac{S_u}{10}\right) = \min\left(\frac{32.0}{6}, \frac{70.0}{10}\right) = \min(5.33, 7.0) = 5.33\ ksi$$

Weld metal allowable stress:

$$F_w = \min\left(\frac{S_y}{6}, \frac{S_u}{10}\right) = \min\left(NA, \frac{75.0}{10}\right) = 7.5\ ksi$$

The ultimate stress of the weld metal is 75 ksi for ER308L electrode material to match the weaker of the two joined base metals.

The calculated stresses and comparisons to allowable values for the 1g critical lift (including a dynamic load factor of 1.15) are summarized in Table 3.9.5-4.

The lower trunnion pockets provided in the bottom ring support the EOS-TC during the various handling and transfer operations. The bearing stress in the bottom ring is analyzed for a bounding load of (1g vertical + 1g horizontal + 1g transverse + 1g dead weight). The maximum bearing stress between the bottom trunnions and the bottom ring is 10.8 ksi.

3.9.5.4.3 Shell Evaluation

A single 3D FEM is prepared for the bounding dimensions of the EOS-TCs, which accounts for the minimum thickness, longest length and bounding DSC weight. The following components were modeled with SOLID185 elements:

- Top ring
- Bottom ring
- Inner shell
- Outer shell
- Lead shielding
- Upper trunnions
- Bottom end plate
- Ram access penetration ring
- Top lid

The parts that are not modeled include the EOS-TC rails, bottom neutron shields, inner and outer neutron shield panel, bottom neutron shield plate, and the bottom cover plate, since these components will not significantly affect the evaluation.

Because all of the components of the EOS-TC are not modeled in the FEM, the densities of various components are modified in order to achieve the overall weight of the EOS-TC135. The total weight of the EOS-TCMAX model is 136,000 lb, which is conservatively higher than the overall weight of the EOS-TC135.

The weld between the top trunnions and top ring is modeled by coupling the nodes in all degrees of freedom. The nodes between inner/outer shell with top/bottom rings are merged together as these locations are not in the high stress locations. Contact between components is created using CONTA173 and TARGE170 surface-to-surface contact elements.

The finite element model for the EOS-TCMAX is shown in Figure 3.9.5-9.

3.9.5.4.4 Results

The stress values in the upper trunnions, shell welds and top and bottom ring are below the allowable values. Table 3.9.5-4 summarizes the calculated stress, allowable stress, and safety margin for each item and load case.

There are two upper trunnion and two lower trunnion pockets on the transfer cask. The upper trunnions are used for lifting and are welded to the cask top ring. The maximum stress in the trunnion and the trunnion to cask top ring weld are evaluated in accordance with the allowables defined by ANSI N14.6.

The maximum stress intensity for the upper trunnion is 93.1 ksi with a margin of 0.22 (10g load). The maximum weld stress is 6.68 ksi with a margin of 0.12 (1g critical lift with 1.15 DLF). The maximum bearing stress for the lower trunnion pocket is 10.8 ksi with a margin of 1.97. The maximum shell stress in the top ring (3g test load) is 32.6 ksi with a margin of 0.31. The maximum stress intensity in the bottom ring (load case HBOT) is 56.3 ksi with a margin of 0.14. The stress contour plots for the 3g test load case and the horizontal transfer load case are shown in Figure 3.9.5-11 and Figure 3.9.5-12, respectively. Since all margins are above zero, the system is shown to be capable of withstanding the prescribed loads.

3.9.5.5 EOS Transfer Cask Neutron Shield Shell Structural Evaluation

The purpose of this section is to summarize the evaluation of the stresses in the neutron shield shell structure of the NUHOMS® EOS-TCs (EOS-TC108, EOS-TC125 and EOS-TC135) due to prescribed loads during fuel loading and transfer operations.

Neutron shield shell is evaluated for all the applied loads during fuel loading and transfer operations as summarized Chapter 2, Table 2-8, except the accident drop loads as the complete loss of neutron shield is assumed in calculating the maximum combined gamma and neutron dose rates. Due to the differences in designs, separate finite element models are setup for the EOS-TC108, EOS-TC125, and EOS-TC135. The evaluation is performed using ANSYS [3.9.5-4].

Material properties, where not explicitly stated, are conservatively taken at 300 °F from the tables in Chapter 8 and the resulting stresses in the neutron shield shell components are compared with the stress criteria listed in Chapter 3, Table 3-5.

3.9.5.5.1 EOS-TC108 Neutron Shield Shell

A 120° segment of the neutron shield shell assembly for EOS-TC108 is modeled. The FEMs are developed using the nominal dimensions per the drawings in Chapter 1, Section 1.3.

Components (neutron shield panel, upper/lower flanges and the I-beams) are modeled using ANSYS SHELL181 3-D shell elements. The elements have 6 degrees of freedom (3 translational and 3 rotational) at each of the four nodes. The interfaces between the mating surfaces are modeled using ANSYS CONTA173 and TARGE170 surface to surface contact elements that allow the transfer of loads. EOS-TC is not modeled explicitly in this model, it is assumed fixed and the interaction between the neutron shield shell inner panel and EOS-TC is simulated using ANSYS CONTA178 node to node contact elements. The interaction between the I-beam faces and the seam plates is simulated using RBE3 constrained equations and ANSYS CONTA175, and TARGE170 node-to-surface contact elements, wherein the RBE3 constrained equation is created between the nodes of the I-beam face to transfer all the forces to the center node onto a single node at the center of the I-beam face. This node is then used to create a node to surface contact between the seam plate surface.

The fillet welds for EOS-TC108 neutron shield assembly are simulated using couplings at the interface of neutron shield inner panel to I-beams and at interface of the neutron shield outer panel to I-beam welds. Welds at other locations are full penetration welds, thus nodes at these weld locations are merged in order to achieve the appropriate behavior.

The FEM for the EOS-TC108 neutron shield assembly is shown in Figure 3.9.5-13.

Horizontal Transfer / Seismic Loads

The horizontal transfer and seismic loads are enveloped by analyzing the neutron shield shell for an internal pressure load of 20 psig and (1g DW + 1g vertical + 1g lateral + 1g axial) accelerations.

Along with this load, the annulus of the neutron shield shell is also subjected to hydrostatic pressure load, which varies linearly with height with maximum at the bottom. Conservatively, a uniform internal pressure equal to the maximum hydrostatic pressure ($p = \rho g d_1 = 0.0361 \times 2.24 \times 90.25 = 7.30$psig) is added. Therefore, the equivalent uniform pressure of 27.5 psig is applied to the model.

This equivalent pressure is applied on the inner walls of the annulus created between the inner neutron shield panel and the outer neutron shield panel. It is also applied on the faces of the I-beams that are exposed to the water.

The neutron shield shell assembly will rest on the EOS-TC. Thus, in order to simulate the effect, ANSYS CONTA178 node-to- node contacts are created between the inner face of the inner panel and the EOS-TC. The EOS-TC surface is not modeled explicitly and the degrees of freedom of free nodes representing the outer surface of the EOS-TC are constrained in all translational directions (UX, UY and UZ).

Nodes at the cut face of 120° segment are constrained in the hoop (UY) direction.

Test Pressure

The EOS-TC108 neutron shield is analyzed in the vertical position and at the room temperature (70 °F) for the test pressure load case.

In addition to hydrostatic pressure due to the water in the neutron shield, an internal pressure of 25 psig (~125% of 20 psig pressure) is also applied for this analysis. The hydrostatic pressure will vary with the height, maximum pressure being at the bottom of the neutron shield shell. This pressure is applied as the triangular varying load. Therefore, the maximum equivalent pressure applied to the model is 31.14 psig.

This equivalent pressure is applied on the inner walls of the annulus between the inner neutron shield panel and the outer neutron shield panel. It is also applied on the faces of the I-beams that are exposed to water.

For pressure test, the neutron shield shell is in the vertical orientation and the nodes at the location of the leg supports are constrained in all directions.

The stresses due to this equivalent pressure in test pressure load are compared with the level B allowable at room temperature.

Vertical Lift

The vertical lift load includes a DLF of 1.15 for pressure load, so the equivalent pressure applied during vertical transfer is 27.06 psig.

This equivalent pressure is applied on the inner walls of the annulus between the inner neutron shield panel and the outer neutron shield panel. It is also applied on the faces of the I-beams that are exposed to the neutron shield.

Thermal Loads

For thermal stress analysis, two temperature distributions from the thermal evaluations documented in Chapter 4 are used. The first load case corresponds to the EOS-TC108 loaded with EOS-37PTH DSC, heat load of 41.8 kW, off-normal hot conditions, outdoor and horizontal position of the TC. The second load case corresponds to the EOS-TC108 loaded with the EOS-89BTH DSC, heat load of 34.44 kW, normal hot conditions, indoor and vertical position of the TC. The temperature distributions are shown in Figure 3.9.5-20.

3.9.5.5.2 EOS-TC125 and EOS-TC135 Neutron Shield Shells

The EOS-TC125 / EOS-TC135 neutron shield shell assembly is analyzed for postulated load conditions using a 3D 180° half-symmetric FEMs. The FEMs are developed using the nominal dimensions per the drawings in Chapter 1, Section 1.3.

All components (EOS-TC shells, neutron shield panel, neutron shield panel support ring plates, and the I-beams) are modeled using ANSYS SOLID185 3-D solid elements. The elements have 3 translational degrees of freedom at each of the eight nodes (no rotational degrees of freedom). The interfaces between the mating surfaces are modeled using ANSYS CONTA173 and TARGE170 surface-to-surface contact elements that allow the transfer of loads.

The welds at the interface of outer shell to I-beams and at the interface of neutron shield plate support ring plates to EOS-TC outer shell are modeled using couplings.

The nodes at slot welds between the I-beam and neutron shield panel are merged in order to achieve appropriate behavior. The weld between neutron shield panel and neutron shield panel support ring are full penetration welds. Thus, nodes at these weld locations are merged in order to achieve the appropriate behavior.

The FEM for the EOS-TC125 neutron shield assembly is shown in Figure 3.9.5-14. It is also representative of the EOS-TC135 neutron shield assembly FEM.

The resulting stresses in the neutron shield shell components are compared with the stress criteria listed in Chapter 3, Table 3-5.

Horizontal Transfer / Seismic Loads

The horizontal transfer and seismic loads are enveloped by analyzing the neutron shield shell for an internal pressure load of 25 psig and (2g vertical + 2g lateral + 2g axial) accelerations.

Along with this load the annulus of the neutron shield shell is also subjected to hydrostatic pressure load which varies linearly with height with maximum at the bottom. Conservatively, a uniform internal pressure equal to the maximum hydrostatic pressure is added. Therefore the equivalent pressure of 40 psig is applied to the model.

This equivalent pressure is applied in the annulus of the neutron shield shell. It is also applied on the faces of the I-Beams which are exposed to the water.

During the horizontal transfer, the EOS-TC is supported by the trunnions and saddle. Therefore, in order to simulate the effect, degree of freedom of nodes at the trunnion locations on the outer surface of the EOS-TC are constrained in axial (upper trunnions) direction and in radial (lower trunnion pockets) direction.

Symmetric boundary conditions are applied at the cut face of the model.

Test Pressure and Vertical Lift

The neutron shield is analyzed in the vertical position and at the room temperature (70 °F) for the test pressure load case.

In addition to hydrostatic pressure due to the water in the neutron shield, an internal pressure of 32 psig (~125% of 25 psig pressure) is also applied for this analysis. The hydrostatic pressure will vary with the height, maximum pressure being at the bottom of the neutron shield shell. The maximum equivalent pressure at the bottom of the cask is calculated to be 38.78 psig. The test pressure load case is enveloped by the horizontal transfer / seismic load case and therefore is not evaluated separately.

Similarly, the maximum pressure during the vertical lift is calculated to be 32.79 psig, which is also enveloped by the horizontal transfer / seismic load case and not evaluated separately.

Thermal Loads

For thermal stress analysis, two temperature distributions from the thermal evaluations documented in Chapter 4 are used. The first load case corresponds to the EOS-TC125 loaded with EOS-37PTH DSC, heat load of 50 kW, off-normal hot conditions, outdoor and horizontal position of the TC. The second load case corresponds to the EOS-TC125 loaded with the EOS-37PTH DSC, heat load of 36.35 kW, normal hot conditions, indoor and vertical position of the TC. The temperature distributions are shown in Figure 3.9.5-19.

3.9.5.5.3 Results

The stress results for the neutron shield shells are summarized in Table 3.9.5-6 and Table 3.9.5-7. The stress contour plots of the EOS-TC108 neutron shield shell for the horizontal transfer/seismic load case are shown in Figure 3.9.5-15 and Figure 3.9.5-16. Also the stress contour plots of the EOS-TC135 neutron shield shell for the horizontal transfer / seismic load case are shown in Figure 3.9.5-17 and Figure 3.9.5-18.

3.9.5.6 EOS Transfer Cask, Trunnion, and Neutron Shield Shell Fatigue Requirements

The transfer cask (TC) and trunnion are designed in accordance with the applicable guidelines of the ASME Code, Section III, Division 1, and Subsection NF for Class 1 vessels, except for the neutron shield tank, which is designed to ASME Code, Section III, Division 1, and Subsection ND. Neither one of these subsections require a fatigue evaluation for low cycle loads. Therefore, the fatigue evaluation is not required for the EOS-TC per ASME code criteria.

3.9.5.7 References

3.9.5-1 Blodgett, O.W., "Design of Welded Structure," published by James F. Lincoln Arc Welding Foundation, June 1966.

3.9.5-2 ANSI N14.6, "Special Lifting Devices for Shipping Containers Weighing 10,000 Pounds or more," 1993.

3.9.5-3 American Society of Mechanical Engineers, "ASME Boiler and Pressure Vessel Code, 2010 Edition with 2011 Addenda.

3.9.5-4 ANSYS Computer Code and User's Manual, Version 14.0.

Table 3.9.5-1
EOS-TCMAX Stress Result Summary Table – 65g Side Drop

STRESS CLASSIFICATION- SERVICE LEVEL D – SUMMARY TABLE				
EOS-TC Components	**Stress Category**	**Maximum Stress (ksi)**	**Allowable Stress (ksi)**	**Max. Stress Ratio**
Outer Shell	P_M	44.14	49.0	0.90
	P_L+P_B	54.72	63.0	0.87
Inner Shell	P_M	45.43	49.0	0.93
	P_L+P_B	50.41	63.0	0.80
Top Cover Plate	P_M	41.58	49.0	0.85
	P_L+P_B	55.78	63.0	0.89
Top Ring	P_M	43.45	49.0	0.89
	P_L+P_B	59.93	63.0	0.95
Bottom Ring	P_M	42.24	49.0	0.86
	P_L+P_B	53.70	63.0	0.85
Bottom End Plate	P_M	47.04	49.0	0.96
	P_L+P_B	50.49	63.0	0.80
RAM Access	P_M	39.41	49.0	0.80
	P_L+P_B	49.40	63.0	0.78
Bottom Neutron	P_M	46.21	49.0	0.94
	P_L+P_B	46.67	63.0	0.74

Table 3.9.5-2
EOS-TCMAX Stress Result Summary Table – 65g Top End Drop

#	Component	Max Stress (ksi) /Stress Ratio			Allowable (ksi)		
		PM	PL	PM+PB	PM	PL	PM+PB
1	Outer Shell	24.4 49.7%	36.3 57.6%	36.3 57.6%	49.0	63.0	63.0
2	Inner Shell	25.7 52.4%	37.9 60.1%	37.9 60.1%	49.0	63.0	63.0
3	Top Cover Plate	12.4 25.2%	18.8 29.8%	18.8 29.8%	49.0	63.0	63.0
4	Top Ring	13.0 26.6%	17.8 28.3%	17.8 28.3%	49.0	63.0	63.0
5	Bottom Ring	3.4 7.0%	6.2 9.9%	6.2 9.9%	49.0	63.0	63.0
6	Bottom End Plate	6.1 12.4%	11.8 18.8%	11.8 18.8%	49.0	63.0	63.0
7	RAM Access Penetration Ring	4.8 9.8%	6.4 10.2%	6.4 10.2%	49.0	63.0	63.0
8	Bottom Neutron Shield Pane	3.8 7.8%	7.0 11.1%	7.0 11.1%	49.0	63.0	63.0

Table 3.9.5-3
EOS-TCMAX Stress Result Summary Table – 65g Bottom End Drop

#	Component	Max Stress (ksi) / Stress Ratio			Allowable (ksi)		
		PM	PL	PM+PB	PM	PL	PM+PB
1	Outer Shell	25.1 51.3%	39.3 62.4%	39.3 62.4%	49.0	63.0	63.0
2	Inner Shell	18.1 37.0%	26.7 42.3%	26.7 42.3%	49.0	63.0	63.0
3	Top Cover Plate	4.1 8.5%	10.8 17.2%	10.8 17.2%	49.0	63.0	63.0
4	Top Ring	1.5 3.1%	2.6 4.1%	2.6 4.1%	49.0	63.0	63.0
5	Bottom Ring	22.5 45.8%	32.5 51.6%	32.5 51.6%	49.0	63.0	63.0
6	Bottom End Plate	16.4 33.5%	32.8 52.1%	32.8 52.1%	49.0	63.0	63.0
7	RAM Access Penetration Ring	25.4 51.8%	29.8 47.3%	29.8 47.3%	49.0	63.0	63.0
8	Bottom Neutron Shield Panel	10.2 20.8%	29.9 47.5%	29.9 47.5%	49.0	63.0	63.0

Table 3.9.5-4
Stress Result Summary Table for the Trunnions
(2 Pages)

Description	Calculated Stress (ksi)	Allowable Stress (ksi)	Margin
Manual Calculation for Upper Trunnions			
Stress intensity at A-A at 6g	55.86	82.80	0.48
Stress intensity at A-A at 10g	93.10	113.70	0.22
Manual Calculation for Weld Stresses and Lower Trunnion Pocket			
Trunnion Base Metal Max Equiv. Stress	5.52	11.40[(1)]	1.07
Weld Metal Max Equiv. Stress	6.68	7.50[(2)]	0.12
Top Ring Base Metal Max Equiv. Stress	4.14	5.33[(1)]	0.29
Load Case :3g (Test Load - Service level B)			
Top Ring Shell Stress (P_m)	16.58	28.46	0.72
Top Ring Shell Stress ($P_m + P_b$)	32.55	42.69	0.31
Bottom Ring Shell Stress (P_m)	10.44	28.46	1.73
Bottom Ring Shell Stress ($P_m + P_b$)	13.37	42.69	2.19
Load Case :DW Upper Trunnion (Service Level A) Vertical TC			
Top Ring Shell Stress (P_m)	6.75	21.40	2.17
Top Ring Shell Stress ($P_m + P_b$)	12.40	32.40	1.61
Top Ring Shell Stress ($P_m + P_b$) + Q	40.13	64.20	0.60
Bottom Ring Shell Stress (P_m)	3.76	21.40	4.69
Bottom Ring Shell Stress ($P_m + P_b$)	4.82	32.40	5.73
Bottom Ring Shell Stress ($P_m + P_b$) + Q	32.54	64.20	0.97
Load Case : DW Lower Trunnion (Service Level A) Vertical TC			
Top Ring Shell Stress (P_m)	1.36	21.40	14.72
Top Ring Shell Stress ($P_m + P_b$)	1.43	32.40	21.59
Top Ring Shell Stress ($P_m + P_b$) + Q	29.16	64.20	1.20
Bottom Ring Shell Stress (P_m)	11.52	21.40	0.86
Bottom Ring Shell Stress ($P_m + P_b$)	23.22	32.40	0.40
Bottom Ring Shell Stress ($P_m + P_b$) + Q	50.94	64.20	0.26
Load Case : Horizontal Transfer on Skid (1g axial) (Service Level B) Horizontal TC			
Top Ring Shell Stress (P_m)	7.39	28.46	2.85
Top Ring Shell Stress ($P_m + P_b$)	13.68	42.69	2.12
Top Ring Shell Stress ($P_m + P_b$) + Q	41.40	64.20	0.55
Bottom Ring Shell Stress (P_m)	17.47	28.46	0.63
Bottom Ring Shell Stress ($P_m + P_b$)	28.56	42.69	0.50

Table 3.9.5-4
Stress Result Summary Table for the Trunnions
(2 Pages)

Description	Calculated Stress (ksi)	Allowable Stress (ksi)	Margin
Bottom Ring Shell Stress $(P_m + P_b) + Q$	56.28	64.20	0.14
Load Case : Horizontal Transfer on Skid (-1g axial) (Service Level B) Horizontal TC			
Top Ring Shell Stress (P_m)	5.25	28.46	4.42
Top Ring Shell Stress $(P_m + P_b)$	8.66	42.69	3.93
Top Ring Shell Stress $(P_m + P_b) + Q$	36.39	64.20	0.76
Bottom Ring Shell Stress (P_m)	16.12	28.46	0.77
Bottom Ring Shell Stress $(P_m + P_b)$	20.43	42.69	1.09
Bottom Ring Shell Stress $(P_m + P_b) + Q$	48.15	64.20	0.33

Notes:

(1) Lower of $S_y/6$ or $S_u/10$

(2) Equal to $S_u/10$

Table 3.9.5-5
Acceptance Criteria for the Stress Evaluation

Item	Stress Type	Service Levels A	Service Level B
Top Ring and Bottom Ring	Primary Membrane (P_m)	S_m	Same as Level A, increased by a factor of 1.33
	Primary Membrane + Bending ($P_m + P_b$)	1.5 S_m	
	Primary Membrane + Bending + Thermal Stress (Q)	3.0 S_m	
Upper Trunnions	Stress Intensity at 6g loads	S_y	
	Stress Intensity at 10g loads	S_u	
	Primary Membrane (P_m)	S_m	Same as Level A, increased by a factor of 1.33
	Primary Membrane + Bending ($P_m + P_b$)	1.5 S_m	
	Primary Membrane + Bending + Thermal Stress (Q)	3.0 S_m	
Welds	Maximum Equivalent Stress for Critical Lift (1g)	$S_u/10$ (Weld Metal and Base Metal)	
		$S_y/6$ (Base Metal)	
	Combined Weld Stress	$\min(0.3xS_u, 0.4xS_y)$	Same as Level A, increased by a factor of 1.33
Bottom Ring	Bearing Stress	S_y	

Table 3.9.5-6
Stress Result Summary for the Neutron Shield Panel model

TC	Load Case(1)	Component	Pm (ksi)	Allowable (ksi)	Ratio	P_m+P_b (ksi)	Allowable (ksi)	Ratio	P_m+P_b+Q (ksi)	Allowable (ksi)	Ratio
125	E2	Neutron Shield Panel	10.92	20.00	0.55	25.57	30.00	0.85	37.69	48.00	0.79
125	E2	I-Beam	4.69	16.60	0.28	6.55	24.90	0.26	16.20	39.84	0.41
135	E2	Neutron Shield Panel	10.92	20.00	0.55	26.18	30.00	0.87	38.30	48.00	0.80
135	E2	I-Beam	5.06	16.60	0.30	6.96	24.90	0.28	16.60	39.84	0.42
108	A1	Neutron Shield Panel	5.18	5.50	0.94	6.77	8.25	0.82	11.40	13.20	0.86
108	A1	I-Beam	1.45	5.50	0.26	7.64	8.25	0.93	12.21	13.20	0.92
108	E1	Neutron Shield Panel	5.23	5.50	0.95	7.07	8.25	0.86	11.70	13.20	0.89
108	E1	I-Beam	1.56	5.50	0.28	8.18	8.25	0.99	12.75	13.20	0.97
108	B1	Neutron Shield Panel	5.86	6.60	0.89	7.80	9.90	0.79	12.43	14.40	0.86
108	B1	I-Beam	1.68	6.60	0.25	8.77	9.90	0.89	13.34	14.40	0.93

Note

(1) The load cases are numbered per Chapter 2, Table 2-8, except E1 and E2 are the enveloping horizontal transfer/seismic load cases as described in the main body of the appendix

Table 3.9.5-7
Weld Stress Result Summary for the Neutron Shield Panel model

TC	Load Case(1)	Weld #	Stress (ksi)	Allowable	Ratio	S (ksi)
125	E2	Transfer Cask Outer Shell to I-Beam Fillet Weld	9.0	13.4	66.9%	20.0
125	E2	Neutron Shield Panel and I-Beam Slot Weld	4.9	13.4	36.7%	20.0
125	E2	Neutron Shield Panel Support and TC Outer Shell	7.9	13.4	58.8%	20.0
135	E2	Transfer Cask Outer Shell to I-Beam Fillet Weld	9.6	13.4	71.5%	20.0
135	E2	Neutron Shield Panel and I-Beam Slot Weld	4.9	13.4	36.7%	20.0
135	E2	Neutron Shield Panel Support and TC Outer Shell	9.3	13.4	68.9%	20.0
108	A1	Neutron Shield Panel Inner and I-Beam	0.8	3.0	26.6%	5.5
108	A1	Neutron Shield Panel Outer and I-Beam	1.3	3.0	44.2%	5.5
108	E1	Neutron Shield Panel Inner and I-Beam	0.9	3.0	29.9%	5.5
108	E1	Neutron Shield Panel Outer and I-Beam	1.4	3.0	47.3%	5.5
108	B1	Neutron Shield Panel Inner and I-Beam	0.9	3.7	25.5%	6.0
108	B1	Neutron Shield Panel Outer and I-Beam	1.5	3.7	41.9%	6.0

Note

(1) The load cases are numbered per Chapter 2, Table 2-8, except E1 and E2 are the enveloping horizontal transfer/seismic load cases as described in the main body of the appendix

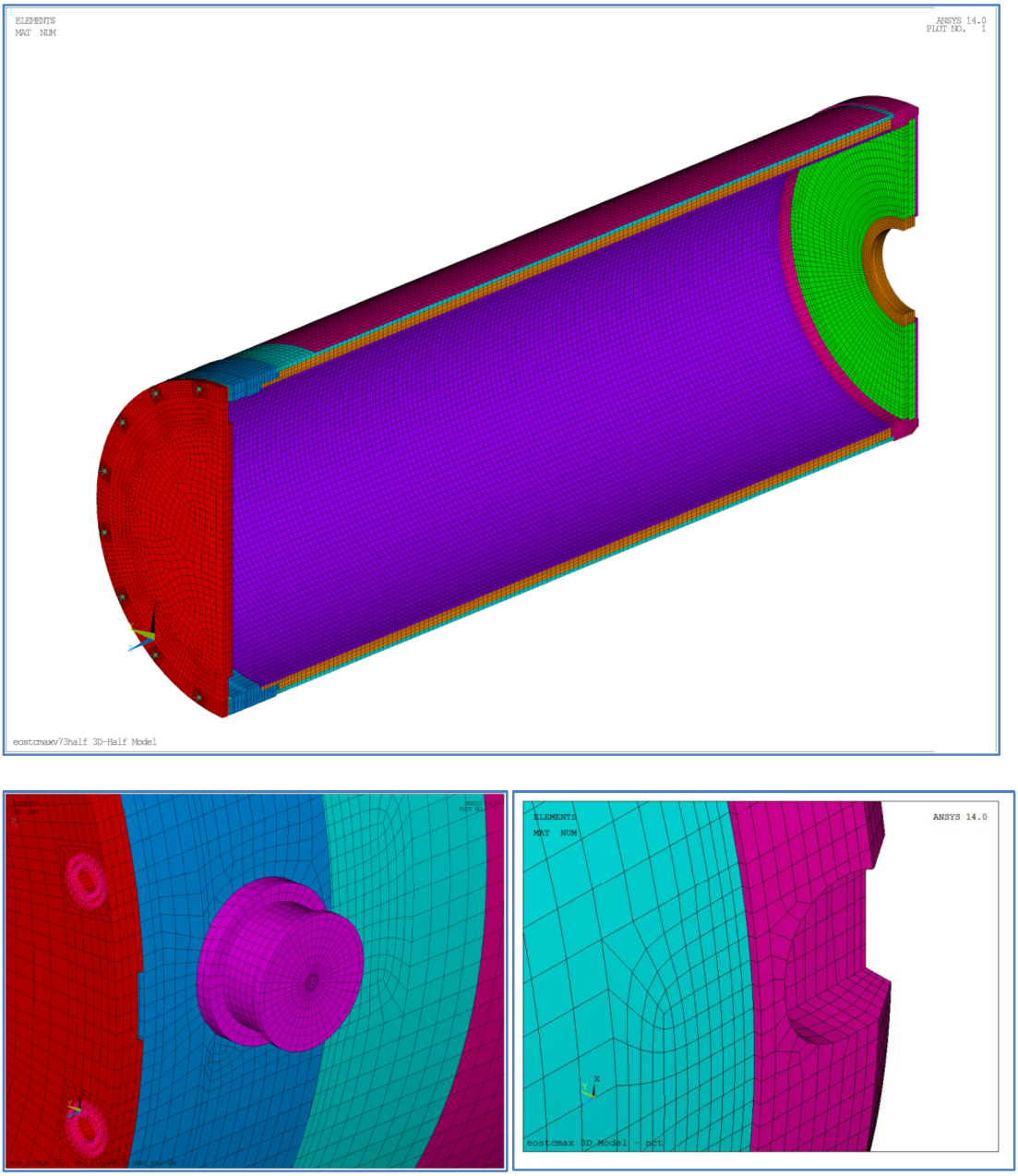

Figure 3.9.5-1
3D Half Symmetric Finite Element Model for Drop Loads

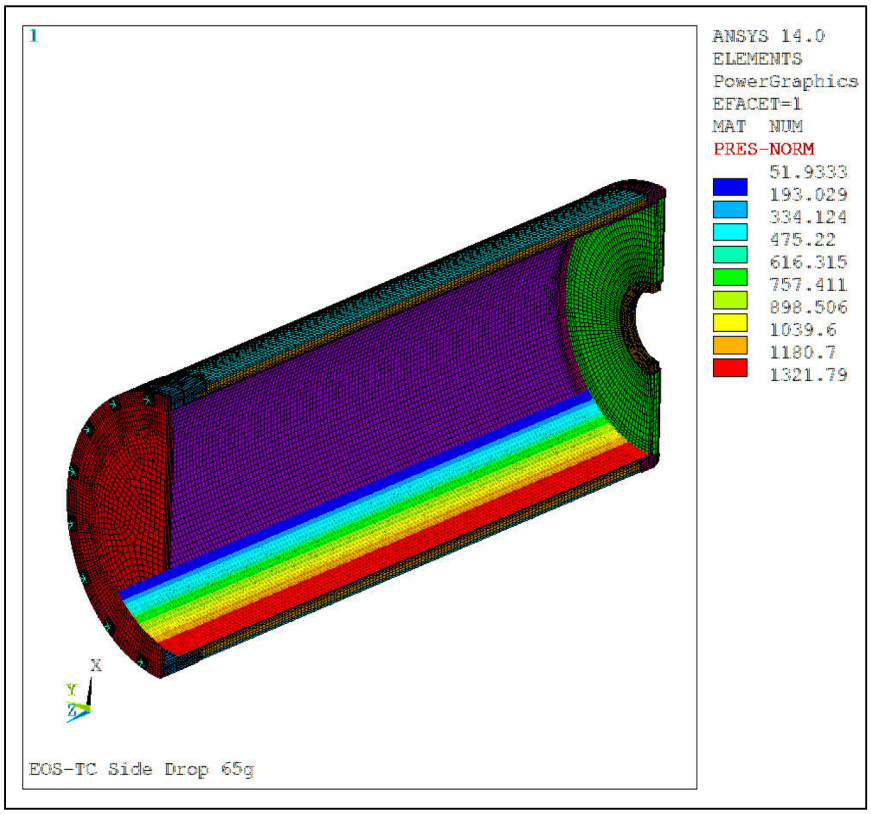

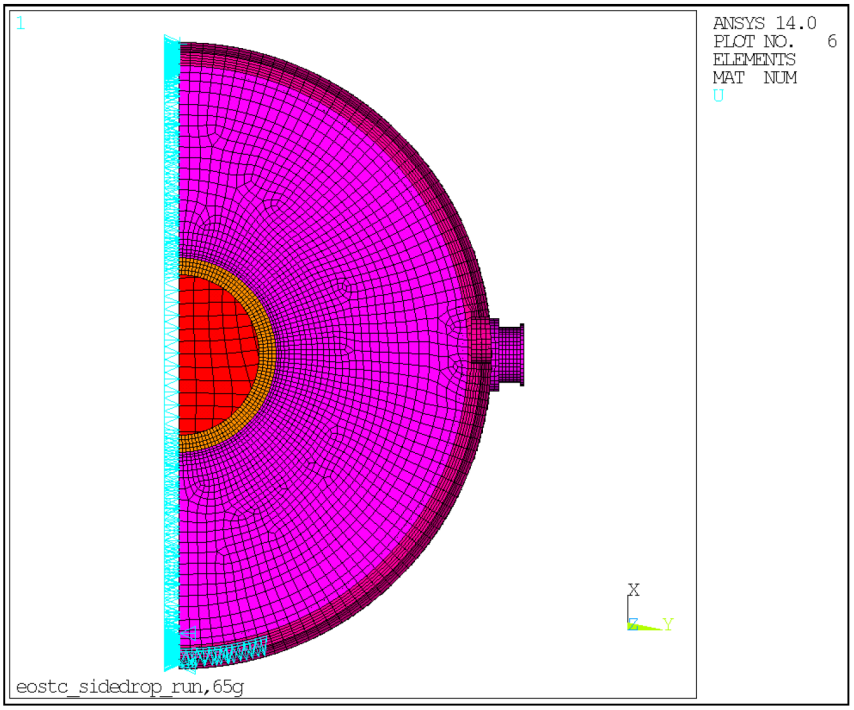

Figure 3.9.5-2
Pressure Load and Boundary Condition Plots – 65g Side Drop

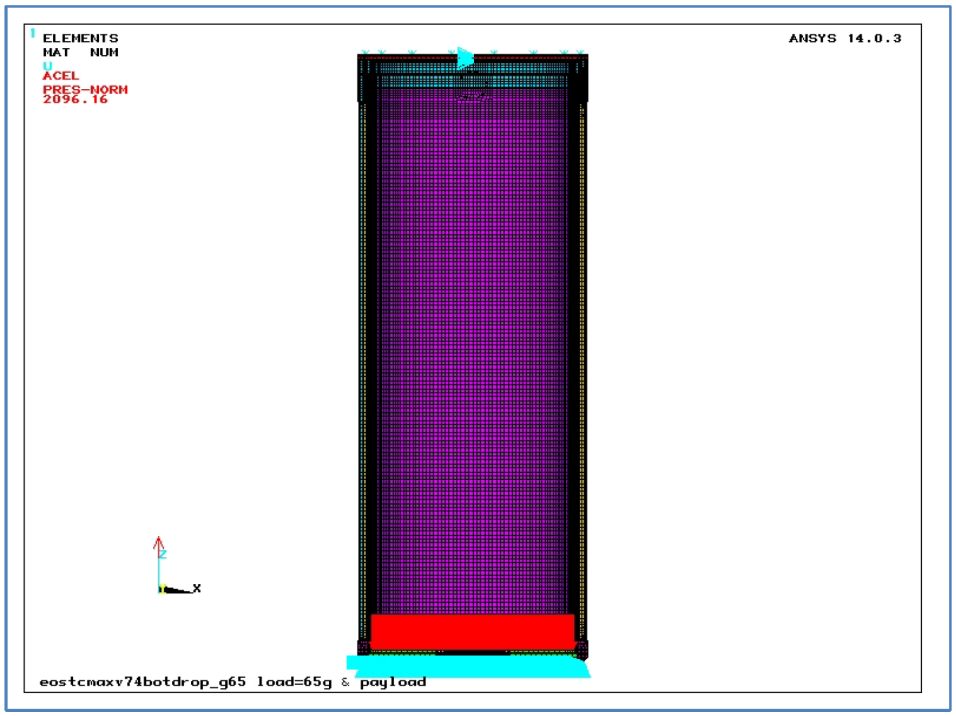

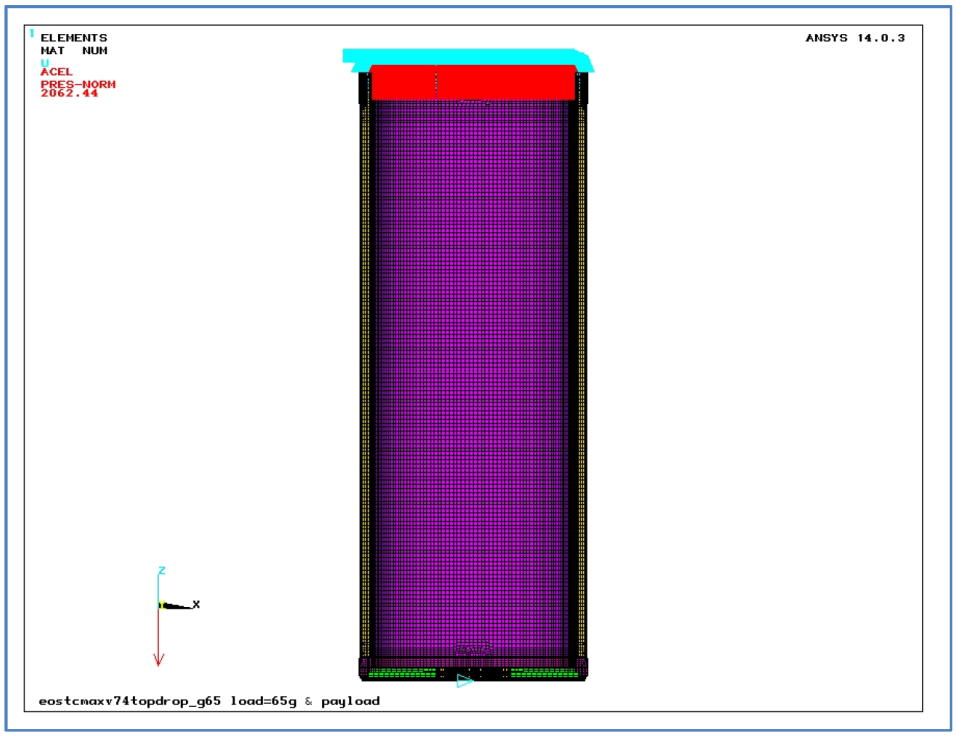

Figure 3.9.5-3
Pressure Load and Boundary Condition Plots – 65g End Drop

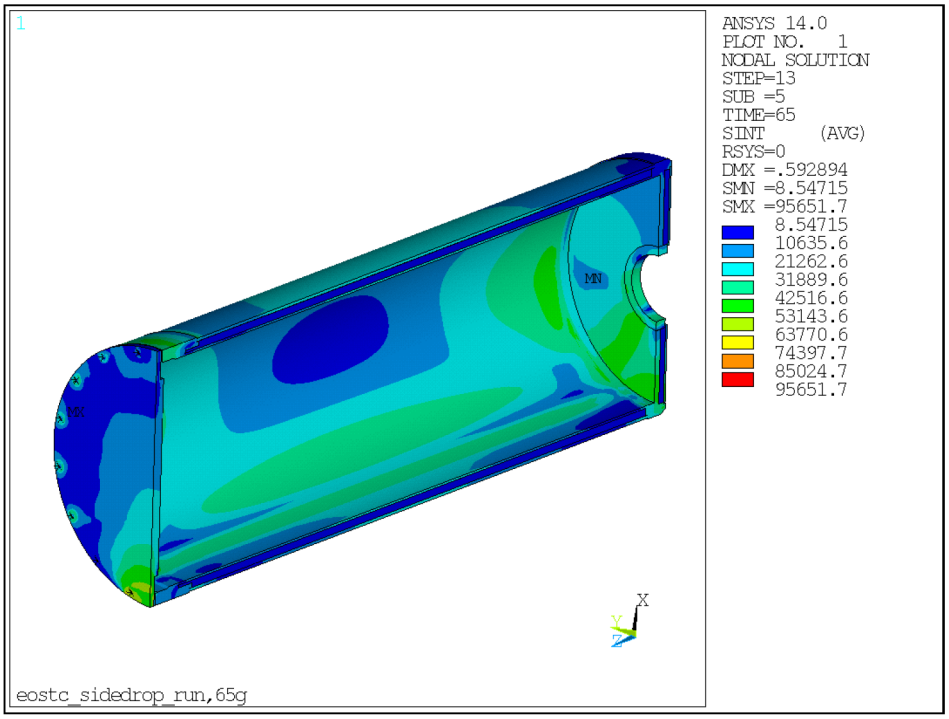

Figure 3.9.5-4
Stress Intensity (psi) plot for EOS-TCMAX – 65g Side Drop

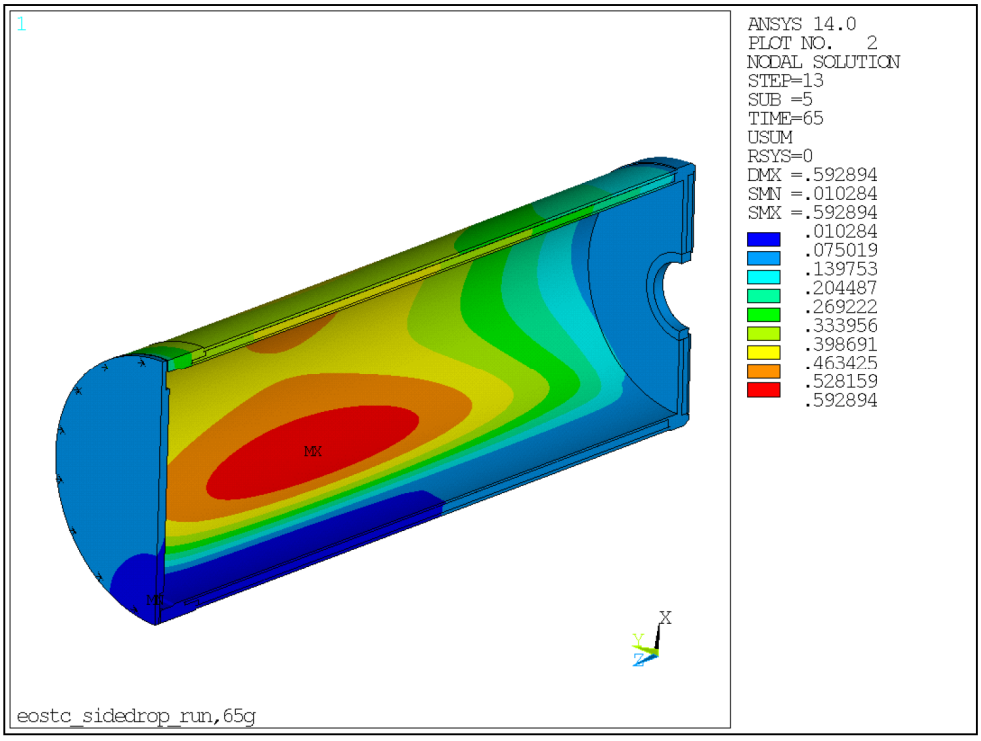

Figure 3.9.5-5
Deformation plot (in.) for EOS-TCMAX (scaled up) – 65g Side Drop

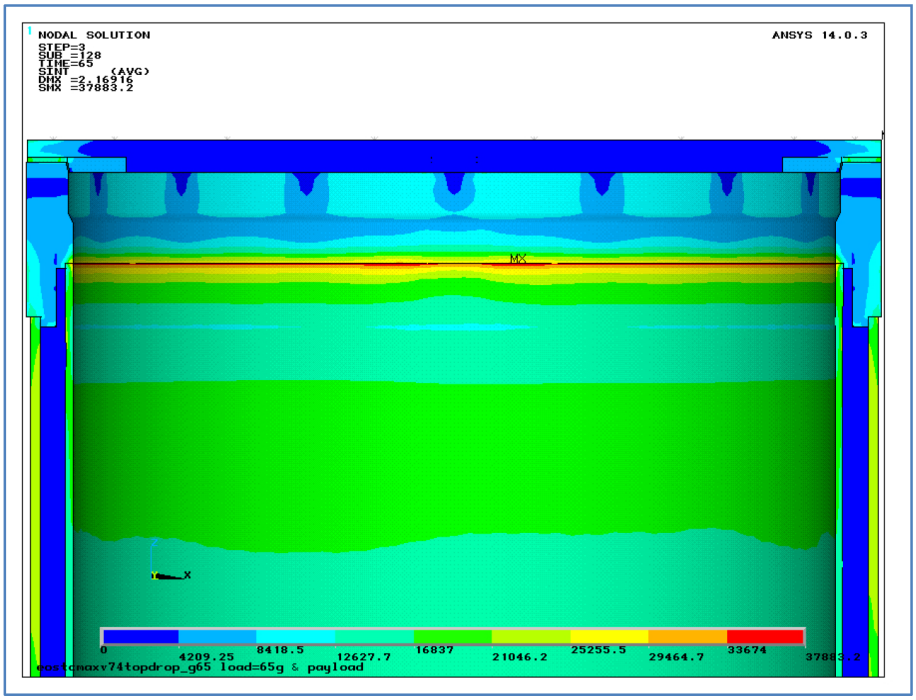

Figure 3.9.5-6
Stress Intensity (psi) plot for EOS-TCMAX – 65g Top End Drop

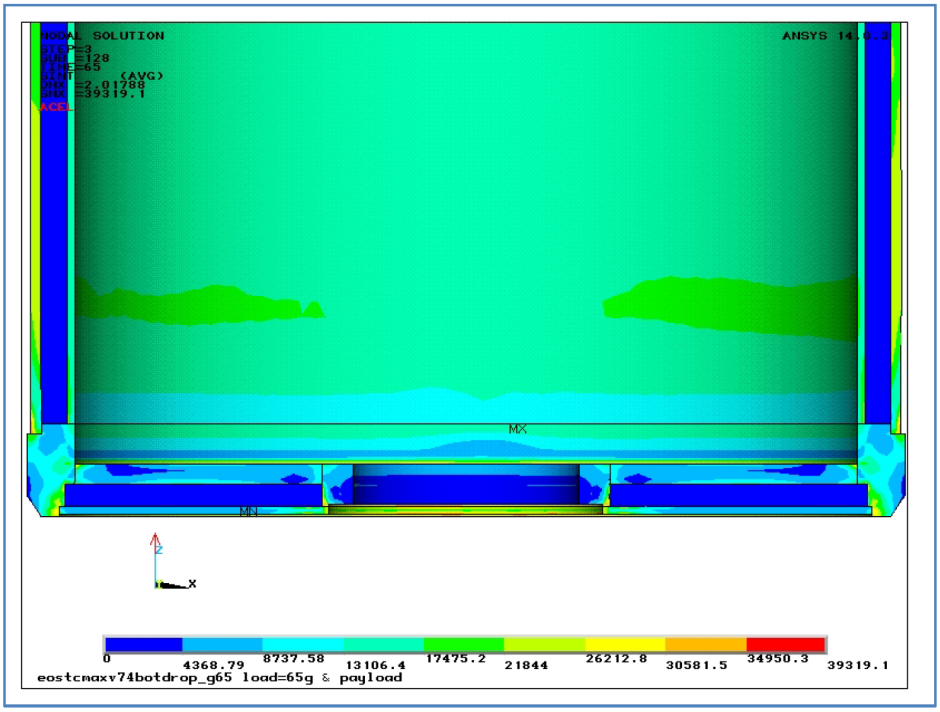

Figure 3.9.5-7
Stress Intensity (psi) plot for EOS-TCMAX – 65g Top End Drop

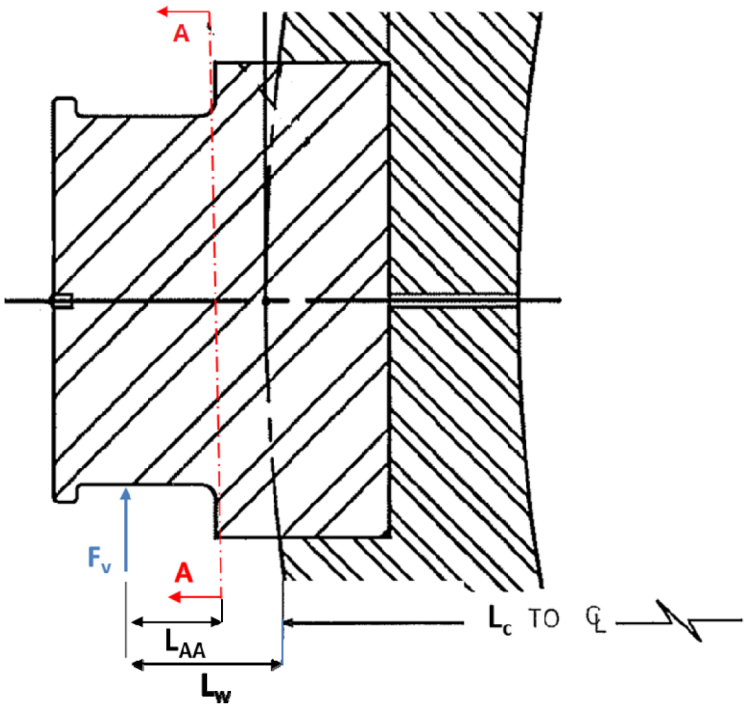

Figure 3.9.5-8
Upper Trunnion Sectional View

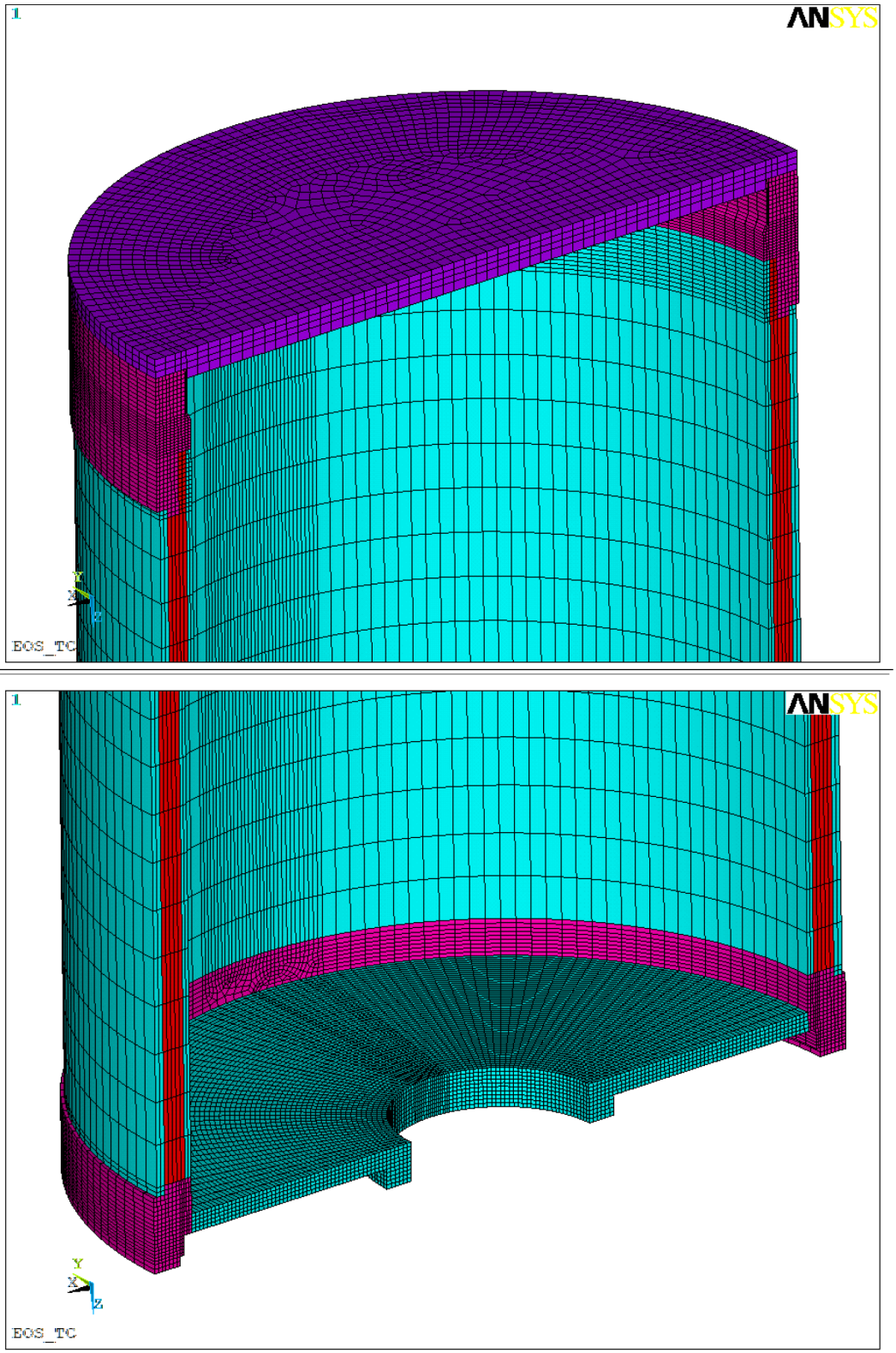

Figure 3.9.5-9
Cut Section Finite Element Model of EOS-TCMAX (Top and Bottom)

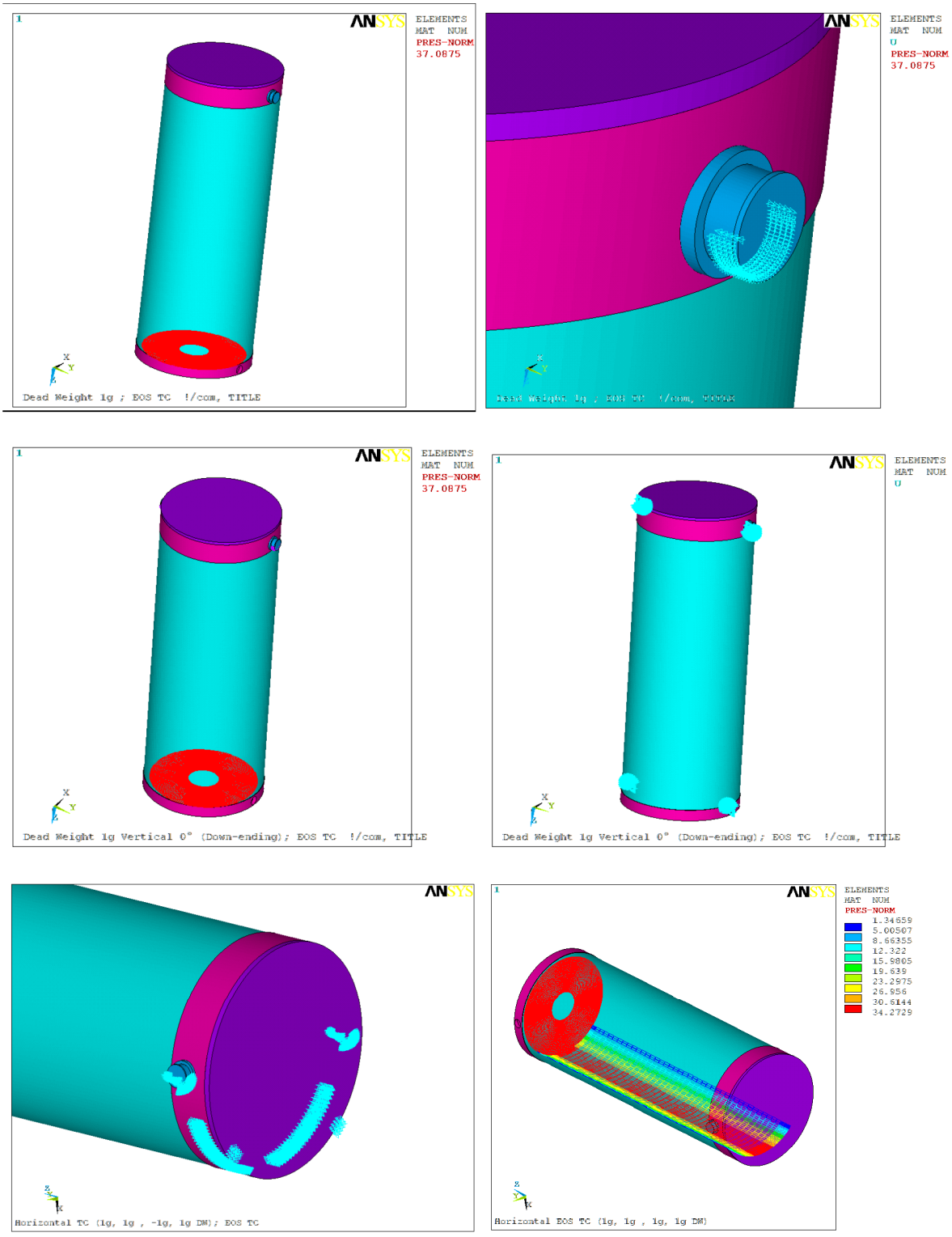

Figure 3.9.5-10
Pressure Load and Boundary Condition Plots

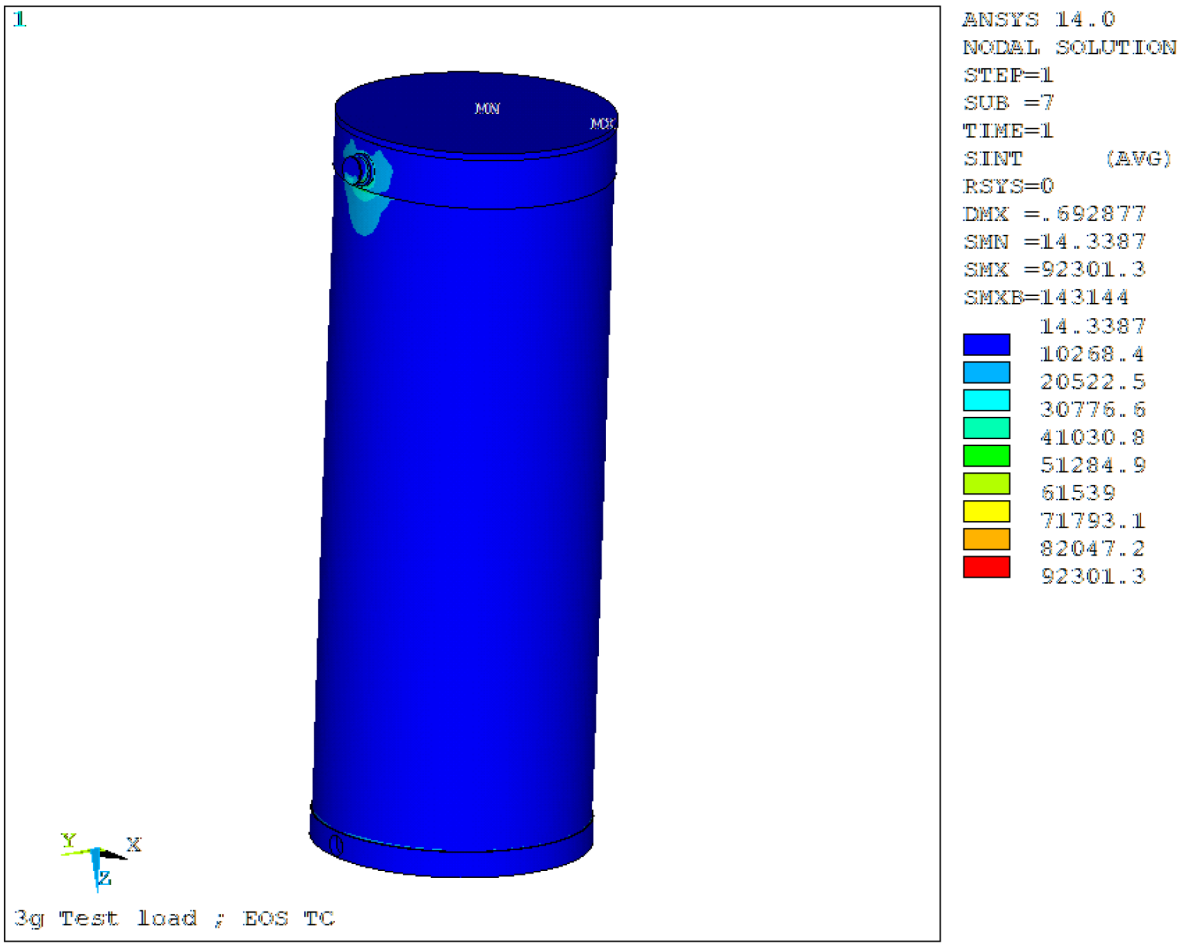

Figure 3.9.5-11
Stress Intensity (psi) Plot for Load Case 3g

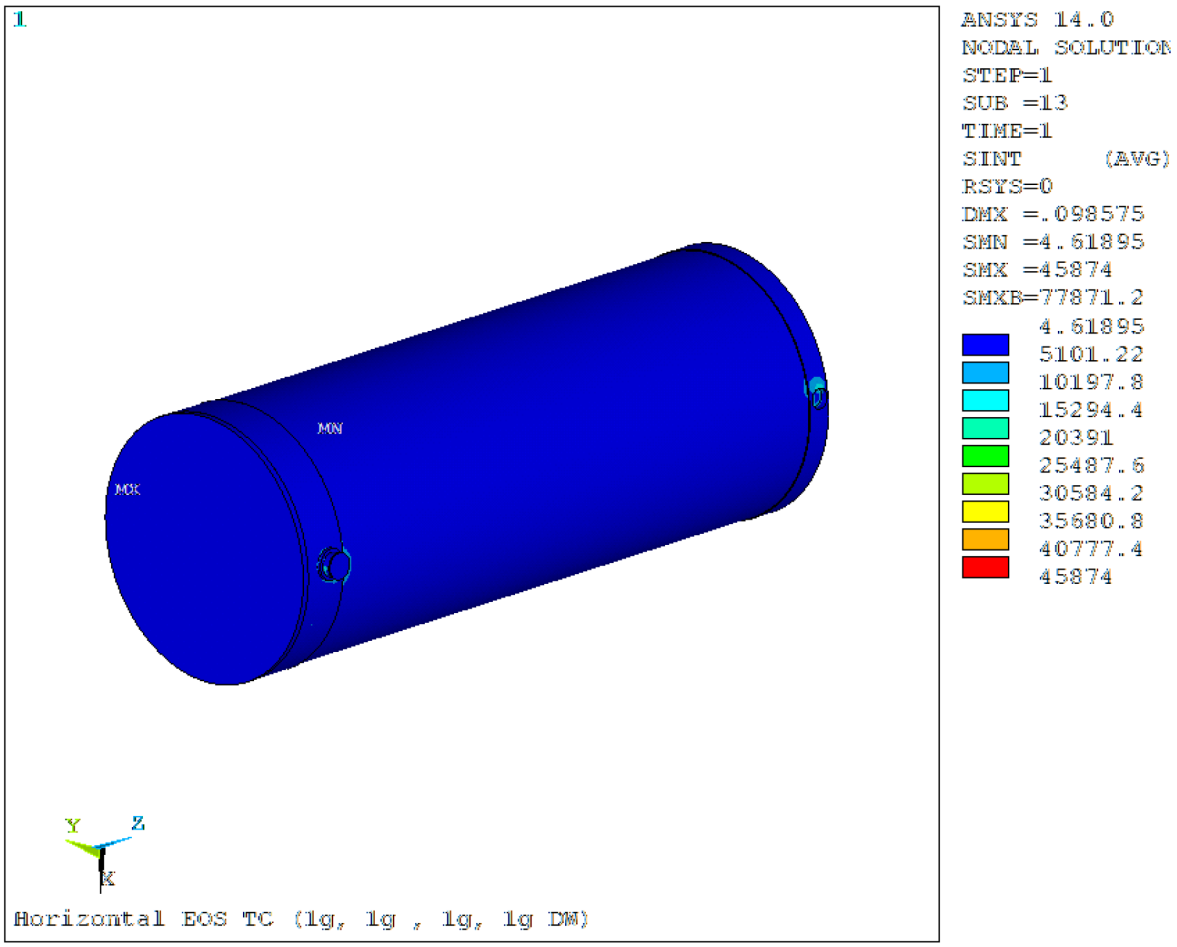

Figure 3.9.5-12
Stress Intensity (psi) Plot for Load Case Horizontal Transfer on Skid

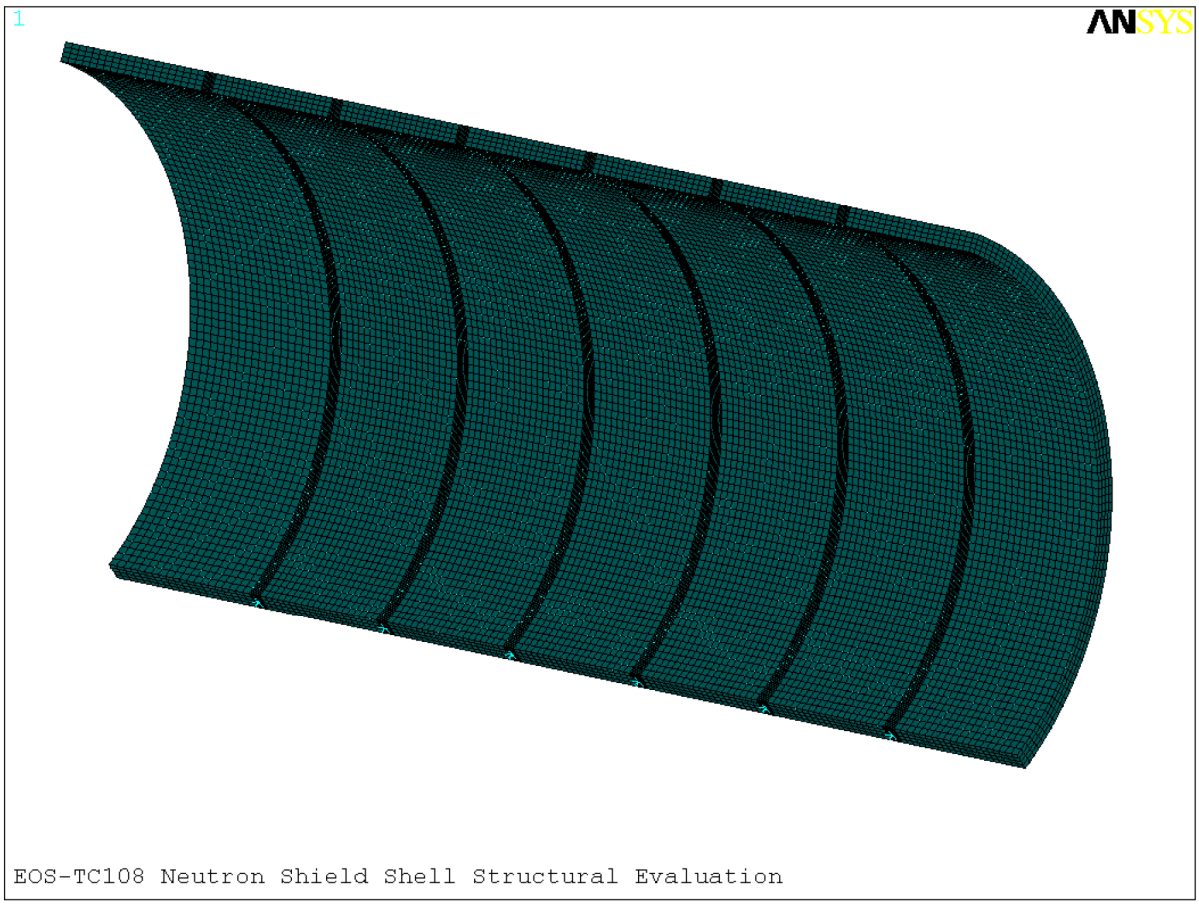

Figure 3.9.5-13
EOS-TC108 Meshed Model

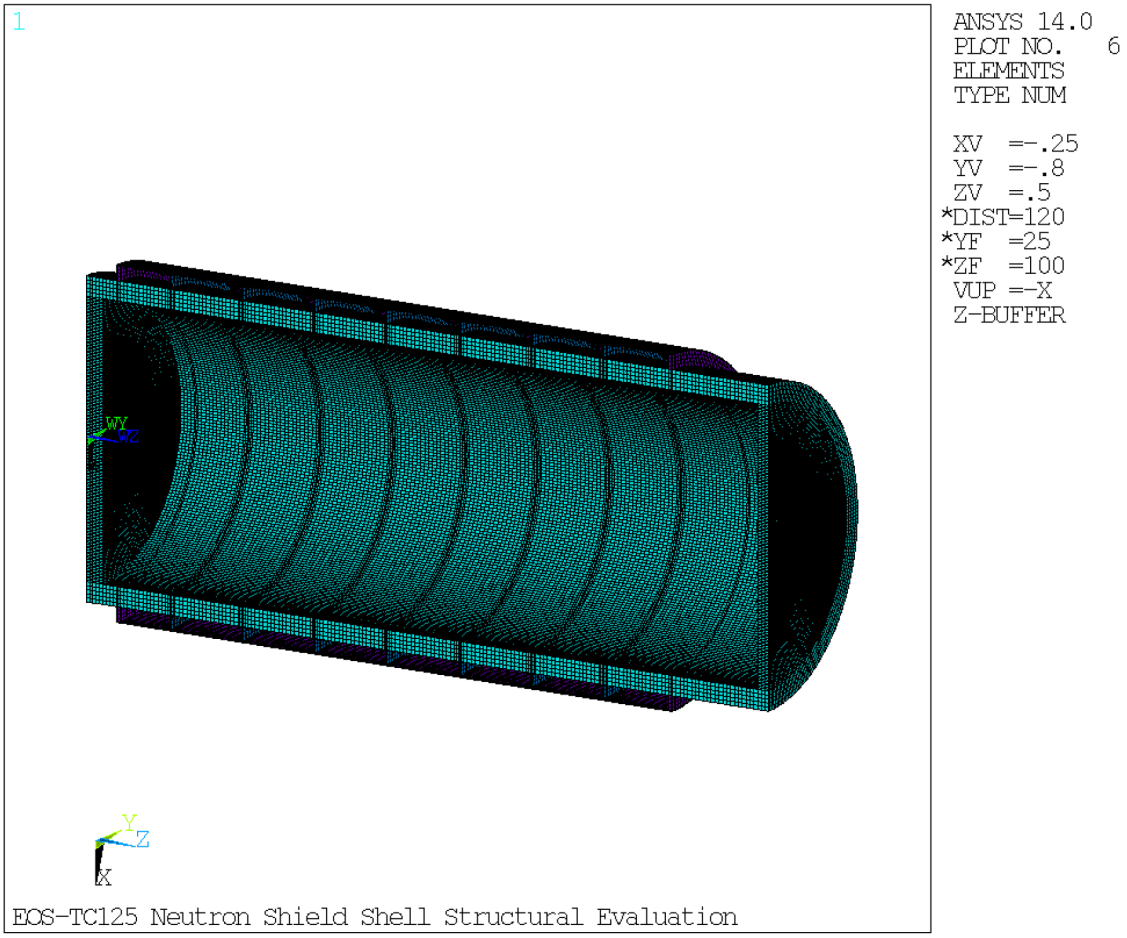

Figure 3.9.5-14
EOS-TC125 Meshed Model

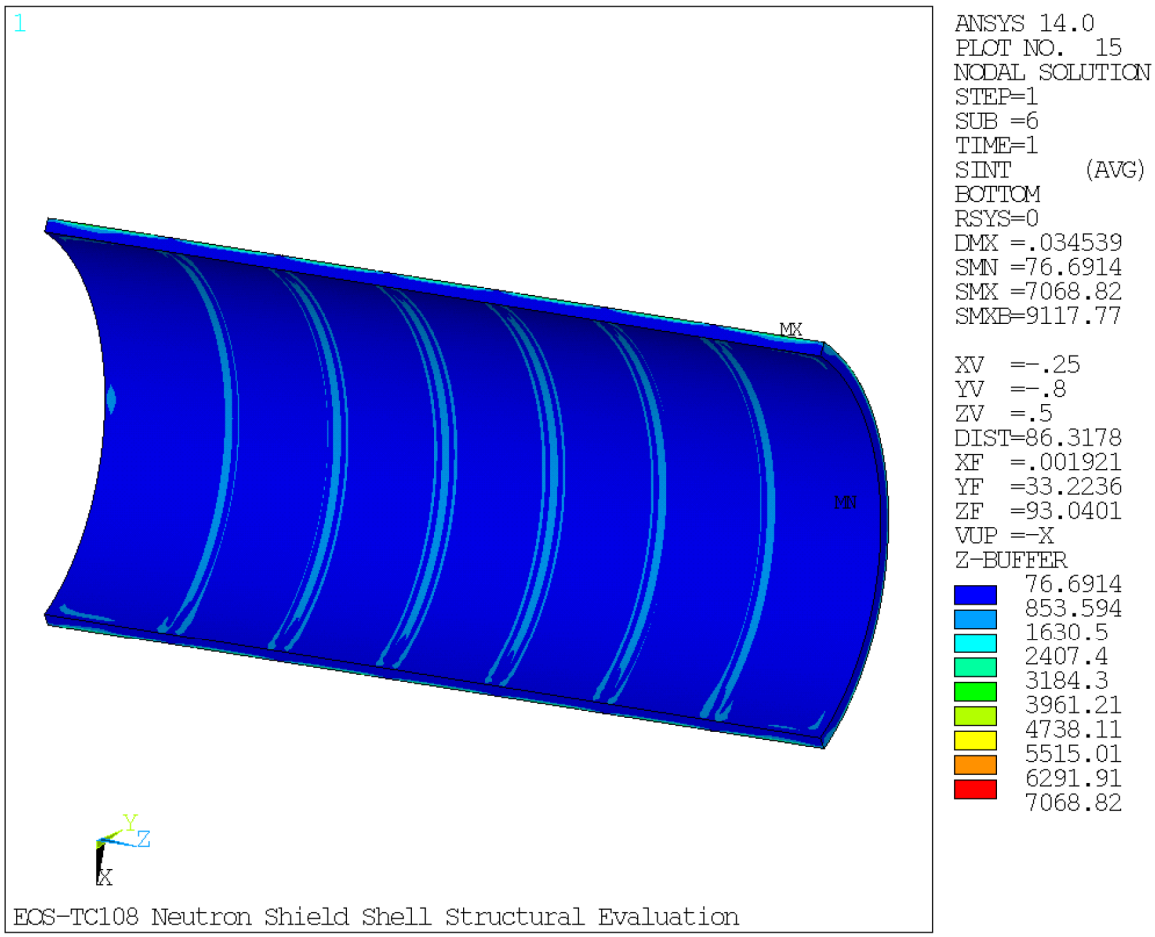

Figure 3.9.5-15
EOS-TC108 Neutron Shield Panel Stress Intensity (P_m+P_b) Plot Load Case E1

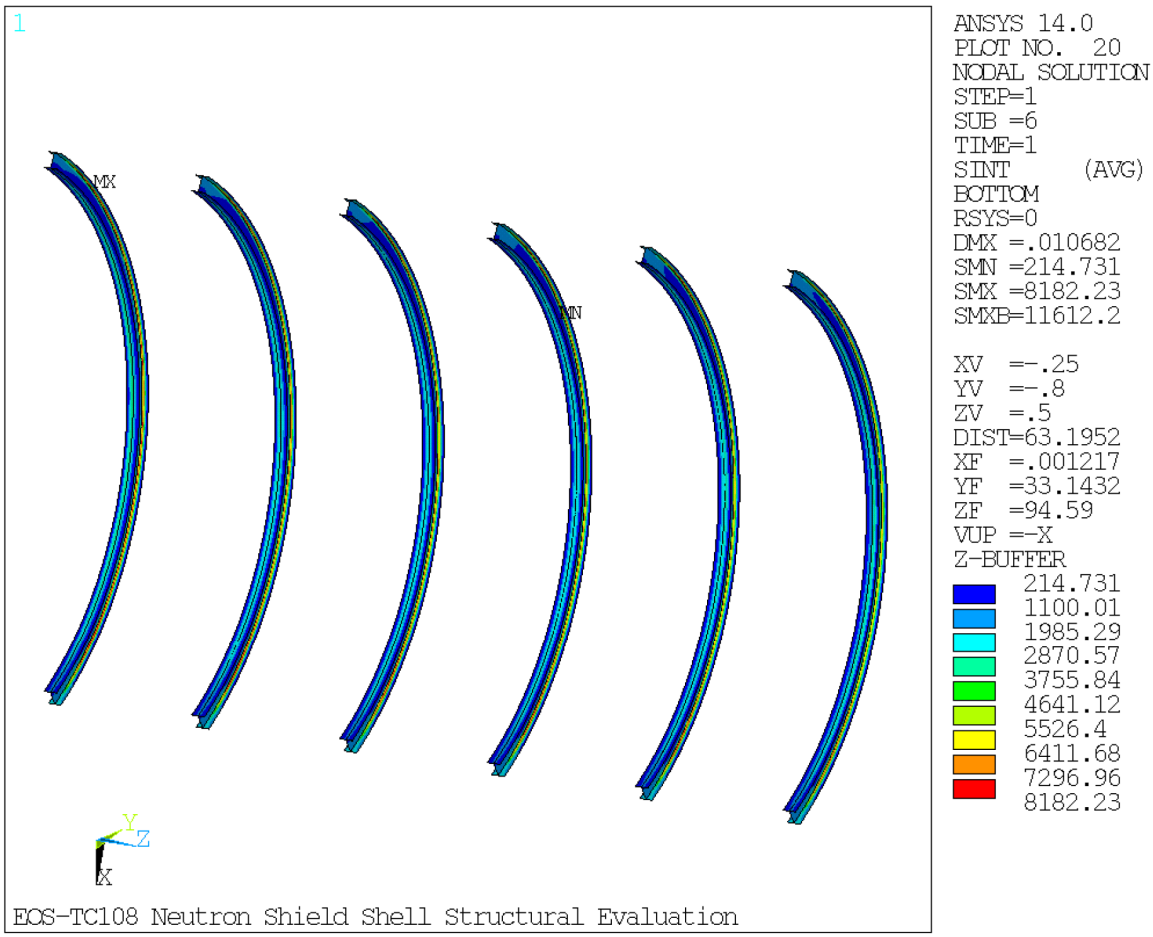

Figure 3.9.5-16
EOS-TC108 I-Beam Stress Intensity (P_m+P_b) Plot Load Case E1

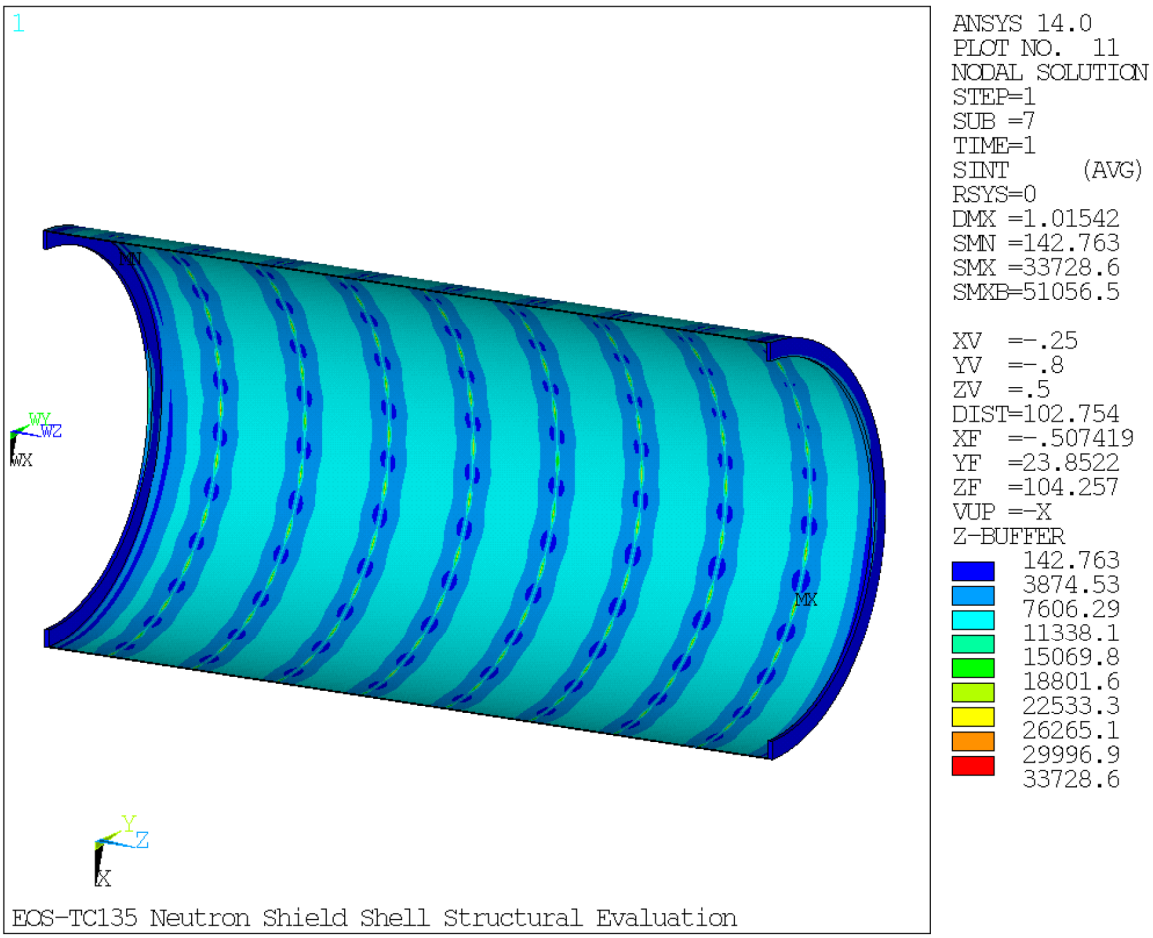

Figure 3.9.5-17
EOS-TC135 Neutron Shield Shell Stress Intensity Plot under Pressure Load (40 psig)

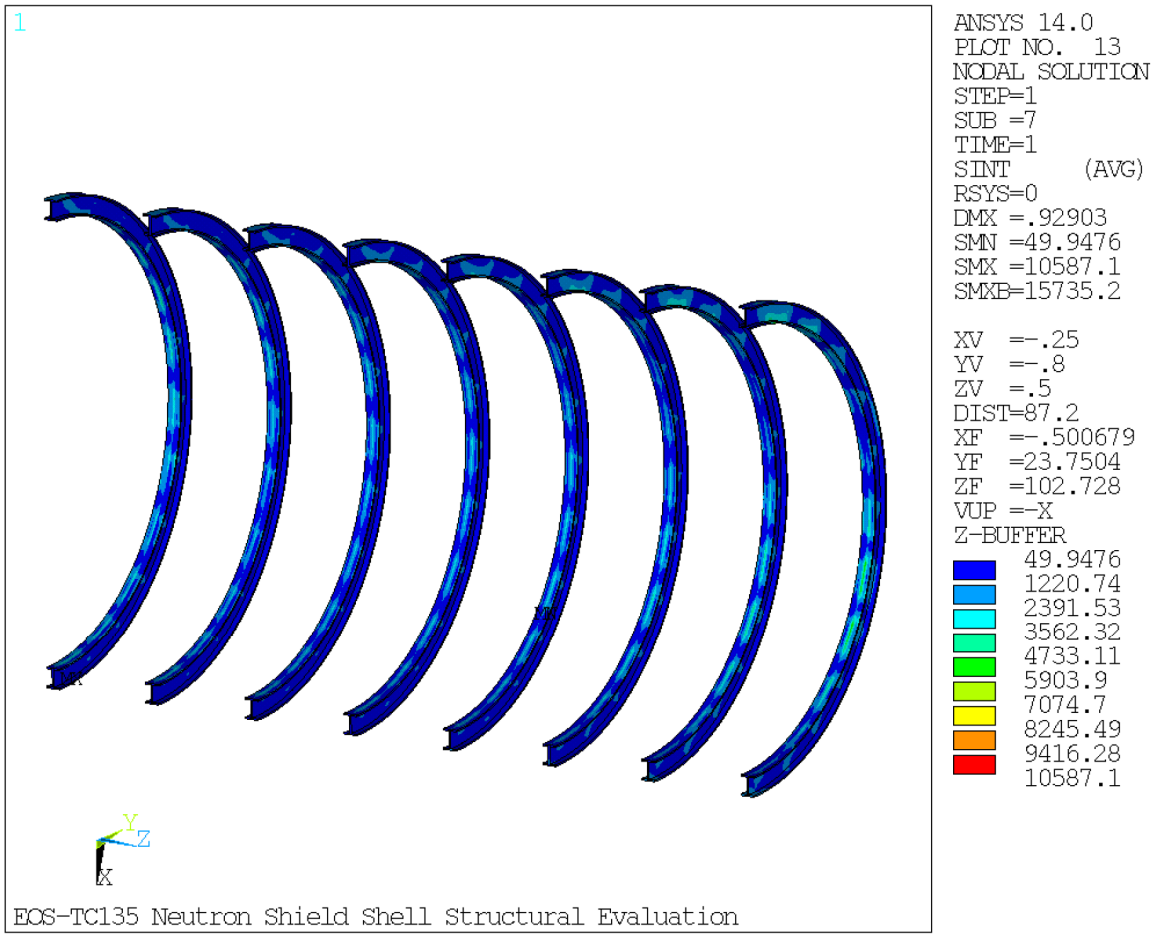

Figure 3.9.5-18
EOS-TC135 I-Beam Stress Intensity Plot under Pressure Load (40 psig)

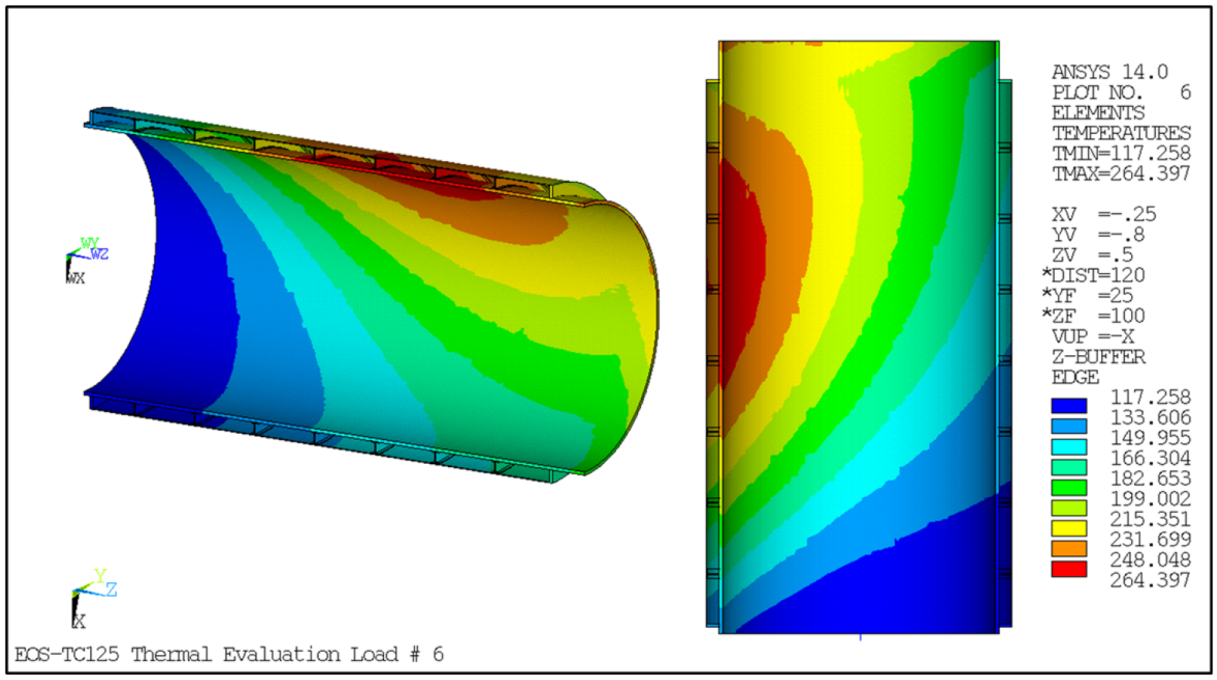

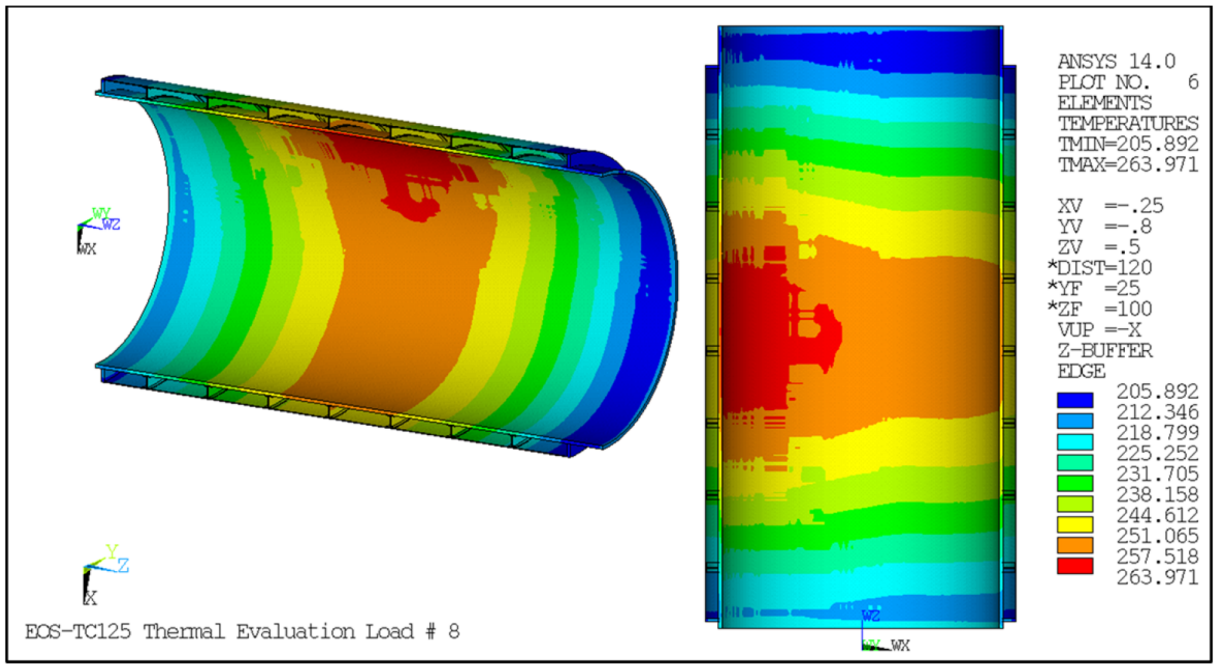

Figure 3.9.5-19
EOS-TC125 Temperature Distribution Plot

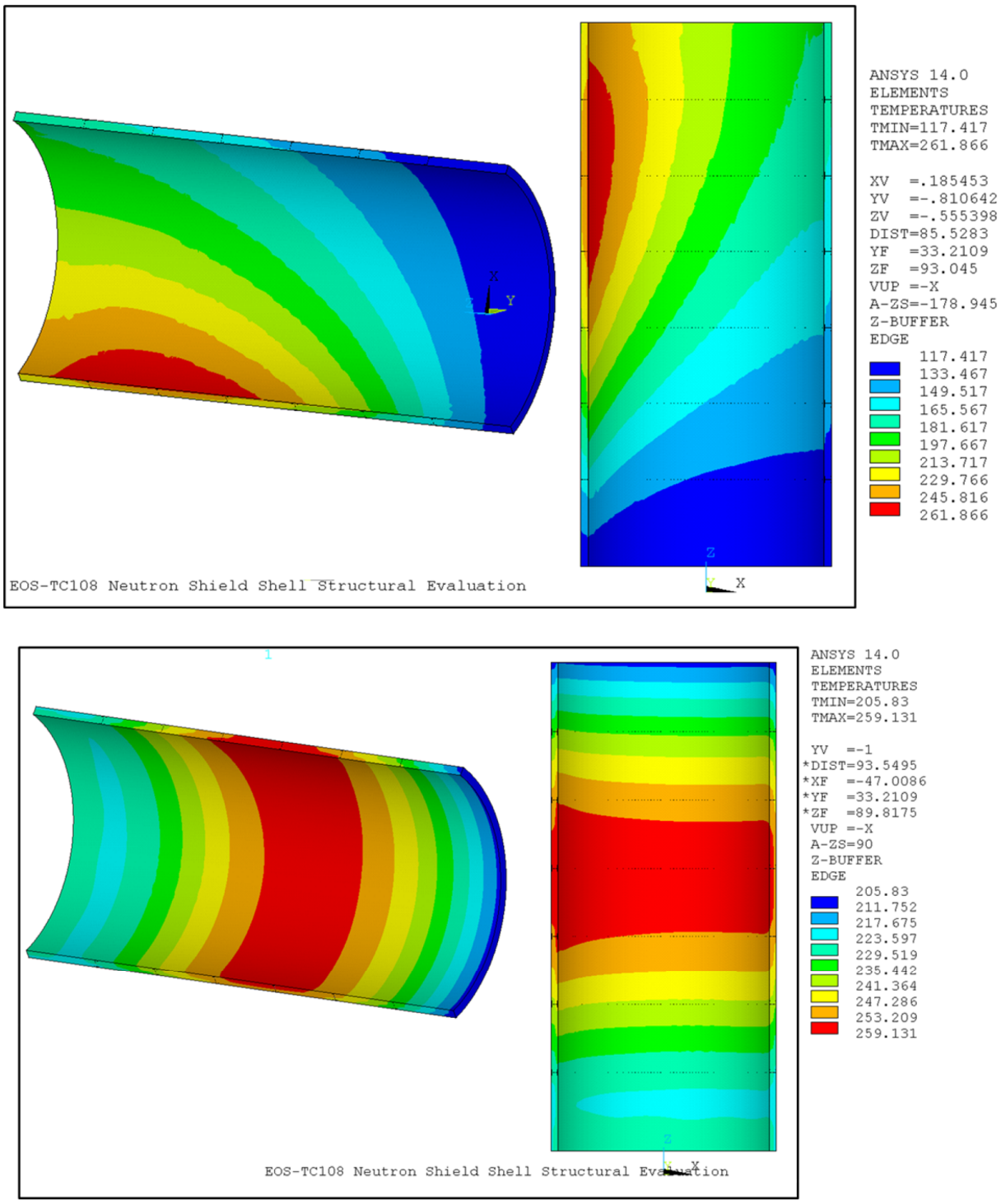

Figure 3.9.5-20
EOS-TC108 Temperature Distribution Plot

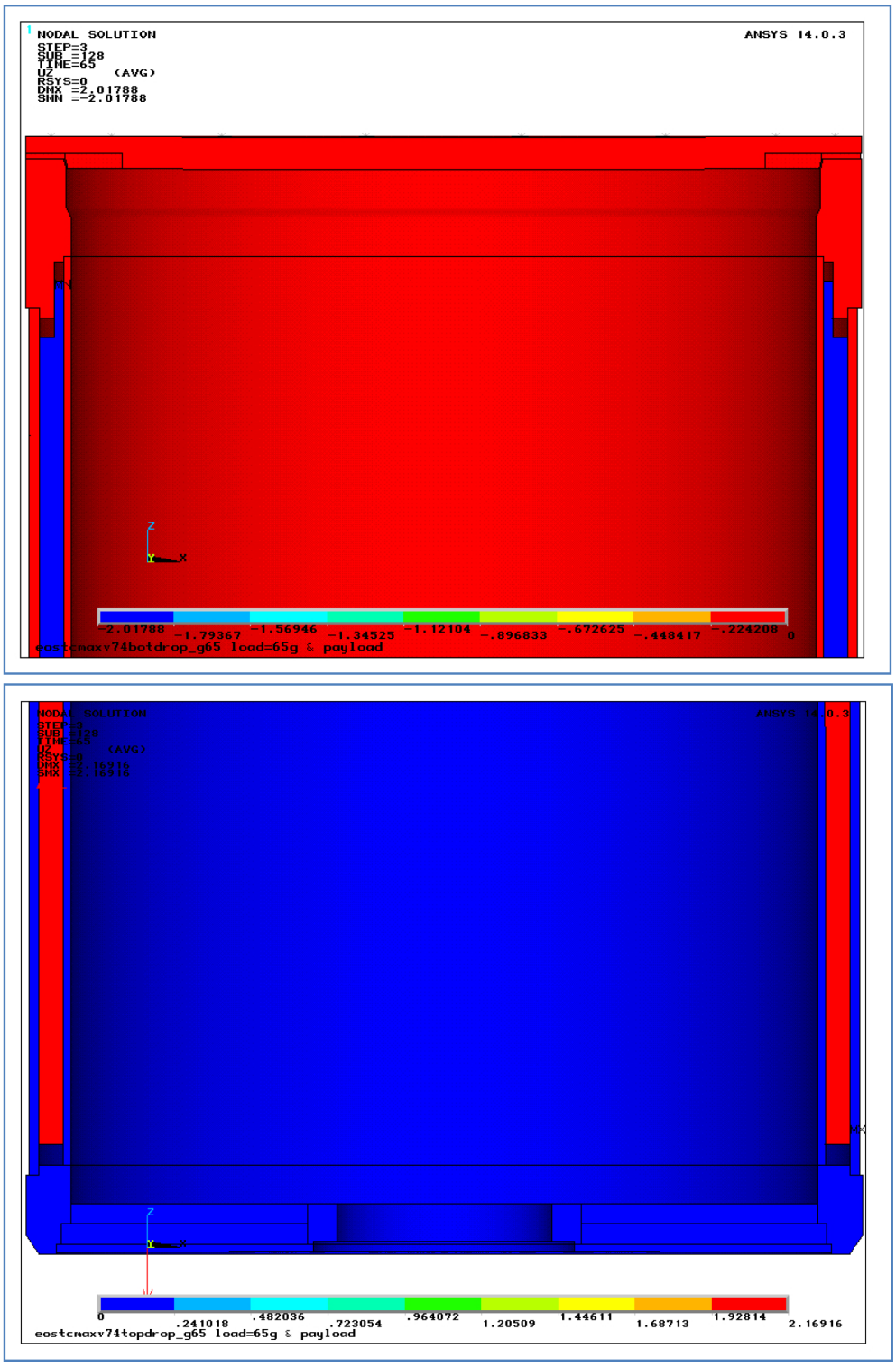

Figure 3.9.5-21
Bottom and Top, respectively, End Drops - Load 65g - Lead Slump Displacements

Proprietary Information on Pages 3.9.6-i through 3.9.6-iv and 3.9.6-1 through 3.9.6-55
Withheld Pursuant to 10 CFR 2.390

APPENDIX 3.9.7
NUHOMS® EOS SYSTEM STABILITY ANALYSIS

Table of Contents

3.9.7 NUHOMS® EOS SYSTEM STABILITY ANALYSIS 3.9.7-1

3.9.7.1 EOS-HSM Stability Evaluation 3.9.7-1

3.9.7.2 EOS Transfer Cask Missile Stability and Stress Evaluation 3.9.7-14

3.9.7.3 References 3.9.7-31

List of Tables

Table 3.9.7-1 Sizes and Weight for Various EOS-HSM Models 3.9.7-33
Table 3.9.7-2 Missile Load Data for EOS-HSM Stability Analysis 3.9.7-33
Table 3.9.7-3 Design Pressures for Tornado Wind Loading 3.9.7-34
Table 3.9.7-4 Summary of EOS-HSM Sliding and Stability Results 3.9.7-35
Table 3.9.7-5 Design-Basis Tornado Missile Spectrum and Maximum Horizontal Speed for EOS-TC Stability Analysis 3.9.7-36
Table 3.9.7-6 Cask and DSC Weights in Different Configuration and Their Geometric Properties 3.9.7-37
Table 3.9.7-7 EOS-TC Analysis Results 3.9.7-38
Table 3.9.7-8 Combined Tornado Effect 3.9.7-39

List of Figures

Figure 3.9.7-1 EOS-HSM Dimensions for Stability Analysis 3.9.7-40

Figure 3.9.7-2 Angle of Rotation from Time-Dependent Analysis Due to Tornado Wind and Massive Missile Loading for EOS- HSM Short 3.9.7-41

Figure 3.9.7-3 Angle of Rotation from Time-Dependent Analysis Due to Tornado Wind and Massive Missile Loading for EOS- HSM Medium 3.9.7-41

Figure 3.9.7-4 Angle of Rotation from Time-Dependent Analysis Due to Tornado Wind and Massive Missile Loading for EOS- HSM Long 3.9.7-42

Figure 3.9.7-5 Sliding Displacement from Time-Dependent Analysis Due to Tornado Wind and Massive Missile Loading for EOS- HSM Short 3.9.7-42

Figure 3.9.7-6 Sliding Displacement from Time-Dependent Analysis Due to Tornado Wind and Massive Missile Loading for EOS- HSM Medium 3.9.7-43

Figure 3.9.7-7 Sliding Displacement from Time-Dependent Analysis Due to Tornado Wind and Massive Missile Loading for EOS- HSM Long 3.9.7-43

Figure 3.9.7-8 Stability of the DSC on the DSC Support Structure 3.9.7-44

Figure 3.9.7-9 Arrangement of EOS-TC, Skid and Transfer Trailer at Rest 3.9.7-45

Figure 3.9.7-10 Stability Geometry of TC on Transfer Trailer 3.9.7-46

Figure 3.9.7-11 Angle of Rotation (Time-Dependent)-Wind and Missile Loading for EOS-TC 3.9.7-47

3.9.7 NUHOMS® EOS SYSTEM STABILITY ANALYSIS

3.9.7.1 EOS-HSM Stability Evaluation

The sliding and overturning stability analyses due to design basis wind, flood, seismic, and massive missile impact loads are performed using hand calculations. The NUHOMS® EOS System consists of a reinforced concrete horizontal storage module (EOS-HSM) loaded with a dry shielded canister (DSC) (EOS-37PTH or EOS-89BTH).

3.9.7.1.1 General Description

The system consists of the dual-purpose (transport/storage) EOS-37PTH and EOS-89BTH DSCs, the EOS-HSM, and the onsite transfer cask (EOS-TC) with associated ancillary equipment. Each EOS-HSM is designed to store a DSC containing up to either 37 pressurized water reactor (PWR) or 89 boiling water reactor (BWR) spent fuel assemblies (SFAs).

The EOS-HSM storage modules can be arranged in both single-row or back-to-back-row arrays, with thick shield walls connected to the EOS-HSM at the ends of the arrays (end shield walls) and at the back end of the module (rear shield walls), if single-row arrays are used.

In the standard configuration, the EOS-HSM consists of two main segments: a base and a roof. The roof is installed on top of the base and is connected to it by bolts/embedments via four stiffened steel brackets located at each of the interior upper corners of the module's cavity. An alternate multi-segment design (EOS-HSMS) is available, consisting of two segments for the base unit connected together with grouted, high-strength threaded bars/embedments or grouted dowels.

3.9.7.1.2 Material Properties

The EOS-HSM assembly is constructed of reinforced concrete and steel. This analysis considers rigid body motions. Therefore, the mechanical properties of the materials are not used as design inputs in this evaluation.

3.9.7.1.3 Mass Properties

The mass properties of the EOS-HSM are listed in Table 3.9.7-1. Bounding values of concrete density (140 pcf, 150 pcf, and 160 pcf) are considered.

3.9.7.1.4 Friction Coefficients

The static analyses are performed using a concrete-to-concrete friction coefficient of 0.6.

3.9.7.1.5 Methodology

The stability of the EOS-HSM unit is evaluated for four load cases that may cause overturning and sliding of a single freestanding module. These four load cases are:

- Tornado-generated wind loads
- Massive missile impact loads
- Flood loads
- Seismic loads

3.9.7.1.6 Assumptions

1. The analyses assume that the dynamic coefficient of friction is equal to the static coefficient. This assumption maximizes the rocking uplift displacements of the EOS-HSM (particularly for the high friction coefficient analysis cases).

2. The differential pressure load caused by the tornado pressure drop does not affect the overall stability of the EOS-HSM and is ignored. The structure is vented, and so any differential pressure is very brief, while the internal and external pressures equilibrate. Since the structure is symmetric, the temporary internal pressure in the EOS-HSM caused by the negative tornado pressure does not cause any unbalanced loads on the EOS-HSM that would cause sliding and/or overturning.

3. This stability evaluation is applicable to both the standard EOS-HSM design, as well as the segmented EOS-HSMS design. The weight and inertia properties of the EOS-HSM and the EOS-HSMS are the same.

3.9.7.1.7 Loads and Boundary Conditions

3.9.7.1.7.1 Earthquake Input

The seismic stability evaluation is performed for a horizontal acceleration of 0.45g and vertical acceleration of 0.30g.

In addition, a 1.1 load factor is added to the seismic load.

3.9.7.1.7.2 Wind and Tornado Input

The EOS-HSM is evaluated for overturning and sliding due to the design basis tornado (DBT) specified in Chapter 2. The DBT is based on the NRC Reg. Guide 1.76 Region I Intensities. The maximum wind speed is 360 mph. The tornado loads are generated for three separate loading phenomena, as follows, which is combined in accordance with Section 3.3.2 of NUREG-0800 [3.9.7-1] (i.e. tornado wind load is concurrent with (additive to) tornado missile loads).

1. Pressure or suction forces created by drag as air impinges and flows past the EOS-HSM with a maximum tornado wind speed of 360 mph.

2. Suction forces due to a tornado generated pressure drop or differential pressure load of 3 psi.

3. Impact forces created by tornado-generated missiles impinging on the EOS-HSM.

Per NUREG-0800, the total tornado load on a structure is combined as follows:

$W_t = W_p$
$W_t = W_w + 0.5W_p + W_m$

Where,

W_t = Total tornado load
W_w = Load from tornado wind effect
W_p = Load from tornado atmospheric pressure change effect
W_m = Load from tornado missile impact effect

Note that W_p is not applicable to the stability analysis as discussed in Section 3.9.7.1.6. Thus, the load combination for tornado loading for this analysis is simplified to:

$W_t = W_w + W_m$

In addition, a 1.1 load factor is added to Dead weight + Tornado load.

The envelope of a range of missiles from Chapter 2 is used for the missile impact load.

As seen from Table 3.9.7-2 the automobile impact on to the EOS-HSM has the maximum momentum and is considered as bounding evaluation.

3.9.7.1.7.3 Flood Input

The EOS-HSM is evaluated for a flood height of 50 feet with a water velocity of 15 fps.

In addition, a 1.1 load factor is added to Dead weight + Flood load per Table 2-7 of Chapter 2.

3.9.7.1.8 Stability Analysis

The load categories associated with the EOS-HSM stability analysis are described in the previous section. The analysis steps and results for each load category are presented in this section.

3.9.7.1.8.1 Design Basis Tornado

The EOS-HSM is evaluated for forces created by drag as air impinges and flows past the EOS-HSM with a maximum tornado wind speed of 360 mph.

For sliding and overturning analysis, it is assumed that the module is subjected to the load due to 218 psf windward pressure loading acting on the end shield wall. The leeward side of the same module is subjected to a wind suction load of 154 psf. A suction of 326 psf is applied to the roof, including the top part of the shield walls. The loads are shown in Table 3.9.7-3.

In addition, missiles loads are combined with the tornado wind load per NUREG-800 [3.9.7-1].

3.9.7.1.8.1.1 Static Overturning Analysis due to Tornado Wind

The loaded EOS-HSM, the rear wall, one corner block, and one end shield wall rotates about B, shown in Figure 3.9.7-1. The other end shield wall and corner block rotates about point A, shown in Figure 3.9.7-1. Conservatively, the overturning of the loaded module with one end shield wall about point B is considered for the stabilizing moment.

In the overturning analysis of the EOS-HSM, the effects of tornado wind forces are first determined. An overturning moment is then calculated and is compared with a stabilizing moment. The minimum safety factor against overturning computed for all the three design lengths of EOS-HSM due to tornado wind is 1.59.

3.9.7.1.8.1.2 Dynamic Overturning Analysis of Tornado Wind Concurrent with Massive Missile Impact Loading

A dynamic analysis based on the conservation of energy is conducted for the combined effects of wind and concurrent massive missile impact loading. The effects of the concurrent massive missile impact loads are used in determining the initial angular momentum from the conservation of angular momentum equation using the wind loads from the previous section. Then the angle of rotation is determined from the conservation of energy of the concurrent loading.

The wind loads are calculated conservatively for EOS-HSM Long:

$$F_{hw} = (F_{windward} + F_{leeward})(L_{base})(h_{HSM+roof})$$

$$F_{vw} = \left(F_{roof}\right)(L_{base})(w_{HSM+shield})$$

The concurrent wind loading is accounted for by reducing the inertia that resists motion in the denominator of the equation.

$$\omega_B = \frac{m_m \cdot d_m \cdot v_i}{m_m \cdot d_m^2 + I_{tot} - \left(\frac{F_{hw}}{g}\right)\left(\frac{h}{2}\right)^2 - \left(\frac{F_{vw}}{g}\right)\left(\frac{w}{2}\right)^2}$$

Where,

F_{hw} = Horizontal tornado wind load
F_{vw} = Vertical tornado wind load
ω_B = Angle of rotation
m_m = Mass of the missile
d_m = Distance from missile impact to floor
v_i = Initial missile velocity
I_{tot} = Total moment of inertia of HSM + Front end shield wall
h = Height of HSM + roof
w = Width of HSM + end shield wall

The conservation of energy is used for overturning.

Rotational Kinetic Energy = Change in Potential Energy – Work Done by Horizontal Wind force

$$\frac{I_{tot}\omega_B^2}{2} = (W - F_{vw}) \cdot r \cdot [\sin(\beta + \theta) - sin\beta] - F_{hw} \cdot r \cdot [\cos(\beta + \theta) - cos\beta]$$

Where,

θ = Angle of tipping
β = Angle from the horizontal to center of gravity (CG) of EOS-HSM (68.3°)
r = Diagonal distance from CG to point B
I_{tot} = Total moment of Inertia of HSM + Left end shield wall
W = Weight of the loaded HSM + Left end shield wall

The loaded EOS-HSM is stable against overturning as tip-over does not occur until the CG rotates past the edge (point B, Figure 3.9.7-1) of the HSM to an angle of more than 90°- 68.3° = 21.7°

A loaded EOS-HSM rotates a maximum of 0.7 degrees, which is less than the 21.7 degrees required to overturn the module.

3.9.7.1.8.1.3 Time-Dependent Overturning Analysis of Tornado Wind Concurrent with Massive Missile Impact Loading

In addition to the dynamic overturning analysis, a time dependent analysis is used to ensure the absence of any overturning.

An approximate relationship for the deceleration of an automobile impacting a rigid wall is given by:

$-\ddot{x} = 12.5g \cdot x$ $Eq. D - 1\ of$ [3.9.7-4]

$-\ddot{x}$ = Deceleration (ft/sec^2)
x = Distance automobile crushes into target (ft)

A force time history is obtained:

$F = 0.625 V_s W_m sin20t$ $Eq. D - 6\ of$ [3.9.7-4]

The overturning moment is:

$$M_{ot} = F \cdot d_m + \frac{F_{hw} h}{2}$$

Where,

d_m = Distance from missile impact to floor
h = Vertical height to the top of EOS-HSM and is a function of rotation

The stabilizing moment is:

$$M_{st} = (W_{HSM} - F_{vw}) \cdot r cos(\beta + \theta) + W_{end\ shield} \cdot r_{end} cos(\gamma + \theta)$$

Where,

W_{HSM}= Weight of the loaded EOS-HSM
r = Diagonal distance from CG to point B
θ = Angle of rotation
r_{end} = Diagonal distance from CG of end shield wall to point B
γ = Angle from horizontal to CG of end shield wall

The moment causing acceleration is:

$$M_{acc} = M_{ot} - M_{st}$$

The angular velocity is:

$$\omega_i = \left[\frac{M_{acc,i} + M_{acc,i-1}}{2} \cdot (t_i - t_{i-1})\right] / I_{tot} + \omega_{i-1}$$

Where,

i = Index for current time step
i-1 = Index for previous time step
I_{tot} = Total moment of Inertia of HSM + Left end shield wall

The angle of rotation is:

$$\theta_i = \left[\frac{\omega_i + \omega_{i-1}}{2} \cdot (t_i - t_{i-1})\right] + \theta_{i-1}$$

The angles of rotation resulting from these analyses are shown in Figure 3.9.7-2 through Figure 3.9.7-4. The governing angle of rotation is 3.12 degrees, which is less than the 21.7 degrees required to overturn the module.

3.9.7.1.8.1.4 Sliding Analysis for Tornado Wind Concurrent with Massive Missile Impact loading

The combined wind + missile impact case is considered for EOS-HSM sliding analysis based on the conservation of energy.

First, the conservation of momentum is used for the sliding analysis.

$$V = \frac{m \cdot v_i}{M/1.07 + m - F_{hw}/386.4}$$

Where,

V = Initial linear velocity of module after impact
v_i = Initial velocity of missile
m = Mass of the missile
M_1 = Mass of empty EOS-HSM Short
M_2 = Mass of end shield wall
M_3 = Mass of governing loaded EOS-89BTH DSC
M = Total mass = $M_1 + M_2 + M_3$
1.07 is the factor used to account for the uncertainty of the concrete density.

Then using the conservation of energy:

$$Friction\ Energy = Initial\ Kinetic\ Energy\ of\ System + Work\ done\ by\ Wind$$

$$\mu \cdot (gM/1.07 - F_{vw})d = \frac{(M/1.07 + m) \cdot V^2}{2} + F_{hw}d$$

Where,

μ = 0.6 coefficient of friction for concrete-to-concrete surfaces
F_{vw} = Uplift force generated by DBT wind pressure on the roof
d = Sliding distance of EOS-HSM
F_{hw} = Sliding force generated by DBT wind pressure

The sliding distance of the EOS-HSM module is calculated to be 1.62 inches.

3.9.7.1.8.1.5 Time-Dependent Sliding Analysis for Tornado Wind Concurrent with Massive Impact Loading

In addition to the dynamic sliding analysis, a time dependent analysis is used to provide a bounding sliding displacement.

The total force causing sliding is:

$$F_{slide} = F + F_{hw}$$

The resisting force from friction is:

$$F_{resis} = \mu(W - F_{vw})$$

Therefore the force causing acceleration is:

$$F_{acc} = F_{slide} - F_{resis}$$

The velocity is:

$$v_i = \left[\frac{F_{acc,i} + F_{acc,i-1}}{2} \cdot (t_i - t_{i-1})\right] / m_{tot} + v_{i-1}$$

Where,

i	=	Index for current time step
i-1	=	Index for previous time step
m_{tot}	=	Total mass of loaded EOS-HSM and both end shield walls including adjustment for density uncertainty

The sliding displacement is:

$$x_i = \left[\frac{v_i + v_{i-1}}{2} \cdot (t_i - t_{i-1})\right] + x_{i-1}$$

The sliding displacements resulting from these analyses are shown in Figure 3.9.7-5 through Figure 3.9.7-7. The governing sliding displacement is 1.30 inches which is bounded by sliding distance of 1.62 inches resulting from dynamic sliding analysis as calculated in Section 3.9.7.1.8.1.4.

3.9.7.1.8.2 Flood Loads

The EOS-HSM is designed for a flood height of 50 feet and water velocity of 15 fps. The module is evaluated for the effects of a water current of 15 fps impinging on the side of a submerged EOS-HSM. Under 50 feet of water, the inside of the module is rapidly filled with water. Therefore, the EOS-HSM components are not evaluated for the 50 feet static head of water.

Calculation of the drag pressure due to design flood is shown in Appendix 3.9.4.

3.9.7.1.8.2.1 Overturning Analysis

The factor of safety against overturning of a single EOS-HSM with shield walls, for the postulated flooding conditions, is calculated by summing moments about the bottom outside corner of a single, freestanding EOS-HSM. The factors of safety against overturning for a single, freestanding EOS-HSM due to the postulated design basis flood water velocity are 1.14, 1.12, and 1.13 for the EOS-HSM Short, EOS-HSM Medium and EOS-HSM Long, respectively.

3.9.7.1.8.2.2 Sliding Analysis

The factor of safety against sliding of a freestanding single EOS-HSM due to the maximum postulated flood water velocity of 15 fps is calculated using methods similar to those described above. The effective weight of the EOS-HSM including the DSC and end shield wall acting vertically downward, less the effects of buoyancy acting vertically upward is calculated. The factors of safety against sliding for a single, freestanding EOS-HSM due to the postulated design basis flood water velocity are 1.12, 1.09, and 1.11 for the EOS-HSM Short, EOS-HSM Medium and EOS-HSM Long, respectively.

3.9.7.1.8.3 Seismic Load

The EOS-HSM is evaluated for maximum values for seismic accelerations of 0.45g in the horizontal direction and 0.30g in the vertical direction. Both the loaded EOS-HSM and the empty EOS-HSM are considered for these loads. The EOS-HSM and one end shield wall rotate about B, shown in Figure 3.9.7-1. The other end shield wall, corner blocks and rear shield walls are conservatively ignored.

The combination of 100% of horizontal acceleration and 40% of vertical acceleration is used.

3.9.7.1.8.3.1 Static Overturning Analysis of the EOS-HSM due to Seismic Load

The stabilizing and overturning moments are calculated and compared, and the case considering the bounding 140 pcf concrete density and the minimum DSC weight to minimize the stabilizing moment is shown below. The stability overturning analysis shown is for the governing EOS-HSM Long model. A factor of 1.07 (150 pcf/140 pcf) reduces the considered mass to the 140 pcf lower bound case. The 160 pcf upper bound is also considered, but not shown here.

Stabilizing Moment = $M_{st} = (W_{HSM} + W_{DSC}) \times d_{HSM-B} + W_{end\_shield\_wall} \times d_{end\_shield\_wall-B}$

$$M_{st} = \left(\frac{330kip}{1.07} + 134kip\right) \times (48in) + \left(\frac{187.1kip}{1.07}\right) \times (124in)$$

$M_{st} = 42{,}900$ kip-in

Where a factor of 1.07 (150pcf/140pcf) is used to account for the uncertainty of the concrete density.

Overturning Moment =

$$M_{ot} = 0.4_{a_v} \times \left(W_{HSM}{}^{x}{}_{HSM} + W_{DSC}{}^{x}{}_{DSC} + W_{wall}{}^{x}{}_{wall}\right) + a_h\left(W_{HSM}{}^{y}{}_{HSM} + W_{DSC}{}^{y}{}_{DSC} + (W_{wall}h_{wall})/2\right)$$

$$M_{ot} = 0.4 \times 0.30g \times \left[\frac{330kip}{1.07} \times 48in + 134kip \times 48in + \frac{187.1kip}{1.07} \times 124in\right] + 0.45g \times \left[\frac{330kip}{1.07} \times 126.5 + 134kip \times 106in + \frac{187.1kip}{1.07} \times 111in\right]$$

M_{ot} = 37,800 kip-in

Where,

W_{HSM}, W_{DSC}	=	Weight of empty HSM and DSC = 330 kip, 134 kip respectively
$d_{HSM\text{-}B}$	=	respective distance between the CG of the HSM and the point of rotation B (Figure 3.9.7-1) =116 in./2 - 10 in. = 48 in.
$d_{end\ shield\ wall\text{-}B}$	=	respective distance between the CG of the end shield wall and the point of rotation B (Figure 3.9.7-1) = 36 in./2 + 116 in. - 10 in.= 124 in.
a_v, a_h	=	vertical and horizontal seismic accelerations
x_{HSM}	=	horizontal distance between the CG of the HSM and the point of rotation B = 48 in. (Figure 3.9.7-1)
x_{DSC}	=	horizontal distance between the CG of the DSC and the point of rotation B = 48 in. (Figure 3.9.7-1)
x_{wall}	=	horizontal distance from the CG of the end shield wall to the point of rotation B = 124 in. (Figure 3.9.7-1)
y_{HSM}	=	vertical distance from the CG of the HSM and the point of rotation B = 126.5 in. (Figure 3.9.7-1)
y_{DSC}	=	vertical distance from the CG of the HSM and the point of rotation B = 106 in. (Figure 3.9.7-1)
h_{wall}	=	vertical distance from the CG of the end shield wall to the point of rotation B = 111 in. (Figure 3.9.7-1)

The maximum acceptable acceleration values before tipping occurs are calculated below:

$$M_{st} = 42{,}900kip \cdot in \geq 1.1M_{ot} = 1.1\left\{0.4_{a_v} \times \left[\frac{330kip}{1.07} \times 48in + 134kip \times 48in + \frac{187.1kip}{1.07} \times 124in\right] + a_h\left[\frac{330kip}{1.07} \times 126.5 + 134kip \times 106in + \frac{187.1kip}{1.07} \times 111in\right]\right\}$$

And assuming $a_v = \frac{2}{3} a_h$

$a = 0.46g, a_v$=0.31g

The safety factor of $M_{st}/1.1M_{ot}$ = 1.03 and is greater than 1 and is the governing safety factor for all load cases. Therefore, it is concluded that the EOS-HSM is stable for seismic loads of up to 0.45g horizontal and 0.30g vertical.

3.9.7.1.8.3.2 Static Sliding Analysis of the EOS-HSM due to Seismic Load

The resisting friction force and horizontal seismic force are calculated and compared and the case considering the bounding 140 pcf concrete density and the minimum DSC weight to minimize the resisting friction force is shown below. The static sliding analysis is shown for the governing EOS-HSM Long model. Cases where the EOS-HSM is loaded versus empty and has one end shield wall versus no shield walls are also considered.

Friction force resisting sliding = $F_{st} = \mu(W_{HSM}+W_{DSC})(1-0.40\ a_v)$

$$F_{st} = 0.6 \times \left(\frac{330kip}{1.07} + 134kip\right) \times (1 - 0.40 \times 0.30)$$

F_{st} = 233 kip

Applied horizontal seismic force = $F_{hs} = a_h\ (W_{HSM}+W_{DSC})$

$$F_{hs} = 0.45 \times \left(\frac{330kip}{1.07} + 134kip\right)$$

F_{hs} = 199kip

Where,

μ	=	friction coefficient = 0.6
a_v, a_h	=	vertical and horizontal seismic accelerations = 0.30g, 0.45g respectively
x, y	=	are the horizontal and vertical distance between the CG and point of rotation B

The maximum acceptable acceleration values before sliding occurs are calculated below:

$$F_{st} = 0.6 \times \left(\frac{330kip}{1.07} + 134kip\right) \times \left(1 - 1.1 \times 0.40_{a_v}\right) \geq 1.1F_{hs}$$
$$= 1.1a_h\left(\frac{330kip}{1.07} + 134kip\right)$$

And assuming $a_v = \frac{2}{3} a_h$

$a = 0.47g, a_v = 0.32g$

The safety factor of $F_{st}/1.1F_{hs}$=1.07 and is greater than 1 and is the governing safety factor for all load cases. Therefore, it is concluded that the EOS-HSM is stable for seismic loads of up to 0.45g horizontal and 0.30g vertical.

3.9.7.1.8.3.3 Seismic Stability of the DSC on DSC Support Structure inside the EOS-HSM

This evaluation is performed for the DSC resting on the support rails inside the EOS-HSM, which includes the stability of the DSC against lifting off from one of the rails during a seismic event and potential sliding off of the DSC from the support structure. The horizontal equivalent static acceleration of 0.45g is applied laterally to the center of gravity of the DSC. The point of rigid body rotation of the DSC is assumed to be the center of the support rail. The applied moment acting on the DSC is calculated by summing the overturning moments.

The stabilizing moment, acting to oppose the applied moment, is calculated and compared with the overturning moment to obtain the maximum acceleration to preclude sliding and overturning of the DSC.

Weight of the DSC = W (kip)

DSC outer radius = $R = 75.5''/2 = 37.8''$

Angle $\theta = 30^\circ$

$Z = 37.75 \sin(30^\circ) = 18.88''$

$Y = 37.75 \cos(30^\circ) = 32.69''$

Vertical Seismic Acceleration = 0.30g

Horizontal Seismic Acceleration = 0.45g

Vertical seismic force (kips) = $W \times 0.30 \times 0.4 = 0.12W = F_v$

Horizontal seismic force (kips) = $W \times 0.45 = 0.45W = F_h$

The overturning moment =
$1.1F_h \times Y = 1.1 \times 0.45W \times 32.69 = 16.18W$ kip-in

The stabilizing moment =
$(W - 1.1F_v) \times Z = (W - 1.1 \times 0.12W) \times 18.88 = 16.39W$ kip-in

Therefore, the margin of safety (*SF*) against DSC lift off from the DSC support rails inside the HSM obtained from this analysis is:

$$SF = \frac{M_{st}}{M_{ot}} = \frac{16.39W}{16.18W} = 1.01$$

The safety factor of M_{st}/M_{ot}=1.01 is greater than 1. Therefore, the DSC is stable against lifting off the DSC support rails in the EOS-HSM. The evaluation to determine the maximum seismic acceleration before any uplift of the DSC occurs is shown.

$$M_{st} = (W - 1.1 \times 0.4a_v W) \times 18.88 \geq M_{ot} = 1.1 \times a_h W \times 32.69$$

And assuming $a_v = \frac{2}{3} a_h$

$a_h = 0.46g, a_v = 0.30g$

Therefore, the maximum horizontal and vertical acceleration are determined to be 0.45g and 0.30g, respectively.

3.9.7.1.8.4 Interaction of EOS-HSM with Adjacent Modules

For the overturning and sliding analyses due to tornado wind plus missile and flood loading, a single module with one end shield wall is considered. For the seismic sliding and overturning analyses in Section 3.9.7.1.8.3, the cases both with and without an end shield wall are considered, where the same weight and moment of inertia is consistently used for sliding force/overturning moment and for friction force/stabilizing moment in each case.

In the actual scenarios, there is either an end shield wall on one side and another module on the other side, or one module on each side. In the case of sliding, the tornado wind plus missile impact loads the end shield wall plus the HSM module and incur a displacement. The maximum displacement is already obtained in Sections 3.9.7.1.8.1.4 and 3.9.7.1.8.1.5 assuming no resisting force from the adjacent module. With the presence of the adjacent module, the displacement can be transferred into a load onto the adjacent module and result in the maximum displacement if it is perfectly elastic (coefficient of restitution = 1). Then this displacement can be transferred into a load for the next adjacent module with a maximum displacement. However, concrete has a much lower coefficient of restitution (COR) of about 0.1. Energy absorption due to contact (due to the low COR=0.1) results in less critical sliding and overturning results. Impact due to sliding would be distributed over the large side/rear wall surface areas. Impact due to tipping would be localized at the free edges/corners of the modules. Any local damage in these corners or edges would not affect the structural, thermal, or shielding performance of the EOS-HSM. Therefore, the displacement of the adjacent module cannot reach the maximum displacement since there is some energy loss. Thus, the maximum displacement obtained in Sections 3.9.7.1.8.1.4 and 3.9.7.1.8.1.5 is conservative and bounding. This conservatism also applies to overturning and the cases due to flood loads.

3.9.7.1.9 Results

For the maximum seismic acceleration of 0.45g horizontal and 0.30g vertical, no sliding will occur. Also, there will be no overturning at this set of seismic accelerations.

For flood, wind, and missile impact, it is also determined that the uplift values are small and so the DSC remains stable on the support rails. For seismic loading, it is also determined that there is no uplift of the DSC.

In the case of an uneven surface of the concrete pad, shims under the end and rear shield walls can be placed to restore the HSM to its horizontal configurations.

Table 3.9.7-4 shows a summary of the bounding results from the analyses in Section 3.9.7.1.8. Thus, a maximum horizontal acceleration of 0.45g and a vertical acceleration of 0.30g can be exerted on the EOS-HSM before any uplift or sliding occurs. Also there is no DSC lift-off due to this seismic loading.

3.9.7.2 EOS Transfer Cask Missile Stability and Stress Evaluation

3.9.7.2.1 General Description

The stability, stresses, and penetration resistance of the EOS-TCs (TC108, TC125 and TC135) due to design basis tornado and missile impact are evaluated in this section.

3.9.7.2.2 Material Properties

The material properties of the cask outer shell, and top cover plate at 400 °F are taken from Chapter 8.

3.9.7.2.3 Assumptions

1. The gust factor value of 0.85 is taken from Section 6.5.8.1 of ASCE 7-05 [3.9.7-5].

2. The bolted bottom cover plate assembly is protected by transfer equipment attached to skid assembly during the transfer operations, and therefore DBT and missile load is not consider for bottom cover plate.

3. The impact between massive missile and EOS-TC is assumed to be perfectly plastic impact and the missile mass is attached to EOS-TC after impact.

4. The stresses in trunnion/saddle due to DBT and missile impact are bounded by seismic loads. The evaluations of trunnions are performed separately in Appendix 3.9.5.

3.9.7.2.4 Design Input/Data

The most severe tornado-generated wind and missile loads specified by Regulatory Guide 1.76 [3.9.7-6] are selected as the design basis.

3.9.7.2.4.1 DBT Velocity Pressure

The DBT Region I intensities are utilized since they result in the most severe loading parameters. For this region, the maximum wind speed is 230 mph, the rotational speed is 184 mph, and the maximum translational speed is 46 mph. The radius of the maximum rotational speed is 150 feet, the pressure drop across the tornado is 1.2 psi and the rate of pressure drop is 0.5 psi per second.

The maximum velocity pressure, q_z, evaluated at height z based on the maximum tornado velocity (v) is calculated using the relationship given in [3.9.7-5].

$$q_z = 0.00256 K_z K_{zt} K_d I (v)^2$$

The maximum tornado wind speed, V, is the resultant of the maximum rotational speed (184 mph) and the translational speed (46 mph) of the tornado.

The design wind force, F, on the EOS-TC due to this velocity pressure, q_z, is $F = q_z G C_f A_f$ lb Section 6.5.15 of Ref. [3.9.7-5]

Where,

G = gust-effect factor =0.85 (Assumption 1)
C_f = Force coefficient = conservatively taken as 0.82 (by linear interpolation of h/D value of 1.69) from Figure 6-21 of [3.9.7-5],
A_f = Projected area normal to the wind and geometry considered is shown in Figure 3.9.7-9 and is calculated for Case E of Table 3.9.7-6. This has a maximum projected area that is conservative.

Projected area of the cask = (Length of the cask, L_c) x (Diameter of the cask, D_c)

Projected area of the skid = (Length of the Skid, L_s) x (Height of the skid, H_s)

Projected area of the trailer = (Length of the trailer, L_t) x (Height of the Trailer, H_t)

Total projected area (Cask +Skid +Trailer),

Design wind force F = 22.36 kips

3.9.7.2.4.2 DBT Generated Missile Parameters

The tornado-generated missile impact evaluation is performed for a spectrum of missiles and are summarized in Table 3.9.7-5.

3.9.7.2.5 Methodology

The following analyses are performed for the cask and components using hand calculations:

- Stability analysis
- Stress analysis
- Penetration analysis

A load factor of 1.1 is applied to the tornado and seismic loads for stability analyses.

3.9.7.2.5.1 Combined Tornado Effects

Individual DBT, missile load, and combination of these loads are calculated assuming these act simultaneously and are shown in Table 3.9.7-8. Since the EOS-TC is vented, the differential atmospheric pressure is neglected.

3.9.7.2.6 Structural Evaluation

3.9.7.2.6.1 Design Basis Wind Pressure Loads

3.9.7.2.6.1.1 Stability Analysis due to DBT Wind Pressure Load

Total weight of the assembly (EOS-TC, skid and the trailer), W_C = Weight of (cask +skid + trailer)

The restoring moment is least for the assembly with minimum weight. Assuming the trailer and skid remain the same, the minimum weight of all the possible EOS-TC and DSC combinations per Table 3.9.7-6, is bounding for the stability analysis.

Considering the minimum weight of EOS-TC108 loaded with EOS-89BTH DSC (Case B, Table 3.9.7-6) is minimum (199.289 kips), a conservative weight of 170 kips is used for the evaluation.

Thus, the restoring moment, M_{st} = (Total weight) x (Half width of the trailer)

Conservatively assuming that the combined geometry of the cask/skid/trailer has a solid vertical projected area and ignoring the reduction in total wind pressure due to the open areas and shape factor, the maximum overturning moment, M_{ot}, for the cask/skid/trailer due to DBT wind pressure is:

$$M_{ot} = 2F \times H$$

Where,

H = Center of the cask/skid/trailer height
F = Design wind pressure
Accounting for the load factor of 1.1 on the overturning moment:

Factor of safety against overturning $= 1.1 \times \frac{M_{st}}{M_{ot}} = 3.92$

3.9.7.2.6.1.2 Stress Analysis

3.9.7.2.6.1.2.1 Stresses in the Cask Shell due to DBT Wind Pressure Load

Assuming the cask is simply supported and subjected to a uniform load, p, over the entire length, thus using Case 8c, Table 13.3 of Ref. [3.9.7-7], Page 650:

Circumferential membrane stress = $\sigma_2 = 0.492 B p R^{\frac{3}{4}} L^{\frac{-1}{2}} t^{\frac{-5}{4}}$

Circumferential bending stress = $\sigma_2' = 1.217 B^{-1} p R^{\frac{1}{4}} L^{\frac{1}{2}} t^{\frac{-7}{4}}$

Axial membrane stress $\sigma_1 = 0.1188 B^3 p R^{1/4} L^{1/2} t^{-7/4}$

Total force = F = 22.36 kips (Section 3.9.7.2.4.1)

Force per inch, p, is maximum for the minimum length of the cask, thus the bounding minimum length, L (EOS-TC108, Case A Table 3.9.7-6) is taken conservatively

p = F / L

B = $[12(1-\nu^2)]^{1/8}$, where ν is the Poisson's ratio (= 0.3 for stainless steel)

Circumferential membrane stress is maximum for the minimum cask length as it is inversely related to the cask length, whereas circumferential bending stress and axial membrane stress is maximum for the maximum cask length since they are directly related to the cask length.

Also, circumferential membrane stress, circumferential bending stress and axial membrane stress are maximum for the maximum cask radius since they are directly related to cask radius:

Bounding minimum cask length = (EOS-TC108, Case A, Table 3.9.7-6)

Bounding maximum cask length = (EOS-TC135, Case E, Table 3.9.7-6)

Bounding maximum cask radius = (EOS-TC135, Case E, Table 3.9.7-6)

Circumferential membrane stress σ_2 = 0.086 ksi

Circumferential bending stress, σ_2 = 3.85 ksi

Axial membrane stress, σ_1 = 1.25 ksi

Primary membrane stress intensity = σ_1 = 0.135 ksf = 0.0009 ksi

Membrane plus bending, S.I. = 5.19 ksi

3.9.7.2.6.1.2.2 Stresses in Top Cover Plate due to DBT Wind Pressure Load

Assuming the plate is simply supported at edges and subjected to a uniform load, q, (load per unit area) over the entire area, thus using Case 10a, Table 11.2 of Roark's Formula for Stress and Strain [3.9.7-7], Page 488 and 509:

$M_c = qa^2 L_{17}$, where $L_{17} = \frac{1}{4}\left\{1 - \frac{1-v}{4}\right\}$ for $r_o = 0$.

Thus, $M_c = \frac{qa^2(3+v)}{16}$

$q = 0.135$ ksf M_c = 0.37 kip-in/in

$\sigma = \frac{6M_c}{t_1^2}$ = 0.21 ksi

Primary membrane stress intensity = σ_m = 0.135 ksf = 0.0009 ksi

Membrane plus bending, S.I. = 0.21 ksi

3.9.7.2.6.2 Massive Missile Impact

3.9.7.2.6.2.1 Stability Analysis due to Massive Missile Impact Load

Stability analysis is done to analyze the most critical impact (Missile B, Table 3.9.7-5) when the missile hits the cask on the side. However, it is conservatively assumed that the missile hits the top most part of the cask as shown in Figure 3.9.7-10.

Using Table 3.9.7-6 and from conservation of momentum,

$$(H_i)_o = (H_a)_o$$

Where,

$(H_i)_o$ is the angular momentum about point O before impact $= R_1 v_i M_m$

$(H_a)_o$ is the angular momentum about point O after impact
$= R_1^2 \omega_i M_m + (I_c)_o \omega_i$

R_1 is the distance from point O to the impact point
v_i is the impact velocity of the missile
M_m is the mass of the missile
M_c is the mass of the cask assembly
ω_i is the angular velocity of the missile about point O just after the impact
$(I_c)_o$ is the mass moment of inertia of the cask about an axis through point O

Therefore, by conserving the momentum before and after the impact:

$$R_1 v_i M_m = R_1^2 \omega_i M_m + (I_c)_o \omega_i$$

$$\omega_i = \frac{R_1 v_i M_m}{R_1^2 M_m + (I_c)_o}$$

From the conservation of energy, $KE_i + PE_i = KE_f + PE_f$

Where,

KE_i is the initial kinetic energy of the cask and missile $= \frac{(I_c)_o \omega_i^2}{2} + \frac{R_1^2 \omega_i^2 M_m}{2}$

KE_f is the final kinetic energy of the cask and missile $= \frac{(I_c)_o \omega_f^2}{2} + \frac{R_1^2 \omega_f^2 M_m}{2}$

PE_i is the initial potential energy of the cask and missile = 0
PE_f is the final potential energy of cask and missile = (weight of the cask) x (change in height of the C.G.)

Therefore:

$$\frac{(I_c)_o \omega_i^2}{2} + \frac{R_1^2 \omega_i^2 M_m}{2} = \frac{(I_c)_o \omega_f^2}{2} + \frac{R_1^2 \omega_f^2 M_m}{2} + w_c h$$

$$\omega_f^2 = \frac{[(I_c)_o + R_1^2 M_m]\omega_i^2 - 2w_c h}{[(I_c)_o + R_1^2 M_m]}$$

From Figure 3.9.7-10 $h = R_2[\sin(\phi + \theta) - \sin(\phi)]$

Hence, $\omega_f^2 = \frac{[(I_c)_o + R_1^2 M_m]\omega_i^2 - 2w_c R_2[\sin(\phi+\theta) - \sin(\phi)]}{[(I_c)_o + R_1^2 M_m]}$

The cask stops rotating when the angular velocity, $\omega_f = 0$ and

$$\omega_i = \frac{R_1 v_i M_m}{R_1^2 M_m + (I_c)_o}$$

Thus, $\sin\phi\cos\theta + \sin\theta\cos\phi = \frac{(R_1 v_i M_m)^2}{2w_c R_2[(I_c)_o + R_1^2 M_m]} + \sin\phi$

$(I_c)_o = (I_c)_{CG} + M_c R_2^2$ (From parallel axis theorem)

Where,

$(I_c)_{CG}$ is the mass moment of inertia of the cask about center of gravity of EOS-TC.

Conservatively, the bounding (maximum) loaded cask weight from Case B (EOS-TC108 with EOS-89BTH DSC) of Table 3.9.7-6 (i.e., 199.29 kips) is taken, which is further decreased to 170 kips such that it is more conservative, because this results in maximum impact force and hence, the maximum primary membrane stress, circumferential membrane and bending stress intensity.

Hence, the total weight of the TC (EOS-TC, Skid and the Trailer), W_c = 170 + 10+ 35 = 215 kips

So the total mass of the TC assembly (EOS-TC, Skid and Trailer), M_c = (215*1000)/32.2 = 6,677.02 lbm

$(I_c)_{CG} = \frac{M_c R_c^2}{2}$ = 43,991.21 ft^2 lbm

$M_c R_2^2$ = 698,769.51 ft^2 lbm

$(I_c)_o$ = 7.43 x 105 ft^2 lbm

By substituting the parameters of cask and stability geometry in above equation, Sin (θ +φ) = 0.015+0.8433 = 0.8583,

Angle of Cask CG about pivot "O" relative to horizontal ,φ = tan-1 (L1/R) where R is the half width of trailer (5.5 ft assumed) and L1 is calculated to be 43 in. +17in. + (87/2) = 103.5 in. = 8.63 ft (See Figure 3.9.7-10). Therefore, φ = 57.49 and Solving above equation, θ = Sin^{-1}(0.8583)-57.49 = 59.13-57.49 = 1.64°

The maximum angle for the tip over the cask occurs when the CG is directly above the point of rotation.

i.e. $\theta_{tip} = 90^{\circ} - \phi = 32.52^{\circ}$ $\theta_{tip} = \tan^{-1} {}^{R}/_{R_2} = \tan^{-1} {}^{5.5}/_{10.6} = 27.42^{\circ}$

Accounting for the load factor of 1.1 on the tornado missile load by increasing the angle of rotation:

Since $\theta_{tip} >> 1.1 \times \theta$, the tip over of the cask does not occur.

3.9.7.2.6.2.2 Stress Analysis

3.9.7.2.6.2.2.1 Stresses in Cask Shell due to Massive Missile Impact Load

The missile impact is analyzed by taking Automobile 16.4 feet x 6.6 feet x 4.3 feet (Case B of Table 3.9.7-5) for evaluation of stresses in cask shell and top cover plates. The stresses in the cask shell due to the massive missile impact will be highest for an impact at the cask mid length. The impact force due to the massive missile is calculated by determining the work done in elevating the cask center of gravity the vertical distance corresponding to the angle of rotation (1.64°) resulting from impact.

The angle of rotation of the cask due to the massive missile impact is 1.64°, therefore, the impact force (*P*) including a dynamic load factor of 2.0 is given by:

P=2.0 x W_c x cos (90°-θ)

Total weight of cask, W_c (EOS-TC, Skid and the Trailer) = 253.30 +10 + 35 = 298.30 kips (Table 3.9.7-6 for enveloping EOS-TC weight)

W_c is considered to be approximately 300 kips, resulting in 17.17 kips

Assuming the cask is simply supported and subjected to a concentrated load, p, over short length 2b (Conservatively taken as 4.3 feet), thus using Case 8b, Table 13.3 of Roark's Formula for Stress and Strain [3.9.7-7], Page 650:

Circumferential membrane stress, $\sigma_2 = 0.130 BpR^{\frac{3}{4}} b^{\frac{-3}{2}} t^{\frac{-5}{4}}$

Circumferential bending stress, $\sigma_2^{'} = 1.56B^{-1}pR^{\frac{1}{4}}b^{\frac{-1}{2}}t^{\frac{-7}{4}}$

Axial membrane stress, $\sigma_1 = 0.153B^{3}pR^{\frac{1}{4}}b^{\frac{-1}{2}}t^{\frac{-7}{4}}$

Force per inch, p, is maximum for the minimum length of Automobile 16.4 feet x 6.6 feet x 4.3 feet (Case B of Table 3.9.7-5):

P = F / minimum dimension of Automobile
B = $[12(1-v^2)]^{1/8}$, where *v* is the Poisson's ratio (= 0.3 for stainless steel)

Also, circumferential membrane stress, circumferential bending stress and axial membrane stress are maximum for the maximum cask radius since they are directly related to cask radius:

Bounding maximum cask radius = EOS-TC135, Case E of Table 3.9.7-6

Circumferential membrane stress σ_2 = 0.39 ksi

Circumferential bending stress σ_2 = 10.03 ksi

Axial membrane stress, σ_1 = 3.27 ksi

Primary Membrane Stress Intensity = 3.27+0.39 = 3.66 ksi

Membrane plus Bending, $S.I. = \sigma_2 + \sigma_2^{'}$ = 13.69 ksi

3.9.7.2.6.2.2.2 Stresses in Top Cover Plate due to Massive Missile Impact Load

The impact on the top cover plate is assumed to be perfectly inelastic impact (Assumption 10) and the automobile (massive missile) is assumed to attach to the EOS-TC after impact.

Let

v_s= Striking velocity of the automobile normal to EOS-TC
w_{mssile}= Weight of missile

The impact force acting on the EOS-TC due to the massive missile automobile will be

W_m =0.625xv_s x w_{mssile} x sin (20t) lbs (Bechtel topical Report, Ref. [3.9.7-4])

Where,

t = time from the instant initial impact (sec)
w_m= 337500 lbs = 337.5 kips

Assuming the plate is simply supported at edges and subjected to a uniform load 'q' (load per unit area) over the entire area, thus using case 10a, Table 11.2 of Ref. [3.9.7-7], Page 509:

$M_c = qa^2 L_{17}$, where $L_{17} = \frac{1}{4}\left\{1 - \frac{1-v}{4}\right\}$ for $r_o = 0$.

Thus, $M_c = \frac{qa^2(3+v)}{16}$

$$M_c = \frac{p}{\pi a^2}\frac{a^2(3+v)}{16} = \frac{p}{\pi}\frac{(3+v)}{16}$$

$$\sigma = \frac{6M_c}{t^2} = \frac{6}{t^2}\frac{p}{\pi}\frac{(3+v)}{16} = 12.59 \text{ ksi}$$

Primary Membrane Stress= Total force acting on the EOS-TC due to massive missile automobile/ Area of top cover plate = 0.06 ksi

Therefore, Primary membrane + bending stress in the top cover plate will be 0.06 +12.59 = 12.65 ksi

3.9.7.2.6.3 Missile Penetration Resistance Analysis

3.9.7.2.6.3.1 Penetration Analysis

In order to evaluate the system for resistance towards the missile penetration, the minimum thickness required to resist the bounding missile (Case A, Table 3.9.7-5) is calculated using two different relations:

- Nelm's formula [3.9.7-8] is used to determine the minimum required thickness for puncture resistance.
- The Ballistic Research Laboratory formula is used to calculate the missile penetration distance and the minimum required thickness for puncture resistance.

It is assumed that the missile is rigid and the mass and velocity of the missile for the evaluation is taken from Table 3.9.7-5.

Nelms' Formula (page 54 of Reference [3.9.7-8])

$E_F / S = 2.4 d^{1.6} t^{1.4}$

Where,

E_F is the incipient puncture energy of the prismatic cask jacket (inch-lbs)
S is the ultimate tensile strength of the jacket material (cask outer shell) (ksi)

t is the thickness of the jacket material (inch)
d is the diameter of the punch/missile (6.625 inch)

Assuming all the kinetic energy of the missile is getting converted to the incipient puncture energy of the prismatic cask jacket.

$$E_F = \frac{1}{2} M_m v_m^{\ 2}$$

Where,

M_m and v_m are the mass and velocity of the missile, respectively.

$$E_F / S = 2.4 d^{1.6} t^{1.4}$$

$$t^{1.4} = 0.281 \Rightarrow t = 0.404 \text{ inch}$$

Ballistic Research Laboratory Relation (page 2-3 of [3.9.7-4])

$$T = \frac{\left(\frac{MV_s^{\ 2}}{2} \right)^{2/3}}{672D}$$

Where,

T is the steel plate thickness to just perforate (inch)
D is the diameter of the punch/missile (= 6.625 inch)
M_s is the mass of the striking missile (= 8.91 lbs.sec^2/ft)
V is the velocity of the striking missile normal to target surface (=135 fps)
T = 0.421 inch

The thickness t_p, of a steel barrier required to prevent perforation should exceed the thickness for threshold of perforations. It is recommended by [3.9.7-4] to increase the thickness, T, by 25 percent to prevent perforation.

Thus, minimum thickness of the barrier should be, $t_p = 1.25T$ inch = 0.526 inch

Out of the thickness calculated by the two methods, the threshold thickness evaluated by Ballistic Research Laboratory relation is bounding. Thus the minimum thickness required to prevent perforation in the EOS-TC is 0.526 inch.

Thickness of the cask outer shell (1 inch) >> 0.526 inch

Thickness of the top cover plate (3.25 inch) >> 0.526 inch

Since the cask shell, and top covers are much thicker than the depth of penetration; demonstrating that during a DBT, the cask is not be penetrated by the missiles specified in Table 3.9.7-5, thus protecting the DSC.

3.9.7.2.6.3.2 Localized Peak Stress Analysis due to Missile Impact Load

In order to evaluate the localized peak stresses occurring due to the missile impact on to the cask, impact force is calculated as follows:

$$F\Delta t = G_f - G_i$$

Where,

Δt is the time of contact =0.05 sec (more conservative than impact time 0.075 sec [3.9.7-4])
G_f is the linear momentum at time $t = t_f = mv_f$
G_i is the linear momentum at time $t = t_i = mv_i$
v is the velocity
m is the mass

Subscripts i and f represent initial and final states, respectively.

$$F = \frac{m(v_i - v_f)}{(t_f - t_i)} = \frac{m(v_i - v_f)}{(\Delta t)}$$

Assuming that the system stops after the impact, i.e. $v_f = 0$

$$F = \frac{m(v_i)}{(\Delta t)} = 24.1 \text{ Kips}$$

The impact force is dynamic as calculated using the rate of change of momentum; hence a dynamic load factor is not required.

3.9.7.2.6.3.2.1 Localized Peak Stresses in the Cask Shell due to Missile Impact Load

Assuming the cask is a cylindrical shell with closed ends and end support, subjected to a uniform radial load, p, over a small area A, thus using Case 8a, Table 13.3 of Roark's Formula for Stress and Strain [3.9.7-7], Page 649:

$$\frac{R}{t} = 43.5$$

r = 3.3125-in. radius of Schedule 40 Pipe (Case A, Table 3.9.7-5)

The localized peak stress region is taken at '2t' away from impact, hence r =5.3125 inches is used to simulate the peak stress region.

$$\frac{A}{R^2} = \frac{\pi(5.3125)^2}{43.5^2} = 0.0469$$

By interpolation,

$$\sigma_2'\left(\frac{t^2}{F}\right) = 0.74$$

$$\sigma_2' = 0.74\left(\frac{F}{t^2}\right) = 0.74\left(\frac{24.1}{1^2}\right) = 17.83 \text{ ksi}$$

By interpolation,

$$\sigma_2\left(\frac{Rt}{F}\right) = 6.37$$

$$\sigma_2 = 6.37\left(\frac{F}{Rt}\right) = 6.37\left(\frac{24.1}{43.5\times 1}\right) = 3.53 \text{ ksi}$$

Force applied by the missile on to the cask = 24.1 kips

Area of missile striking face = $\frac{\pi}{4}\times 6.625^2 = 34.47\, in^2$

Therefore, radial membrane stress $\sigma_3 = \frac{24.1}{34.47} = 0.70\, ksi$

As the weight of the missile (287 lb) is much less than the weight of the overall cask, thus stresses in the axial direction (σ_1) will be negligible.

Therefore, conservatively Primary Membrane stress

$\sigma_m = \max(\sigma_1+\sigma_2, \sigma_2+\sigma_3, \sigma_3+\sigma_1) = 3.53+0.70 = 4.23\, ksi$

Primary Membrane plus Bending stress, $\sigma_m+\sigma_b = 4.23+17.83 = 22.06\ ksi$

3.9.7.2.6.3.2.2 Localized Peak Stresses in Top Cover Plate due to Missile Impact Load

Assuming the top cover plate is a circular plate simply supported at the edges and subjected to a uniform load over a small area A of radius r_o, thus using case 16, Table 11.2 of Roark's Formula for Stress and Strain, Page 514 [3.9.7-7]:

$$M_{\max} = \frac{W}{4\pi}\left[(1+v)\ln\left(\frac{a}{r_o'}\right)+1\right] \text{ at r = 0}$$

Where, a is the plate outer radius = 43.5 inch

r_o = 5.3125 inches
W is the load = 24.1 kips
t is the thickness of the top cover plate = 3.25 inches
M_{max} = 7.16 Kip-in/in

$$\sigma = \frac{6M_{max}}{t^2} = 4.07 \text{ ksi}$$

Force applied by the missile onto the cask = 24.1 kips
Area of missile striking face = 34.47 in^2
Therefore, radial membrane stress = 24.1/34.47 = 0.70 ksi
Primary membrane plus bending stress = 4.07+ 0.70 = 4.77 ksi

3.9.7.2.6.4 Stability Analysis for EOS-TC due to Seismic Load

During any seismic event in a loaded EOS-TC in the horizontal position on the skid and the trailer, it will be subjected to overturning moment. The peak ground acceleration in the horizontal (a_h) and the vertical direction (a_v) due to seismic event is 0.45 g and 0.30 g, respectively.

An overturning moment due to seismic load is calculated assuming the seismic load is acting on the cask center from the ground. The vertical seismic load is combined with the horizontal load using the 100-40-40 combination method (i.e., 40% of the vertical component acting simultaneously with 100% of the horizontal component). The stability analysis due to seismic overturning moment is performed below:

The overturning moment produced in the cask due to seismic effect is:

$$M_{ot} = a_h \times W \times L_1 + 0.4a_v \times W \times R$$

This overturning moment is resisted by the restoring moment:

$$M_{st} = W \times R$$

The variables are defined as follows:

a_h = horizontal seismic acceleration = 0.45g

W = weight of cask (results are independent of cask weight)

L_1 = vertical location of cask center of gravity = $\frac{\left(17+43+\frac{87}{2}\right)}{12} = 8.63$ feet
(Figure 3.9.7-9 and Figure 3.9.7-10)

R = horizontal distance from point of rotation to cask center of gravity = $\frac{11ft}{2} = 5.5$ feet (Figure 3.9.7-9 and Figure 3.9.7-10)

The factor of safety against overturning, including a load factor of 1.1 on the overturning moment is:

$$\frac{M_{st}}{1.1M_{ot}} = \frac{W \times R}{1.1(a_h \times W \times L_1 + 0.4a_v \times W \times R)} = \frac{5.5}{1.1(0.45 \times 8.63 + 0.4 \times 0.30 \times 5.5)} = 1.10$$

The maximum acceptable acceleration value before tipping occurs is calculated below:

$$a_v = \frac{2}{3}a_h$$

$$M_{st} > 1.1M_{ot} \rightarrow W \times R > 1.1\left(a_h \times W \times L_1 + 0.4\frac{2}{3}a_h \times W \times R\right)$$

$$\frac{R}{1.1} > a_h\left(L_1 + 0.4\frac{2}{3} \times R\right)$$

$$a_h < \frac{R}{1.1\left(L_1 + 0.4\frac{2}{3} \times R\right)} = \frac{5.5}{1.1(8.63 + 0.267 \times 5.5)} = 0.49g$$

$$a_h = 0.49, \quad a_v = 0.33g$$

The safety factor against overturning is 1.10 based on the design basis accelerations and including a load factor of 1.1 on the overturning moment. The EOS-TC can have up to 0.49g horizontal seismic acceleration and 0.33g vertical seismic acceleration before the cask can start to overturn. Therefore, the EOS-TC will maintain its stability during the seismic event.

3.9.7.2.6.5 Analysis of Cask for DBT Wind Load and DBT Missile Load Combination

Per NUREG-0800, the total tornado load on a structure is combined as follows:

$W_t = W_p$
$W_t = W_w + 0.5W_p + W_m$

Where,

W_t = Total tornado load
W_w = Load from tornado wind effect
W_p = Load from tornado atmospheric pressure change effect
W_m = Load from tornado missile impact effect

Note that W_p is not applicable to the stability analysis as discussed in Section 3.9.7.1.6. Therefore, the load combination for tornado loading for this analysis is simplified to:

$W_t = W_w + W_m$

The envelope of a range of missiles listed in Table 3.9.7-5 is used for the missile impact load evaluation. The automobile missile, with a size of 16.4 ft x 6.6 ft x 4.3 ft (Case B of Table 1), impact on to the EOS-TC has the maximum momentum and is considered as the bounding case.

3.9.7.2.6.5.1 Overturning Analysis due to Concurrent Tornado Loads

A dynamic analysis for the combined effects of wind and concurrent massive missile impact loading is conducted. The effects of the concurrent missile impact loads are used in determining the initial angular momentum from the conservation of angular momentum equations using the wind loads from the previous section. Then the angle of rotation is determined from the conservation of the concurrent loading.

Angular velocity of the missile about point O just after the impact is:

$$\omega_i = \frac{R_1 v_i M_m}{R_1^2 M_m + (I_c)_o}$$

The concurrent wind load is accounted for by reducing the inertia that resists motion in the denominator of the equation of angular velocity of the missile about point O just after the impact

$$\omega_i = \frac{R_1 v_i M_m}{R_1^2 M_m + (I_c)_o - W_w \times L_1^2}$$

Where R_1, v_i, M_m and $(I_c)_o$ are defined in Section 3.9.7.2.6.2.1

Using the relation presented in Section 3.9.7.2.6.2.1 and reducing the inertia that resists motion in the denominator of the equation,

$$Sin(\theta + \phi) = \frac{(R_1 v_i M_m)^2}{2 w_c R_2 [(I_c)_o + R_1^2 M_m - W_w \times L_1^2]} + \sin\phi$$

$$Sin(\theta + \phi) = 0.0174 + 0.8433$$

$$(\theta + \phi) = Sin^{-1}(0.8607) = 59.40°$$

$$\theta = 59.40° - 57.49° = 1.91°$$

The maximum angle for the tip over of the cask occurs when the CG is directly above the point of rotation. The maximum angle for tip over calculated in Section 3.9.7.2.6.2.1 is $\theta_{tip} = 32.51°$. Since $1.1\theta \times < 1/3\ \theta_{tip}$, tip over of the EOS-TC cask will not occur.

3.9.7.2.6.5.2 Time-Dependent Overturning due to Concurrent Tornado Loads

In addition to the dynamic overturning analysis, a time dependent analysis is used to ensure the absence of any overturning.

An approximate relationship for the deceleration of an automobile impacting a rigid wall is given by:

$$-\ddot{x} = 12.5g * x \quad [3.9.7\text{-}4]$$

Where,$-\ddot{x} = 12.5g \cdot x$Eq. D-1of[3.9.7-4]

$-\ddot{x}$ = Deceleration (ft/sec^2)
x = Distance automobile crushes into target (ft)

A force time history is obtained:

$$W_m = 0.625 \times v_s \times w_{missile} \times \sin(20t)$$

The overturning moment is:

$$M_{ot} = W_m \times L + q_z \times L_\theta^{\ 2} \times L_T$$

Where,

L_θ = Height to the top of the cask system, which is dependent on rotation θ.
L = Initial height of the cask system
L_T = Length of the trailer
q_z = DBT velocity pressure

And the stabilizing moment is:

$$M_{st} = W_c * R_2 * Cos(\phi + \theta)$$

The moment causing acceleration is:

$$M_{acc} = M_{ot} - M_{st}$$

The angular velocity is:

$$\omega_i = \frac{\left[\frac{M_{acc,i} + M_{acc,i-1}}{2} * (t_i - t_{i-1})\right]}{(I_c)_o} + \omega_{i-1}$$

Where,

i = index for the current time step
$i-1$ = index for the previous time step

The angle of rotation is:

$$\theta_i = \left[\frac{\omega_i + \omega_{i-1}}{2} * (t_i - t_{i-1})\right] + \theta_{i-1}$$

Accounting for the required load factor of 1.1 on the design basis tornado, the angle of rotation resulting from the analysis is shown in Figure 3.9.7-11. The governing angle of rotation is 7.55 x 1.1 = 8.31 degrees, which is less than the (1/3) x tip angle (Θ_{tip}) = (1/3) x 32.51° = 10.84°. The factor of safety against tipping is 10.84/8.31 = 1.30. Therefore, the EOS-TC will not tip over due to wind concurrent with massive missile impact load combination.

3.9.7.2.7 Results

The factor of safety against tip overturn is greater than 1 for the individual DBT wind pressure load and seismic load. Also, the angle of rotation (θ) due to massive missile impact load, concurrent tornado loads is less than critical tipping angle ($1/3x\theta_{tip}$). Therefore, EOS-TC remains stable on the trailer during transfer operations. The primary membrane intensity and combined membrane plus bending stresses due to DBT and missile impact are calculated to be below the allowable stresses. The maximum missile penetration depth is found to be 0.526 inch, which is less than the thickness of the EOS-TC outer shell and top cover plate of 1 inch and 3.25 inches, respectively.

The resultant stresses for the bounding individual DBT, missiles impact and combined tornado load are summarized in Table 3.9.7-7 and Table 3.9.7-8, respectively.

3.9.7.3 References

3.9.7-1 NUREG-0800, Standard Review Plan, "Missiles Generated by Natural Phenomena", Revision 2, U.S. Nuclear Regulatory Commission, July 1981.

3.9.7-2 American Society of Civil Engineers, ASCE 7-10, "Minimum Design Loads for Buildings and Other Structures."

3.9.7-3 Raymond C. Binder, "Fluid Mechanics," Prentice-Hall, Inc, 1943.

3.9.7-4 Bechtel Report BC-TOP-9A Rev. 2, "Topical Report – Design of Structures for Missile Impact," September 1974.

3.9.7-5 American Society of Civil Engineers Standard, ASCE 7-05, "Minimum Design Loads for Buildings and Other Structures," (Formerly ANSI A58.1).

3.9.7-6 U.S. Nuclear Regulatory Commission, Regulatory Guide 1.76, "Design Basis Tornado for Nuclear Power Plants," Revision 1, March 2007.

3.9.7-7 R.G Budynas and W.C Young, "Roark's Formula for Stress and Strain," Eighth Edition, McGraw-Hill Book Company.

3.9.7-8 H. A. Nelms, "Structural Analysis of Shipping Casks, Effects of Jacket Physical properties and Curvature on Puncture Analysis," Vol.3, ORNL TM-312, Oak Ridge National Laboratory, Oak Ridge Tennessee, June 1968.

Table 3.9.7-1
Sizes and Weight for Various EOS-HSM Models

EOS-HSM Module	Total Length of EOS-HSM (in.)	Nominal Weight of Empty HSM (lbs.)
EOS-HSM Short	228	292,000
EOS-HSM Medium	248	314,000
EOS-HSM Long	268	330,000

Table 3.9.7-2
Missile Load Data for EOS-HSM Stability Analysis

Missile	Mass (lbs.)	Dimensions	Velocity (fps)	Momentum (lbs-fps)
Utility Wooden Pole	1,124	13.5-inch Diameter 35 feet Long	180	202,320
Armor Piercing Artillery Shell	276	8-inch Diameter	185	51,060
Steel Pipe	750	12-inch Sch. 40 15 feet Long	154	115,500
Automobile	4,000	20 ft^2 Contact Area	195	780,000

Table 3.9.7-3
Design Pressures for Tornado Wind Loading

Wall Orientation (1)	Velocity Pressure (psf)	Ext. Pressure Coefficient (2)	Int. Pressure Coefficient (3)	Max/Min Design Pressure (psf) (4)
Front	253.8	0.680	± 0.18	218
Left	253.8	-0.595		-197
Rear(5)	253.8	-0.425		-154
Right	253.8	-0.595		-197
Top	253.8	-1.105		-326

Notes:

1. Wind direction assumed to be from front. Wind loads from other directions may be found by rotating above table values to desired wind direction.
2. These values are calculated using the external pressure coefficients from Figure 27.4-1 of [3.9.7-2] times the gust effect factor (0.85) from Section 26.9 of [3.9.7-2].
3. Internal pressure coefficient from Table 26.11-1 of [3.9.7-2].
4. These values are computed based on Equation 27.4-1 of [3.9.7-2].
5. The bounding C_p of -0.5 from an L/B ratio of 0-1 is used for wind in all directions from Figure 27.4-1 of [3.9.7-2].

Table 3.9.7-4
Summary of EOS-HSM Sliding and Stability Results

Loading	Tornado Wind + Missile		Flood		Seismic for Loaded EOS-HSM with End Shield Wall	
Result	Maximum Sliding Distance (in)	Maximum Rocking Uplift[3] (°)	Safety Factor against Sliding	Safety Factor against Tipping	Maximum Acceleration before Sliding[1] (horiz / vert) (g)	Maximum Acceleration before Tipping[2] (horiz / vert) (g)
EOS-HSM Short	1.62	3.4	1.12	1.14	0.45 / 0.30	>0.45 / 0.30
EOS-HSM Medium	1.62	2.8	1.09	1.12	0.45 / 0.30	>0.45 / 0.30
EOS-HSM Long	1.62	2.4	1.11	1.13	0.45 / 0.30	>0.45 / 0.30

Notes:

1. Maximum acceleration to preclude sliding is 0.47g / 0.32g, but seismic load is limited to 0.45g / 0.30g based on static stability analysis of DSC on the support structure.
2. Maximum acceleration to preclude tipping is 0.46g / 0.31g, but seismic load is limited to 0.45g / 0.30g based on stability analysis of DSC on the support structure.
3. A 1.1 required factor is applied for the wind load to the angles from Figure 3.9.7-2 to Figure 3.9.7-4.

Table 3.9.7-5
Design-Basis Tornado Missile Spectrum and Maximum Horizontal Speed for EOS-TC Stability Analysis

Case #	Missile [1]	Weight (lbs)	Horizontal Impact Velocity [2] (fps)
A	Schedule 40 Pipe (ϕ 6.625 inch x 15 ft long) [5]	287	135
B	Automobile (16.4 ft x 6.6 ft x 4.3 ft) [3][4]	4000	135
C	Solid Steel Sphere (ϕ 1 inch)	0.147	26

Notes:

1. Missiles are assumed to strike at 90 degrees to the surface with the longitudinal axis of the missile parallel to the striking angle.
2. Vertical striking velocity is 67% of the horizontal.
3. Automobile missile (Case B) bounds all other cases for stability and stresses and therefore only Case B is evaluated for stability and associated stresses.
4. The automobile missile (Case B) considered to impact at all altitudes less than 30 ft above all grade levels within 0.5 mile of the plant structure.
5. Schedule 40 pipe (Case A) bounds all other items for penetration resistance and for local stresses and therefore Case A is evaluated for the penetration resistance.

Table 3.9.7-6
Cask and DSC Weights in Different Configuration and Their Geometric Properties

CASE	Configuration	Cask without NSP Assembly[1] (lbs)	DSC Weight[2] (lbs)	Minimum Weight (lbs)	Maximum Weight (lbs)	Cask Diameter[1] (inches)	Length[1] (inches)
A	TC108/37PTH	86,289	119,000	205,289	220,289	85.5	206.76
			134,000				
B	TC108/89BTH	86,289	113,000	199,289	206,289	85.5	206.76
			120,000				
C	TC125/37PTH	108,802	119,000	227,802	242,802	87	208.01
			134,000				
D	TC125/89BTH	108,802	113,000	221,802	228,802	87	208.01
			120,000				
E	TC135/37PTH	119,230	119,000	238,230	235,230	87	228.59
			134,000				

Note:

1. Weight of TC without NSP assembly and their geometric parameter in different configuration is taken from Section 3.2.
2. Weight of 37PTH and 89BTH DSC weights are taken from Section 3.2.

Table 3.9.7-7
EOS-TC Analysis Results

Load Description	Stress Category	Calculated Stress (ksi)		Allowable Stress (ksi)	Impact Force (kips)
		Cask Shell	Top Cover Plate		
Wind Pressure Loads	Primary Membrane	1.34	0	39	22.36
	Membrane + Bending	5.19	0.21	58.5	
Massive Missile	Primary Membrane	3.66		39	17.17
	Membrane + Bending	13.69		58.5	
	Primary Membrane		0.06	39	337.5
	Membrane + Bending		12.65	58.5	
Penetration Resistance	Primary Membrane	4.23	0.70	39	24.1
	Membrane + Bending	22.06	4.77	58.5	

Table 3.9.7-8
Combined Tornado Effect

Load Description	Stress Category	Combined Stress (ksi)		Allowable stress (ksi)
		Cask Shell	Top Cover Plate	
Wind pressure load + Massive Missile	Primary Membrane	5.0	0.06	39
	Membrane + Bending	18.88	12.86	58.5

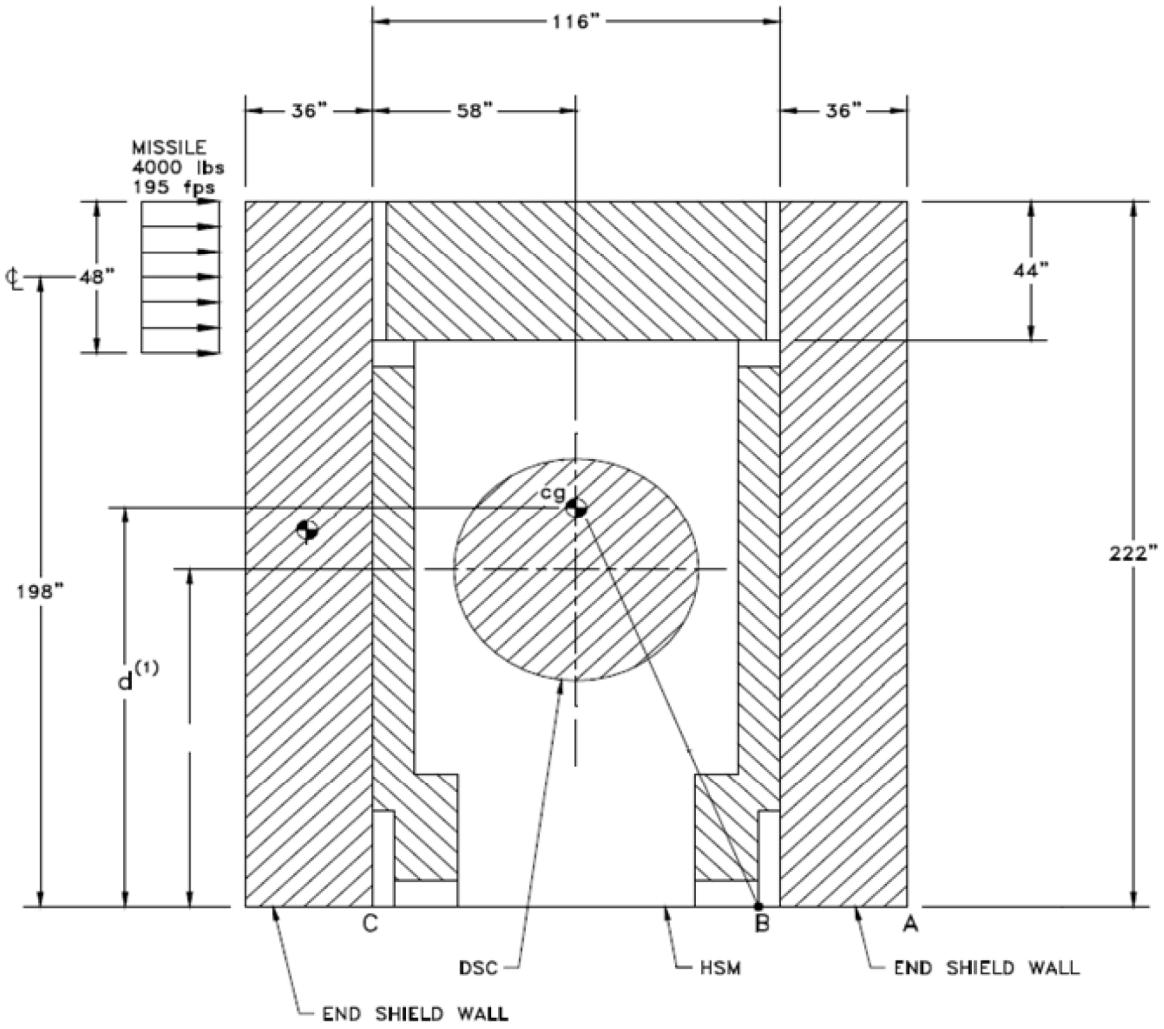

(1) d = distance to CG of EOS-HSM

Figure 3.9.7-1
EOS-HSM Dimensions for Stability Analysis

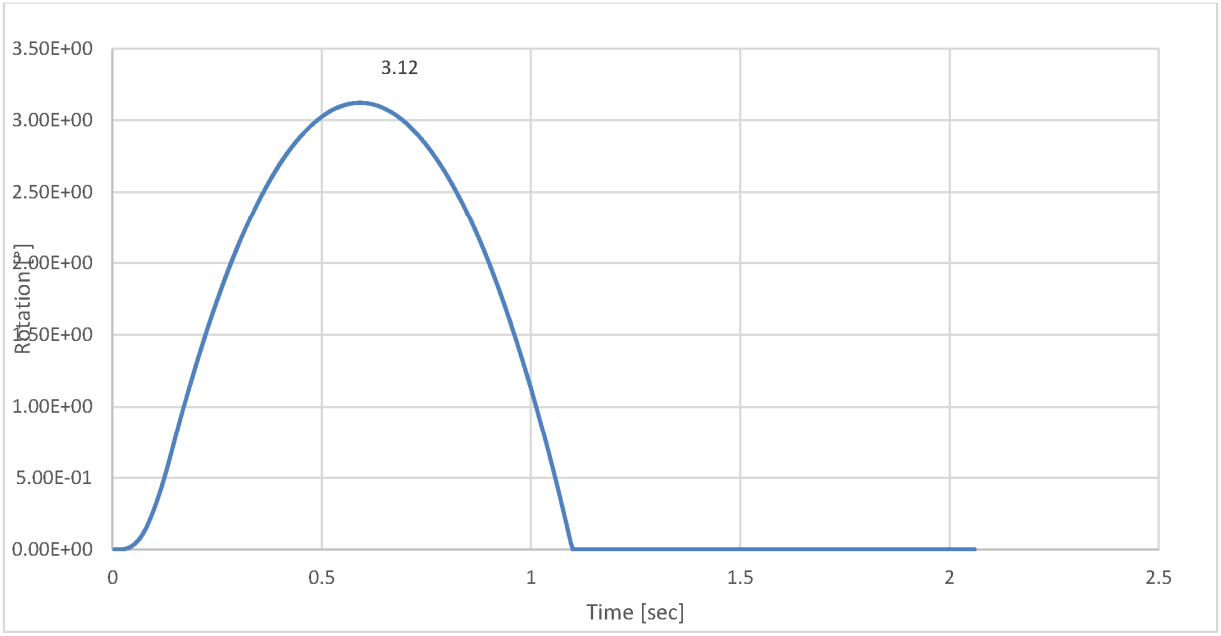

Figure 3.9.7-2
Angle of Rotation from Time-Dependent Analysis Due to Tornado Wind and Massive Missile Loading for EOS- HSM Short

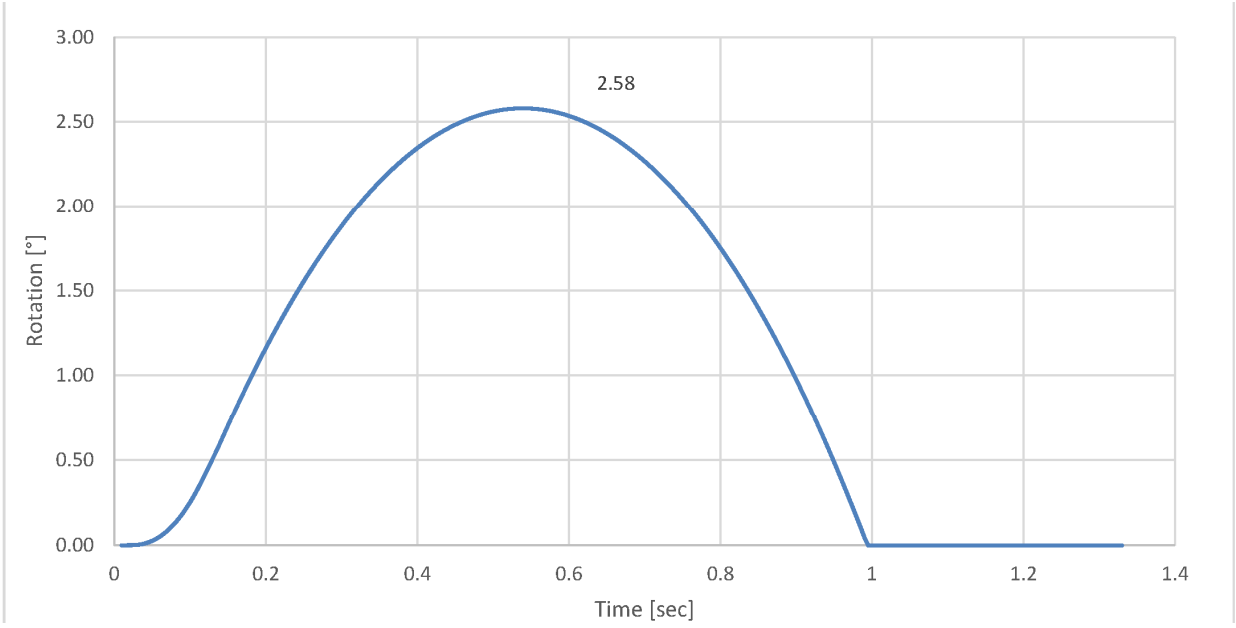

Figure 3.9.7-3
Angle of Rotation from Time-Dependent Analysis Due to Tornado Wind and Massive Missile Loading for EOS- HSM Medium

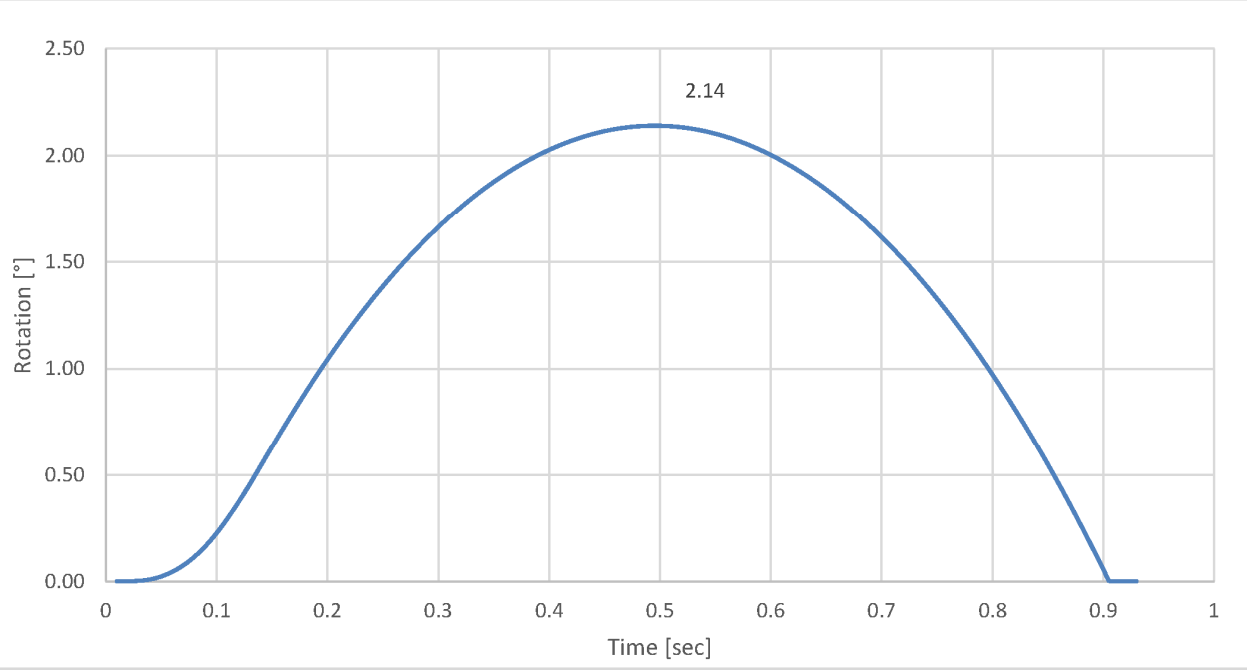

Figure 3.9.7-4
Angle of Rotation from Time-Dependent Analysis Due to Tornado Wind and Massive Missile Loading for EOS- HSM Long

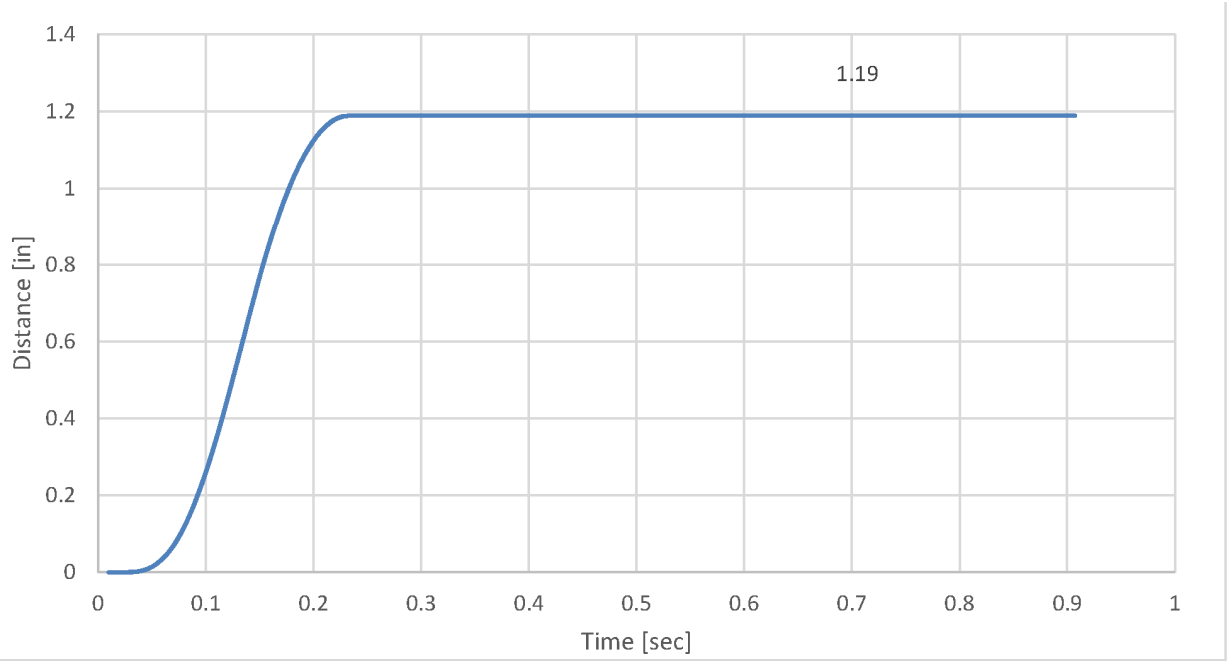

Figure 3.9.7-5
Sliding Displacement from Time-Dependent Analysis Due to Tornado Wind and Massive Missile Loading for EOS- HSM Short

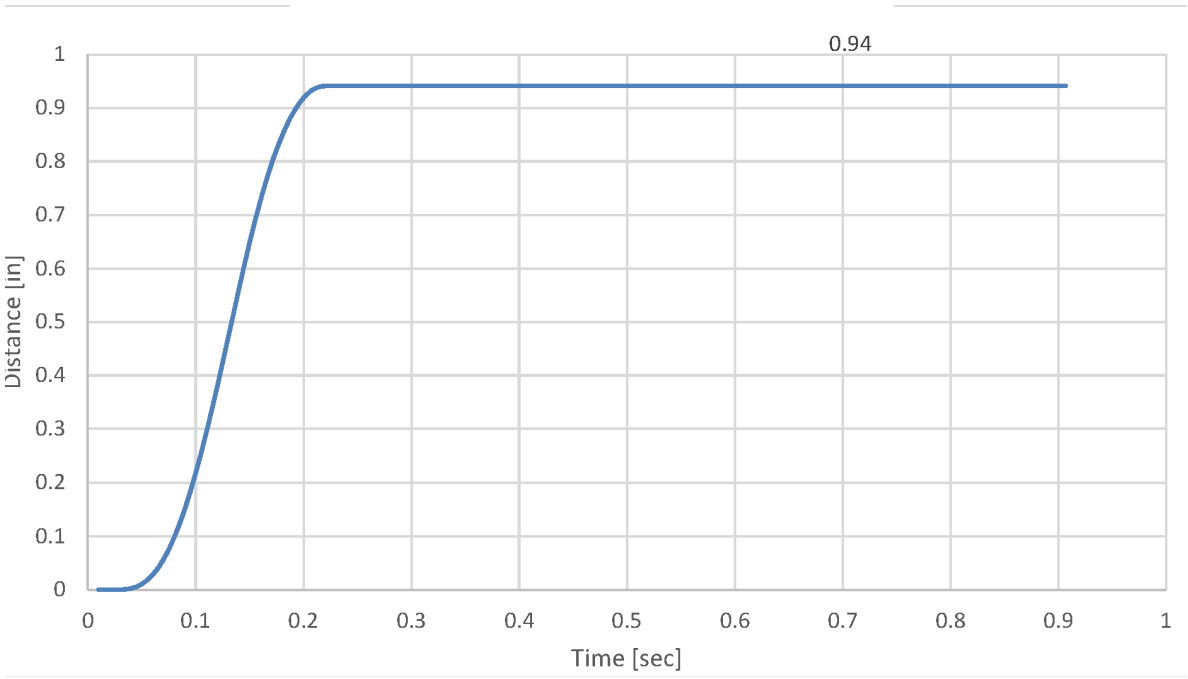

Figure 3.9.7-6
Sliding Displacement from Time-Dependent Analysis Due to Tornado Wind and Massive Missile Loading for EOS- HSM Medium

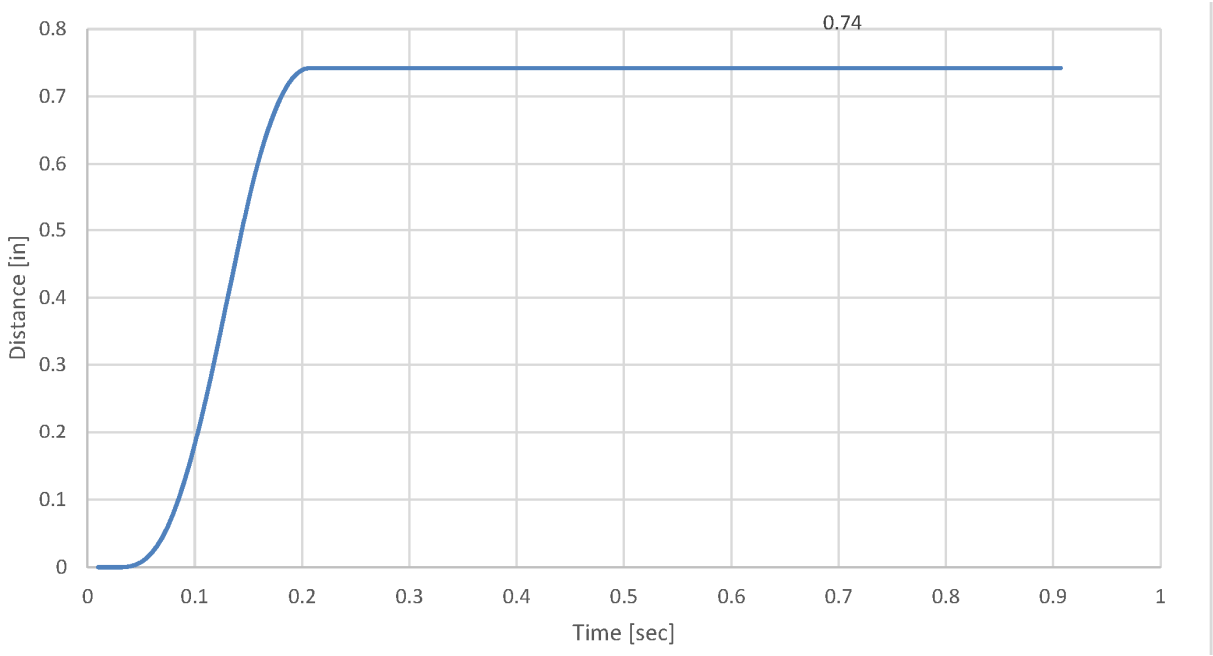

Figure 3.9.7-7
Sliding Displacement from Time-Dependent Analysis Due to Tornado Wind and Massive Missile Loading for EOS- HSM Long

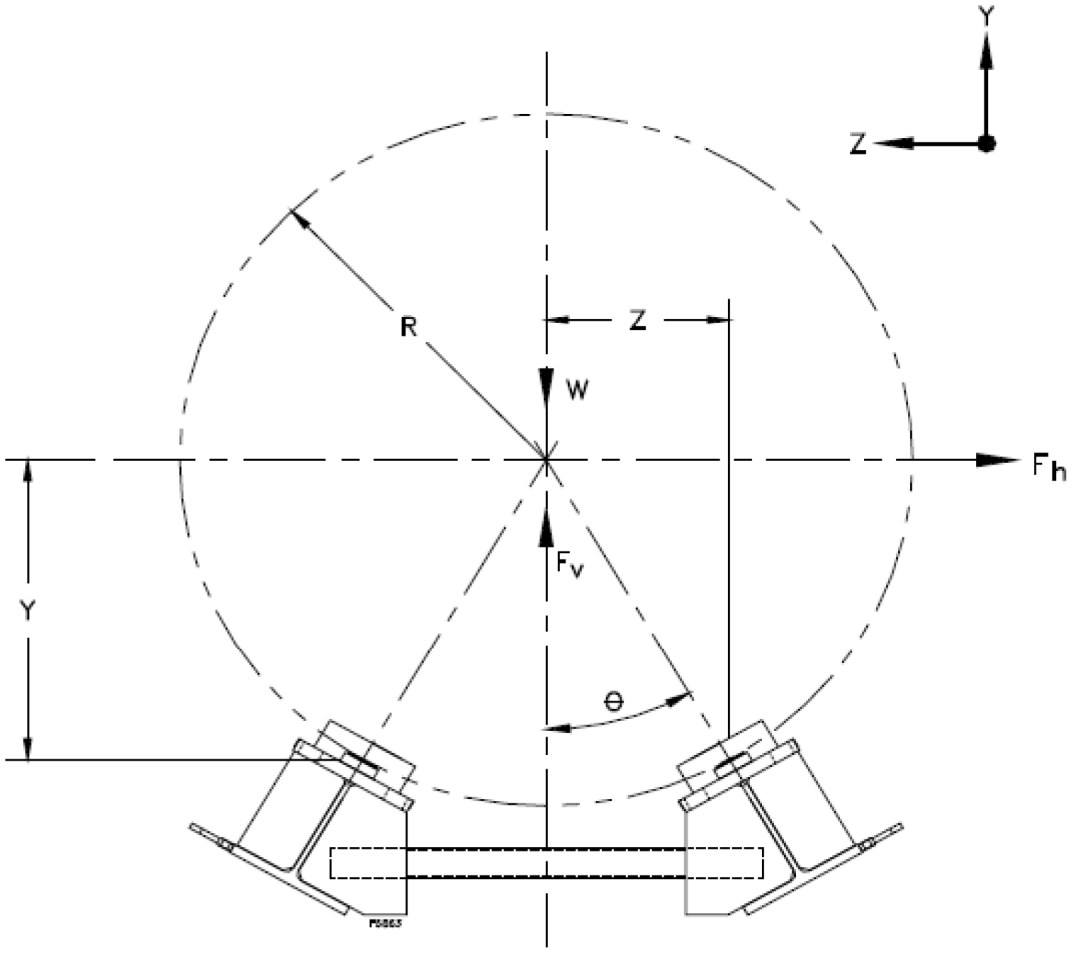

Figure 3.9.7-8
Stability of the DSC on the DSC Support Structure

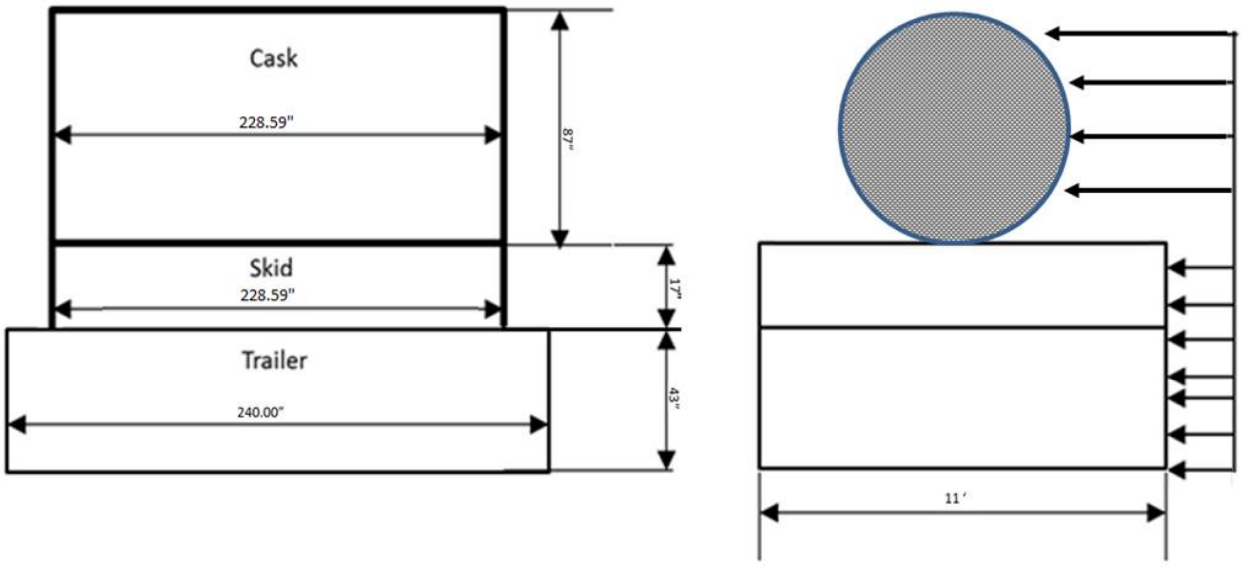

Figure 3.9.7-9
Arrangement of EOS-TC, Skid and Transfer Trailer at Rest

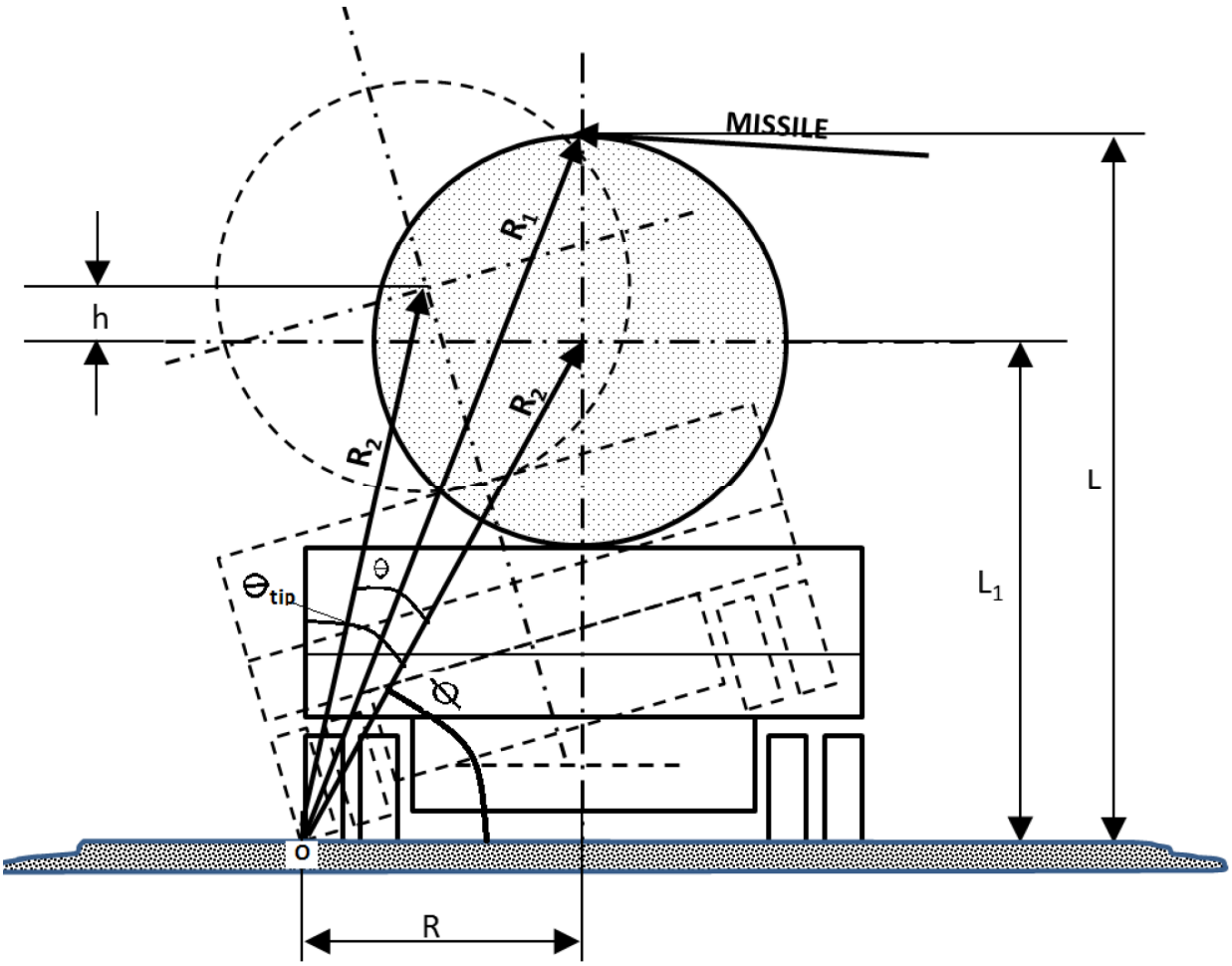

Figure 3.9.7-10
Stability Geometry of TC on Transfer Trailer

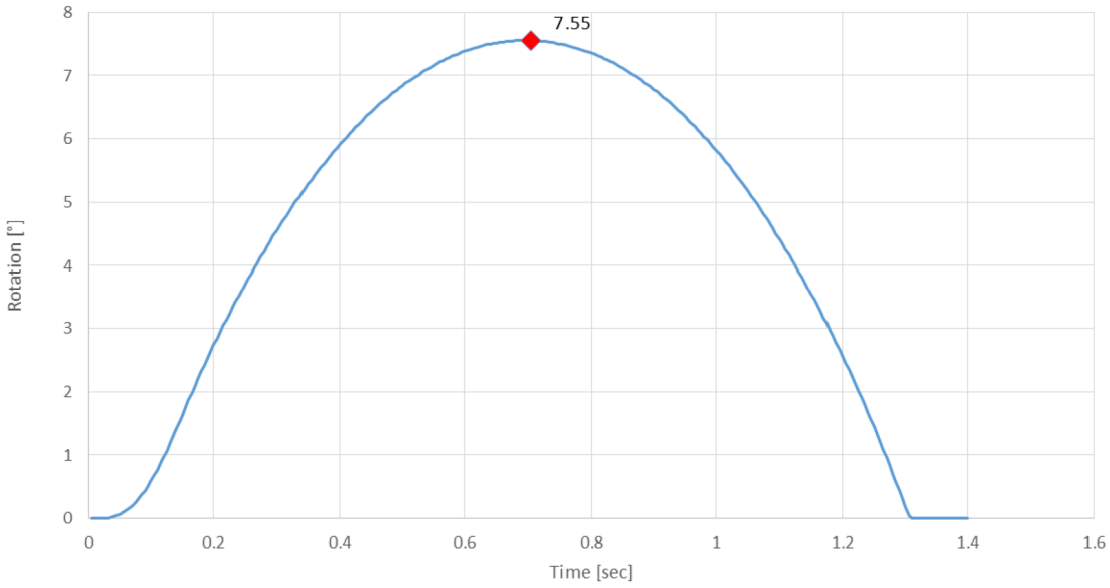

Figure 3.9.7-11
Angle of Rotation (Time-Dependent)-Wind and Missile Loading for EOS-TC